

Fatigue Life Assessment of 30CrNiMo8HH Steel Under Variable Amplitude Loading

by

Elfaitori Ibrahim

A thesis
presented to the University of Waterloo
in fulfillment of the
thesis requirement for the degree of
Master of Applied Science
in
Mechanical Engineering

Waterloo, Ontario, Canada, 2012

© Elfaitori Ibrahim 2012

AUTHOR'S DECLARATION

I hereby declare that I am the sole author of this thesis. This is a true copy of the thesis, including any required final revisions, as accepted by my examiners.

I understand that my thesis may be made electronically available to the public.

Elfaitori Ibrahim

Abstract

The actual service loading histories of most engineering components are characterized by variable amplitudes and are sometimes rather complicated. The goal of this study was to estimate the fatigue life of nickel-chromium-molybdenum 30CrNiMo8HH steel alloy under axial and pure torsion variable amplitude loading (VAL) conditions. The investigation was directed at two primary factors that are believed to have an influence on fatigue life under such loading conditions: load sequence and mean stress. The experimental work for this research included two-step loading, non-zero mean strain loading, and VAL tests, the results of which were added to previously determined fully reversed strain-controlled fatigue data. The effect of load sequence on fatigue life was examined through the application of the commonly used linear damage accumulation rule along with the Manson and Marco–Starkey damage accumulation methods, the latter of which takes load sequence into account. Based on the two-step experimental results, both the Manson and Marco–Starkey methods were modified in order to eliminate the empirically determined constants normally required for these two methods. The effect of mean stress on fatigue life was investigated with the use of three life prediction models: Smith–Watson–Topper (SWT), Fatemi–Socie (FS), and Jahed–Varvani (JV). The cycles from the VAL histories were counted using a rainflow counting procedure that maintains the applied strain sequence, and a novel method was developed for the estimation of the total energy density required for the JV model. For two-step loading and for all three fatigue models employed, the modified damage accumulation methods provided superior fatigue life predictions. However, regardless of the damage accumulation method applied, the most satisfactory fatigue life correlation for VAL was obtained using the energy-based JV model.

Acknowledgements

I would like to express my greatest gratitude to my supervisor, Professor Hamid Jahed, for his guidance, encouragement, and support. I also wish to thank Dr. Mohammad Noban for his helpful consultations and feedback.

I gratefully acknowledge the financial assistance of General Dynamics Land Systems (GDLS), and I am also thankful to the Libyan Ministry of Higher Education and Scientific Research (MOHESR) for granting me an MASc scholarship.

I greatly appreciate the valuable discussions and thoughts contributed by my colleagues: Seyed Behzad Behravesh, Dr. Jafar Al Bin Mousa, Dr. Amin Eshraghi, Dr. Morvarid Karimi Ghovanlou, Ali Roostaei, and Mi Chengji. I would also like to thank Barbara Trotter for proofreading and copyediting my thesis.

Last but not least, I wish to thank my family and my friends for their continuous support and encouragement throughout this work.

Dedication

*To the soul of my brother Nasef
I dedicate this thesis*

Table of Contents

| | |
|--|------|
| AUTHOR'S DECLARATION | ii |
| Abstract | iii |
| Acknowledgements | iv |
| Dedication | v |
| Table of Contents | vi |
| List of Figures | viii |
| List of Tables | xi |
| <i>Chapter 1</i> Introduction | 1 |
| 1.1 Background | 1 |
| 1.2 Motivation | 2 |
| 1.3 Plan and Objectives | 3 |
| 1.4 Thesis Layout | 4 |
| <i>Chapter 2</i> Literature Review | 5 |
| 2.1 Introduction | 5 |
| 2.2 VAL Elements | 6 |
| 2.2.1 Cycle Counting Methods | 6 |
| 2.2.2 Damage Accumulation and Load Sequence Effect | 8 |
| 2.2.3 Effect of the Mean Stress | 12 |
| 2.3 Monotonic, Cyclic, and Fatigue Properties | 15 |
| 2.3.1 Monotonic Properties | 15 |
| 2.3.2 Cyclic Properties | 17 |
| 2.3.3 Fatigue Properties | 18 |
| 2.4 Fatigue Life Prediction Models | 21 |
| 2.4.1 Smith–Watson–Topper Model | 22 |
| 2.4.2 Fatemi–Socie Model | 23 |
| 2.4.3 Jahed–Varvani Model | 23 |
| 2.5 Previous Studies of Variable Amplitude Loading | 28 |
| <i>Chapter 3</i> Experimental Program | 29 |
| 3.1 Introduction | 29 |
| 3.2 Material and Specimens | 30 |
| 3.3 Testing Equipment and Standards | 31 |

| | |
|---|----|
| 3.4 Experimental Results and Material Properties | 32 |
| 3.4.1 Monotonic Tests | 32 |
| 3.4.2 Constant Amplitude Loading Tests | 33 |
| 3.4.3 Two-Step Loading Tests..... | 37 |
| 3.4.4 Mean Strain Loading Tests..... | 41 |
| 3.4.5 Variable Amplitude Loading Tests..... | 53 |
| <i>Chapter 4</i> Fatigue Life Prediction..... | 56 |
| 4.1 Introduction | 56 |
| 4.2 Cycle Counting Method | 57 |
| 4.3 Damage Accumulation Method..... | 62 |
| 4.4 Total Energy Estimation Method | 68 |
| 4.5 Fatigue Life Predictions | 70 |
| 4.5.1 Constant Amplitude Loading Tests | 70 |
| 4.5.2 Two-Step Loading Tests..... | 72 |
| 4.5.3 Mean Strain Loading Tests..... | 75 |
| 4.5.4 Variable Amplitude Loading Tests..... | 77 |
| <i>Chapter 5</i> Summary, Conclusions, and Recommendations | 81 |
| 5.1 Summary | 81 |
| 5.2 Conclusions | 83 |
| 5.3 Recommendations | 83 |
| <i>Appendix A</i> Hysteresis Loops..... | 85 |
| <i>Appendix B</i> MATLAB Code for the Rainflow Counting Method..... | 95 |
| Bibliography | 99 |

List of Figures

| | |
|--|----|
| Figure 2.1: Simplified rainflow counting method [10]: (a) original history; (b) rearranged history; (c), (d), (e) cycle counting and removal of cycles counted; (f) counting results | 7 |
| Figure 2.2: Two-step loading: (a) CAL stress blocks; (b) S–N _f curve [4]..... | 9 |
| Figure 2.3: Applying Manson’s approach to two-step loading: (a) HL; (b) LH [18]..... | 10 |
| Figure 2.4: Nonlinear damage curves for the Marco–Starkey theory [19]..... | 12 |
| Figure 2.5: Phenomena associated with mean loading: (a) cyclic creep; (b) mean stress relaxation [23] | 13 |
| Figure 2.6: Monotonic properties [3] | 15 |
| Figure 2.7: Coefficients of cyclic stress–strain curve: (a) axial; (b) shear | 17 |
| Figure 2.8: Stress–life curve: (a) axial curve; (b) shear curve..... | 19 |
| Figure 2.9: Strain–life curve: (a) axial curve; (b) shear curve..... | 20 |
| Figure 2.10: Total energy–life curve: (a) axial curve; (b) shear curve | 21 |
| Figure 2.11: Plastic and positive elastic energy densities [22]..... | 24 |
| Figure 2.12: Behaviour of Masing materials [22] | 26 |
| Figure 2.13: Estimation of plastic energy for non-Masing materials: (a) non-Masing material; (b) master curve [22]..... | 26 |
| Figure 3.1: Specimen geometry [mm]..... | 30 |
| Figure 3.2: Testing machine | 31 |
| Figure 3.3: Extensometers employed: (a) uniaxial; (b) biaxial | 32 |
| Figure 3.4: Monotonic stress-strain curves: (a) axial curve; (b) shear curve | 33 |
| Figure 3.5: Cyclic stress–strain curves | 35 |
| Figure 3.6: Strain–life curves: (a) axial curve; (b) shear curve | 36 |
| Figure 3.7: Total energy–life curves: (a) axial curve; (b) shear curve | 37 |
| Figure 3.8: Two-step experiments: (a) HL test; (b) LH test | 38 |
| Figure 3.9: SP7-HL hysteresis loops: [$\epsilon_{a_high} = 0.50\%$; $\epsilon_{a_low} = 0.25\%$] | 39 |
| Figure 3.10: SP19-HL hysteresis loops: [$\gamma_{a_high} = 1.00\%$; $\gamma_{a_low} = 0.50\%$]..... | 40 |
| Figure 3.11: Two-level factorial experiments at intersections of (a) uncoded values and (b) coded values..... | 41 |
| Figure 3.12: SP4 hysteresis loops: [$\epsilon_a = 0.30\%$; $\epsilon_m = 0.15\%$]..... | 43 |
| Figure 3.13: Residual plots: (a) including the ϵ_m term; (b) excluding the ϵ_m term | 45 |

| | |
|--|----|
| Figure 3.14: Predictions of fatigue life and plastic strain based on the axial empirical relations: (a) non-zero mean strain tests; (b) zero mean strain tests | 46 |
| Figure 3.15: SP33 hysteresis loops: [$\gamma_a = 0.80\%$; $\gamma_m = 0.50\%$] | 47 |
| Figure 3.16: Predictions of fatigue life and plastic strain based on the shear empirical relations: (a) non-zero mean strain tests; (b) zero mean strain tests | 48 |
| Figure 3.17: Effects of strain amplitude on fatigue life: (a) pure axial loading; (b) pure torsion loading | 49 |
| Figure 3.18: Effects of mean strain on fatigue life: (a) pure axial loading; (b) pure torsion loading .. | 50 |
| Figure 3.19: Comparison of stress levels in mean strain experiments: (a) maximum stress; (b) mean stress; (c) stress amplitude | 52 |
| Figure 3.20: Effect of mean strain on fatigue life, including zero-mean strain tests: (a) pure axial loading; (b) pure torsion loading | 53 |
| Figure 3.21: SP28 loading blocks: (a) first block; (b) subsequent blocks | 54 |
| Figure 3.22: SP57 Loading block | 54 |
| Figure 3.23: SP28 hysteresis loops | 55 |
| Figure 4.1: Rainflow counting flow chart | 58 |
| Figure 4.2: SP28 cycle counting steps | 59 |
| Figure 4.3: Applying Manson's approach to two-step loading ($S-2N_f$ curve) | 63 |
| Figure 4.4: Applying Manson's approach for two-step loading (ϵ_a-2N_f ; γ_a-2N_f ; $\Delta E_{AX}-2N_f$; $\Delta E_{SH}-2N_f$ curves) | 64 |
| Figure 4.5: Schematic representation of Marco-Starkey damage curves | 66 |
| Figure 4.6: Application of the Marco-Starkey theory for (a) HL, (b) LH, (c) VAL | 67 |
| Figure 4.7: Mean stress relaxation: (a) axial loading; (b) shear loading | 68 |
| Figure 4.8: Total energy-strain amplitude curves: (a) pure axial loading; (b) pure torsion loading .. | 69 |
| Figure 4.9: Predicted versus calculated total energy density: (a) pure axial loading; (b) pure torsion loading | 70 |
| Figure 4.10: Fatigue life predictions for CAL tests: (a) SWT; (b) FS; (c) JV | 71 |
| Figure 4.11: Miner's rule and fatigue life predictions for two-step loading: (a) SWT; (b) FS; (c) JV | 73 |
| Figure 4.12: Manson's approach and fatigue life predictions for two-step loading: (a) SWT; (b) FS; (c) JV | 74 |
| Figure 4.13: Marco-Starkey theory and fatigue life predictions for two-step loading: (a) SWT; (b) FS; (c) JV | 75 |

| | |
|---|----|
| Figure 4.14: Fatigue life predictions for mean strain tests: (a) SWT; (b) FS; (c) JV | 76 |
| Figure 4.15: Miner’s rule and fatigue life predictions for VAL: (a) SWT; (b) FS; (c) JV | 78 |
| Figure 4.16: Manson’s approach and fatigue life predictions for VAL: (a) SWT; (b) FS; (c) JV | 79 |
| Figure 4.17: Marco–Starkey theory and fatigue life predictions for VAL: (a) SWT; (b) FS; (c) JV .. | 80 |
| Figure A.1: Two-step hysteresis loops for axial loading..... | 85 |
| Figure A.2: Two-step hysteresis loops for shear loading | 86 |
| Figure A.3: Hysteresis loops for axial mean strain | 87 |
| Figure A.4: Hysteresis loops for shear mean strain..... | 89 |
| Figure A.5: Counted cycles and hysteresis loops for VAL [without repeated cycles]..... | 90 |
| Figure A.6: VAL history and hysteresis loops [with repeated cycles]; same counted cycles as for SP28 but with each cycle counted (except the largest) repeated 50 times within the block | 93 |
| Figure B.1: SP28 input file for VAL history | 95 |

List of Tables

| | |
|---|----|
| Table 3.1: Vickers hardness number of 30CrNiMo8HH steel | 30 |
| Table 3.2: Chemical composition of 30CrNiMo8HH steel [1] | 30 |
| Table 3.3: Monotonic properties | 33 |
| Table 3.4: Fully reversed CAL experimental results [2] | 34 |
| Table 3.5: Cyclic stress–strain parameters | 34 |
| Table 3.6: Strain-based fatigue parameters | 35 |
| Table 3.7: Energy-based fatigue parameters | 36 |
| Table 3.8: Axial two-step experimental results | 38 |
| Table 3.9: Torsional two-step experimental results | 40 |
| Table 3.10: Axial mean strain experimental results | 43 |
| Table 3.11: Shear mean strain experimental results | 47 |
| Table 3.12: Comparison of plastic energy in mean strain experiments | 51 |
| Table 3.13: VAL experimental results | 55 |
| Table 4.1: SP28 cycle counting results | 62 |

Chapter 1

Introduction

1.1 Background

In solid mechanics, the term “fatigue of materials” refers to the cumulative damage occurring under cyclic loading conditions. The investigation of failure due to fatigue includes consideration of a number of metallurgical aspects, such as dislocations, slip bands, and microcracks. Real-world engineering components are subjected to cyclic loading with, in most cases, variable amplitudes. Structures such as aircraft, automobiles, offshore structures, and nuclear power stations are all subject to fluctuating loading. The consequences of fatigue failure can be catastrophic: sudden failure in an aircraft engine, an automobile wheel, or a nuclear pipe could lead to significant loss of life and property. Consideration of failure due to fatigue is therefore an essential element in the design of components that are subjected to cyclic loading.

A number of approaches have been proposed and categorized with respect to determining fatigue damage: stress-based, strain-based, and energy-based. Stress-based approaches were developed as early as 1850 and are considered the simplest fatigue prediction methods. However, those approaches

were created as a means of predicting fatigue life at low loading levels and hence are appropriate only for the high-cycle fatigue (HCF) regime. For the low-cycle fatigue (LCF) regime in which plastic strain is dominant, strain-based approaches are more suitable. Both stress and strain terms are associated with energy-based and critical plane approaches, and the deformation behaviour of the material is therefore incorporated into these fatigue-damage models. Whichever approach to fatigue prediction is utilized, a number of fatigue parameters must be obtained through constant amplitude loading (CAL) experiments.

While engineering structures are subject primarily to variable amplitude loading (VAL), which can be generated from external conditions such as wind gusts, road roughness, or ocean waves, fatigue characterization experiments are nevertheless conducted under CAL. The prediction of fatigue life under VAL based on the fatigue properties obtained from the results of CAL experiments requires the consideration of several additional parameters, including the load sequence effect, the mean stress effect, and appropriate cycle counting and damage accumulation methods.

1.2 Motivation

Nickel-chromium-molybdenum 30CrNiMo8HH steel alloy provides excellent tensile and yield strength, along with a high degree of hardness, stiffness, and fatigue resistance. These properties have led to its wide use in a variety of engineering components, such as power trains, chemical plants, drive shafts, aircraft structures, and turbine blades [1]. Because the cost of failure of such components could be enormous, all expected failure modes including fatigue must be taken into consideration during the design process.

The typical type of loading for the above applications of the alloy is VAL. For fatigue prediction modeling, fully reversed CAL experiments are usually performed in order to determine fatigue properties. For VAL histories, however, the amplitudes are constantly changing, thus entailing a high possibility of non-zero mean stress. The estimation of the fatigue life of a component subjected to VAL requires that the load sequence and mean stress effects be accounted for. The majority of the available studies related to VAL account for mean stress based on the damage prediction model utilized; however, the application of the simplest damage accumulation method fails to incorporate the effect of load sequence.

The estimation of fatigue life under VAL is a topic of ongoing interest, with no universally accepted approach. The lack of knowledge about this topic with respect to 30CrNiMo8HH steel alloy and the

interest expressed by General Dynamics Land Systems (GDLS) led to a decision to attempt to shed addition light on the estimation of fatigue life under VAL relative to this material. For this research, the load sequence effect was examined using a variety of damage accumulation methods, and the mean stress effect was explored using three different fatigue life prediction models.

1.3 Plan and Objectives

The main objective of this research was to acquire insight into the estimation of the fatigue life of 30CrNiMo88HH steel under VAL. For the fatigue parameters obtained from fully reversed CAL tests to be used for fatigue life predictions under VAL, the effects of two factors must be taken into consideration: load sequence and mean stress. Monotonic and fully reversed CAL data were already available from previous studies of 30CrNiMo88HH steel [1, 2]. Several strain-controlled two-step and non-zero mean strain experiments were conducted in order to investigate the effects of load sequence and mean stress on fatigue life, respectively. The final step was to conduct axial and torsional VAL experiments for evaluation purposes. The specific objectives of this study can thus be summarized as follows:

1. Obtaining the monotonic properties from the available data and performing additional experiments as necessary.
2. Determining the strain-based and energy-based fatigue properties of 30CrNiMo88HH steel alloy based on the CAL data available.
3. Examining the effect of load sequence on fatigue life based on the two-step fatigue data through the application of several damage accumulation methods along with a cycle counting method that maintains the applied strain sequence.
4. Applying three fatigue life prediction models to the mean strain data and evaluating their predictions.
5. Developing proper fatigue model for 30CrNiMo88HH that combines the life prediction models, the damage accumulation approaches, and the cycle counting method in order to obtain optimal fatigue life correlations under VAL conditions.

1.4 Thesis Layout

This thesis is comprised of five chapters. The current chapter summarizes the importance of taking fatigue failure into account in the design process and the value of considering the approaches available in the literature. It also explains the motivation behind the research and its specific objectives. The literature review provided in Chapter 2 introduces the factors that affect fatigue life under VAL and the methods available for taking those factors into account. Monotonic, cyclic, and fatigue properties are described along with the fatigue life prediction models currently employed. Chapter 3 defines the material investigated and presents the testing procedures, followed by a discussion of the experimental results, material properties, and observations based on the tests conducted. Chapter 4 contains an analysis of the findings of the experiments performed along with suggested methods for estimating fatigue life. The last chapter includes the summary, conclusions, and recommendations for possible future research.

Chapter 2

Literature Review

2.1 Introduction

The current chapter includes an overview of variable amplitude loading (VAL) and the factors that require consideration with respect to the estimation of fatigue life. Section 2.2 discusses the elements included in VAL histories, including cycle counting, damage accumulation, and the effects of mean stress. Monotonic, cyclic, and fatigue properties are then presented in section 2.3. Section 2.4 introduces the three fatigue life prediction models employed in this study: Smith–Watson–Topper (SWT), Fatemi–Socie (FS), and Jahed–Varvani (JV). The chapter concludes with an analysis of the methods used for estimating plastic energy density.

2.2 VAL Elements

Because the fatigue properties of engineering materials are determined through experiments conducted under constant amplitude loading (CAL), additional factors must be taken into account when the fatigue life is estimated for a component subjected to VAL conditions. VAL blocks are comprised of varied loading amplitudes in a specific order with, in most cases, a non-zero mean stress level. The estimation of fatigue life under such loading conditions must therefore include consideration of the effects on fatigue life of the load sequence and the mean stress. Another consideration associated with the prediction of fatigue life under VAL conditions is the development of a method of extracting CAL cycles from the VAL histories, a method known as cycle counting.

2.2.1 Cycle Counting Methods

Although most service loading histories are VAL in nature, fatigue properties are obtained through sets of experiments under CAL conditions. For these fatigue properties to be used for the estimation of fatigue lives under actual service loading, the VAL histories must be decomposed into CAL cycles by means of a cycle counting method. With the use of a damage accumulation method, the overall damage caused by the VAL block can then be ascertained based on the sum of the individual amounts representing the damage caused by each cycle counted. The damage accumulation methods are explained in detail in the subsection 2.2.2. Several approaches have been proposed for counting cycles, some of which are discussed below.

Early literature reports of cycle counting approaches include methods such as level-crossing counting, peak counting, and simple range counting. Examples of the application of these methods are available in [3-5]. The method most commonly used, however, is the rainflow counting method, first proposed by Matsuishi and Endo in 1968 [6]. This method is based on the decomposition of the VAL history into peaks and valleys, followed by the counting of the cycles based on the ranges of the reversals. A variety of procedures and algorithms associated with the rainflow counting method are reported in the literature [7-10]. However, the procedure most frequently used is the one described in ASTM Standard E1049-85 [10], which is known as the simplified rainflow counting for repeating histories and is illustrated in Figure 2.1.

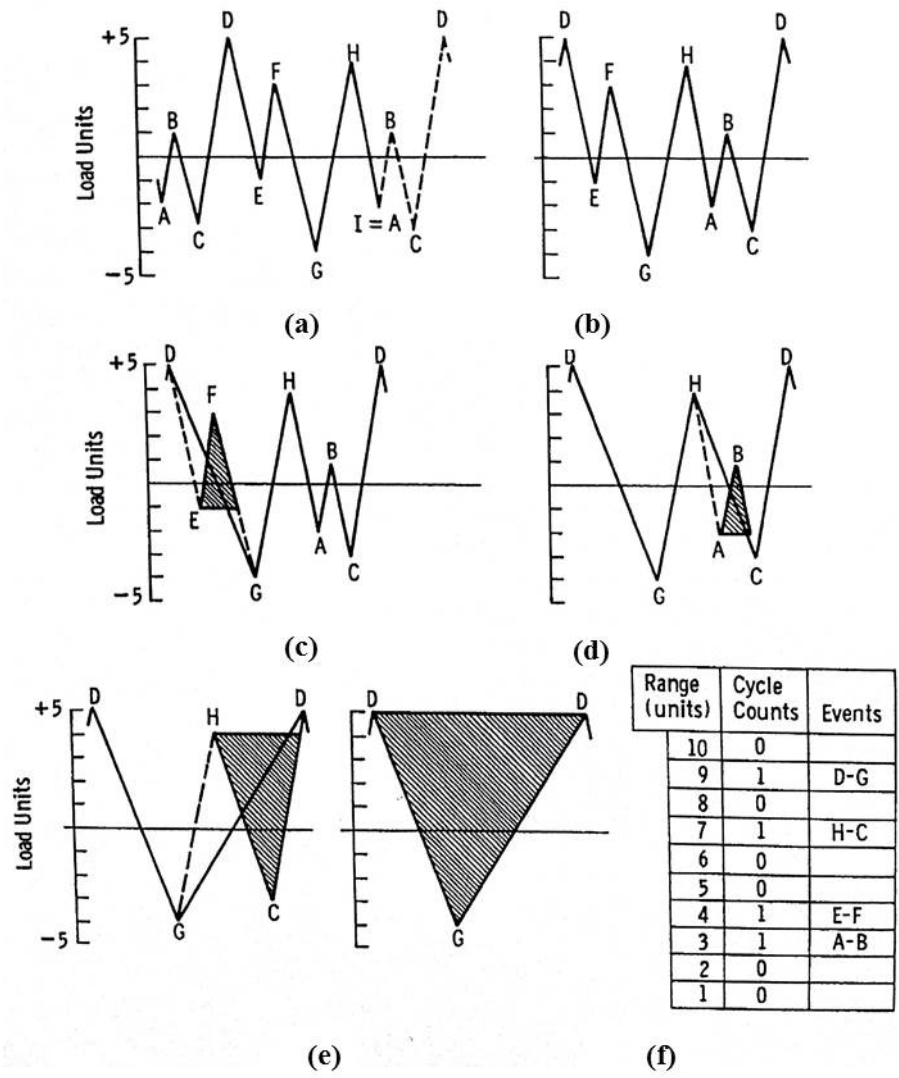


Figure 2.1: Simplified rainflow counting method [10]: (a) original history; (b) rearranged history; (c), (d), (e) cycle counting and removal of cycles counted; (f) counting results

The counting steps for the example shown in the figure can be summarized as follows:

1. Rearrange the original VAL history (Figure 2.1 (a)) to start with the highest peak (or lowest valley) and move the preceding reversals to the end of the history (Figure 2.1 (b)).
2. Start counting from the first point and count the cycle if the range of the reversal is equal to or greater than the previous range (Figure 2.1 (c)).
3. After a cycle has been counted, remove the preceding reversal (e.g., EF in Figure 2.1 (c)) and start the counting again.

4. The cycle counting is completed after the last (largest) cycle (DGD in Figure 2.1 (e)) has been counted.

Although the above counting procedure is recommended by ASTM for repeated VAL blocks, the rearrangement of the history could change the effect of the load sequence on fatigue life, especially for longer VAL blocks or for blocks that contain several repeated cycles.

Another rainflow counting algorithm for longer VAL blocks was proposed by Glinka and Kam [11]. Their method involves no rearrangement of the histories or prior knowledge of the complete VAL history. Because load sequence was one of the factors under investigation in the research for this thesis, an approach similar to that of the Glinka–Kam algorithm was utilized for counting the cycles, as discussed in detail in section 4.2.

2.2.2 Damage Accumulation and Load Sequence Effect

Each counted CAL cycle obtained based on the methods described in the previous section causes individual damage that is dependent on its amplitude and mean stress levels. The overall damage caused by the VAL block can then be obtained from the sum of those individual damage amounts. The term damage accumulation refers to the method by which the individual damage amounts are summed. Numerous approaches to damage accumulation have been reported in the literature [5, 12], some of which require empirically determined constants and are quite complicated. The approaches discussed in the following subsections are among those that can be implemented simply: the linear damage rule, Manson’s approach, and the Marco–Starkey theory.

2.2.2.1 Linear Damage Rule (Miner’s Rule)

The linear damage rule, also known as Miner’s rule, was proposed initially by Palmgren in 1924 [13] and later by Miner in 1945 [14]. It states that the damage fraction caused by n_i cycles at applied stress amplitude σ_i (or ε_i in strain-controlled tests) is defined as

$$D_i = \frac{n_i}{N_{f_i}} \quad (2.1)$$

where n_i = number of applied cycles at the i^{th} loading level
 N_{f_i} = fatigue life until failure at the applied loading level

Miner's rule assumes that failure occurs when the summation of the damage fractions at different loading levels equals one ($\sum_i D_i = 1$). For the two-step loading test shown in Figure 2.2, with a known number of applied cycles at the first step (n_1), the number of cycles at the second step (n_2) can be estimated based on Miner's rule as

$$n_2 = \left(1 - \frac{n_1}{N_{f1}}\right) N_{f2} \quad (2.2)$$

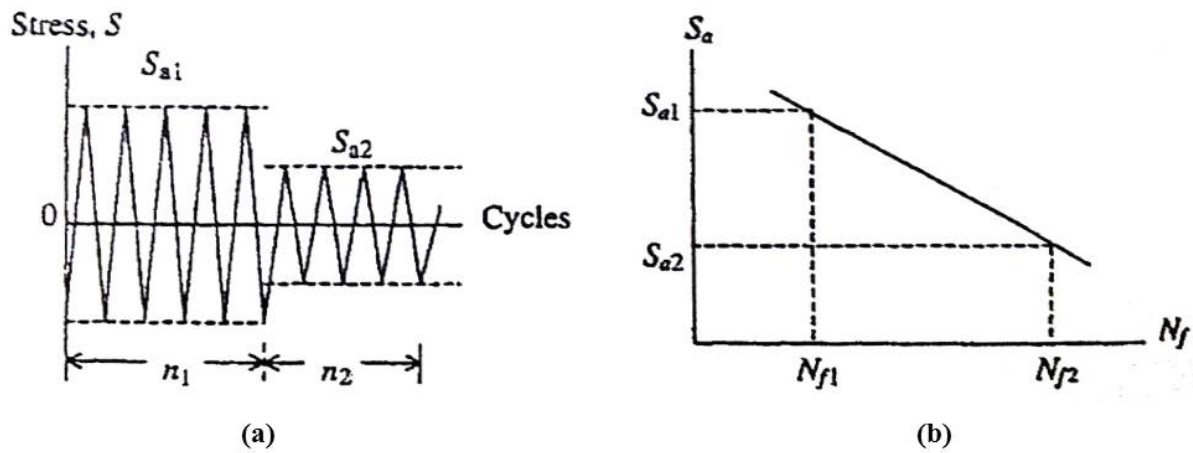


Figure 2.2: Two-step loading: (a) CAL stress blocks; (b) S– N_f curve [4]

Although it is still widely used as a damage accumulation method, the linear damage rule has associated deficiencies. First, it fails to account for the effect of load sequence on fatigue life. For example, it predicts identical fatigue life for both two-step high-low (HL) and low-high (LH) tests, which is inconsistent with experimental observations [3, 12, 15]. The second drawback of the linear damage rule is the assumption of a constant rate of damage accumulation regardless of past histories. Experiments show that, for the HL tests, the sum of the damage fractions is less than one, but for the LH tests, it is greater than one [5, 12, 15]. Miner's rule also ignores the reduction in the endurance limit caused by the inclusion of some cycles above the endurance limit of the virgin material [16].

2.2.2.2 Manson's Approach

To overcome some of the shortcomings of Miner's rule, Manson et al. [17, 18] proposed a cumulative damage approach based on the modification of the stress–life line (or the fatigue life curve in general). They suggested rotating the S–N line about a convergence point, which is considered to be a material constant. Figure 2.3 shows schematically the application of Manson's approach for two-step loading.

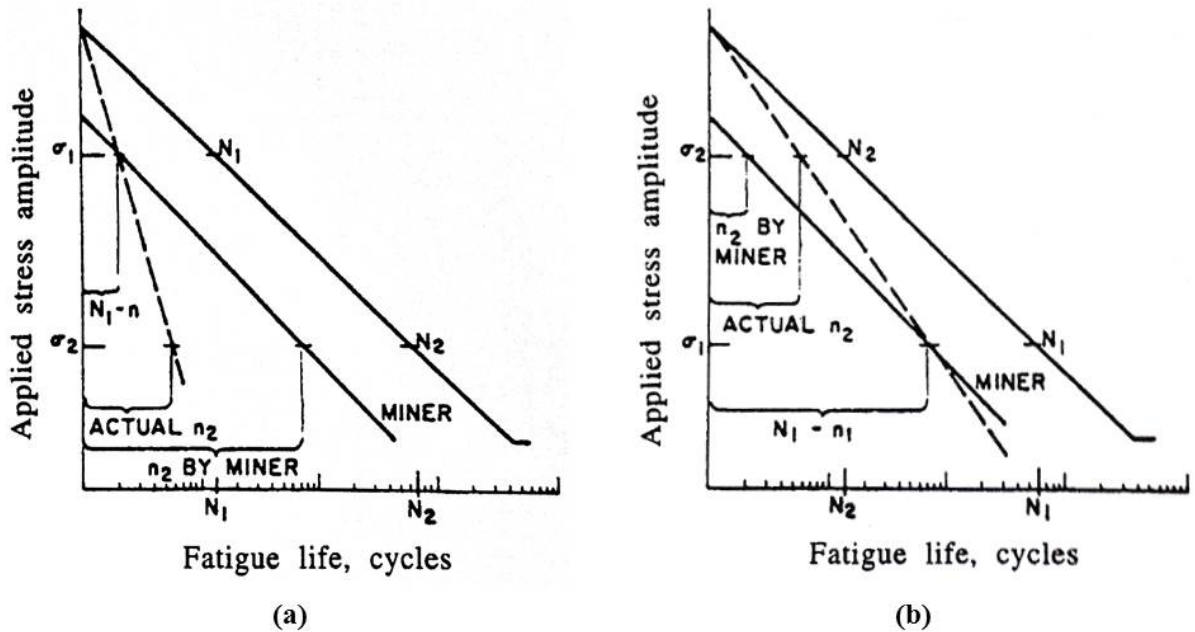


Figure 2.3: Applying Manson's approach to two-step loading: (a) HL; (b) LH [18]

As can be seen from the figure, the new S–N line (dashed line) can be obtained based on the two points it passes through. The first point, regarded as a material constant, is located on the original line and is suggested to fall within the range of 10^2 – 10^3 cycles. The second point is obtained as

$$N(x) = N_1 - n_1 \quad (2.3)$$

where N_1 = fatigue life until failure at the 1st stress level
 n_1 = number of cycles applied at the 1st step

In two-step loading experiments, the revised S–N line includes consideration of the effect of the load sequence on fatigue life because it predicts lower fatigue life for the HL test than for the LH test. Manson’s approach also accounts for the reduction in the endurance limit through the extension of the modified S–N line to meet the fatigue life at the knee of the original fatigue curve. However, experimental results show that the reduction in the fatigue limit is not as great as suggested with this approach [16]. A drawback of Manson’s approach is the empirically determined constant that is required for the convergence point. For this research, this deficiency was overcome by relating the convergence point to the second point, as discussed in section 4.3.

2.2.2.3 Marco–Starkey Theory

Another attempt to address the shortcomings of Miner’s rule was the first nonlinear damage accumulation theory, which was proposed by Marco and Starkey [19]. This theory is based on experimental observations that show that the sum of the damage fractions (n_i/N_i) is less than one for HL tests but greater than one for LH tests. The method can be expressed as the following power relation:

$$D = \left(\frac{n_i}{N_i}\right)^{\chi_i} \quad (2.4)$$

where χ_i is a value related to the i^{th} loading level obtained based on empirical relations.

Multiple damage curves result from Equation (2.4) at different values for the exponents χ_i , as shown in Figure 2.4.

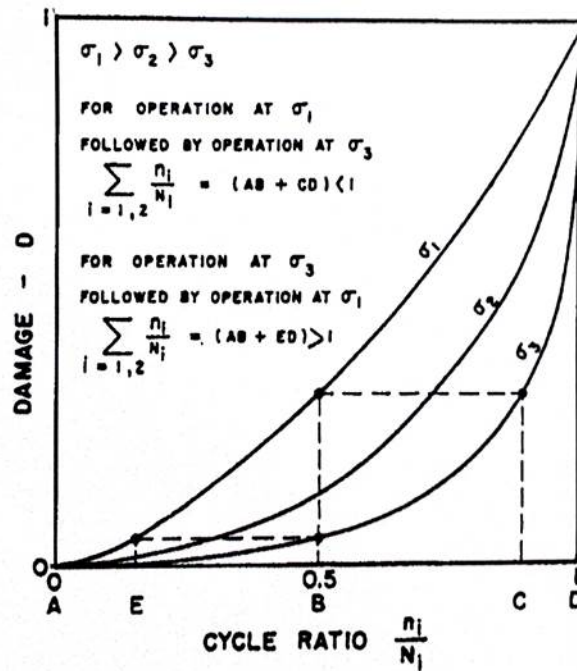


Figure 2.4: Nonlinear damage curves for the Marco–Starkey theory [19]

This figure shows that the critical value at which failure is expected to occur is dependent on the sequence of the applied load. Based on the Marco–Starkey theory, for the HL test ($\sigma_1\sigma_3$), the critical value predicted is expected to be less than one, whereas for the LH test ($\sigma_3\sigma_1$), the critical value is expected to be greater than one, results that agree with experimental observations. However, performing the additional experiments required in order to find the values for the exponents x_i can be considered a disadvantage of this approach. As a means of avoiding extra experiments, the modification incorporated for this research was to relate the values for the exponents to the predicted values of the fatigue lives rather than to those of the applied load. Section 4.3 provides details.

2.2.3 Effect of the Mean Stress

Mean stress, which is the mean value of the maximum and minimum stresses, is an important factor that affects fatigue life during both load-controlled and strain-controlled tests, and it is very likely to be found in VAL histories. For axial loading, it is believed that tensile mean stress causes greater damage, which consequently decreases fatigue life, while compressive mean stress increases it [3, 4, 20, 21]. In the high-cycle fatigue (HCF) regime, the effect of mean stress can be examined through either load-controlled or strain-controlled tests because the response of the material is primarily

elastic. However, in the low-cycle fatigue (LCF) regime during strain-controlled tests, the mean stress effect becomes noticeable only if half-life mean stress exists [20, 22]. Depending on the type of mean loading, two distinct phenomena can be observed. For load-controlled tests with positive mean stress, cyclic creep (or ratcheting strain) is expected, whereas in strain-controlled tests with positive mean strain, mean stress relaxation is more likely [4, 23]. Figure 2.5 shows these two phenomena schematically.

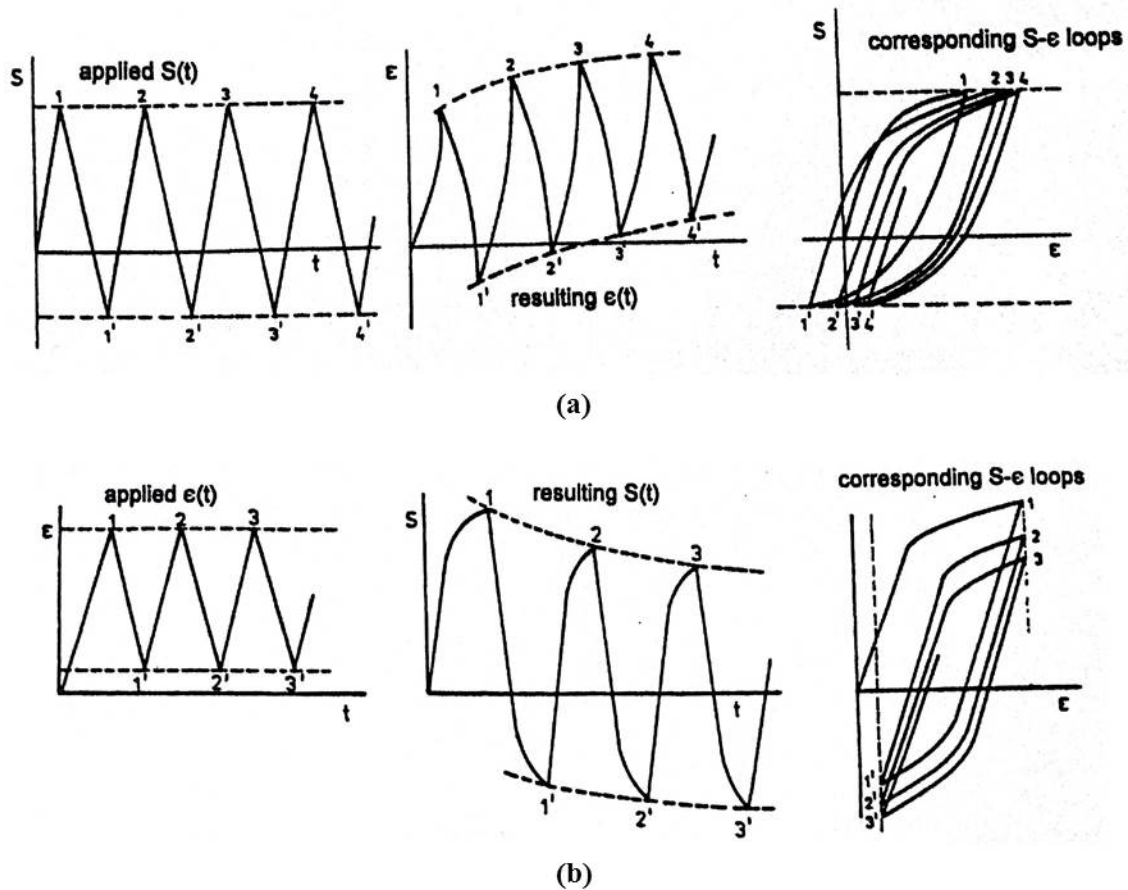


Figure 2.5: Phenomena associated with mean loading:
 (a) cyclic creep; (b) mean stress relaxation [23]

Mean stress relaxation and cyclic creep affect fatigue life in opposite ways. While mean stress relaxation eliminates the effect of the applied mean strain, cyclic creep causes additional damage to the material, which results in a reduction in fatigue life [22]. In stress-life approaches, the modified Goodman diagram [4] is commonly used as a means of incorporating the effects of mean stress in the HCF regime [24].

During strain-controlled fatigue tests, mean stress relaxation (Figure 2.5 (b)) is a common phenomenon that indicates a decrease in the mean stress over subsequent cycles. The rate of mean stress relaxation becomes significant in the LCF regime, which negates the effect of the applied mean strain [3, 25]. A number of methods have been proposed in order to account for the effect of mean stress on fatigue life during strain-controlled tests. Assuming that the effect of mean strain on fatigue life is noticeable only in the HCF regime, Morrow [26] suggested subtracting the mean stress, σ_m , from the elastic component of the Coffin–Manson equation, as presented in the Equation (2.5).

$$\varepsilon_a = \frac{\sigma_f' - \sigma_m}{E} (2N_f)^b + \varepsilon_f' (2N_f)^c \quad (2.5)$$

where σ_f' = fatigue strength coefficient
 σ_m = mean stress
 b = fatigue strength exponent
 ε_f' = fatigue ductility coefficient
 c = fatigue ductility exponent
 $2N_f$ = number of reversals to failure

Another suggestion for addressing the mean stress effect is to subtract it from both the elastic and the plastic terms, as proposed by Manson and Halford [27]:

$$\varepsilon_a = \frac{\sigma_f' - \sigma_m}{E} (2N_f)^b + \varepsilon_f' \left(\frac{\sigma_f' - \sigma_m}{\sigma_f'} \right)^{c/b} (2N_f)^c \quad (2.6)$$

For the three damage models employed in the research for this thesis, the mean stress effect was taken into account in different ways. In the SWT and FS models, the correction for mean stress is determined based on the maximum stress on the critical planes, whereas in the JV model, the positive elastic energy is the parameter that covers the effect of mean stress on fatigue life, as discussed in section 2.4.

2.3 Monotonic, Cyclic, and Fatigue Properties

The properties of any material are typically determined through sets of experiments conducted in pre-specified conditions. Monotonic properties are established through the application of a gradually increasing load/displacement until the point of failure, whereas cyclic and fatigue properties are ascertained through sets of CAL experiments conducted with differing applied load/strain levels. The following subsections provide a brief description of the testing procedures and the determination of the properties.

2.3.1 Monotonic Properties

For monotonic tension and compression properties, tests involve controlling the stress rate, strain rate, or crosshead speed, whereas for monotonic torsion properties, tests typically entail regulating the torque and measuring the angle of twist. Additional details about monotonic axial and torsional experiments are available in ASTM standards [28] and [29], respectively. The yield strength revealed by monotonic tests is commonly defined based on the 0.2 % strain offset. Figure 2.6 shows a schematic of the engineering and the true stress–strain curves.

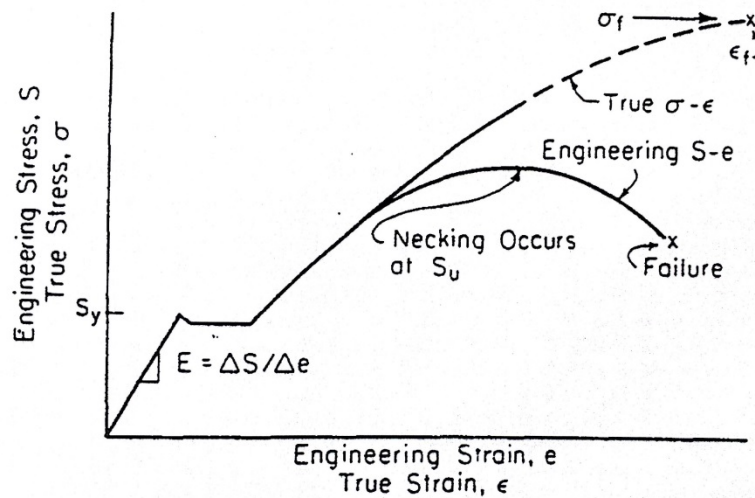


Figure 2.6: Monotonic properties [3]

The engineering axial strain is calculated from the applied/measured displacement as

$$\varepsilon = \frac{\Delta l}{l_0} \quad (2.7)$$

where Δl = applied/measured displacement
 l_0 = extensometer gage length

The engineering shear strain is calculated from the angle of twist as

$$\gamma = \phi \times \frac{\pi}{180} \quad (2.8)$$

where ϕ is the applied/measured angle of twist in degrees.

For solid-bar specimens, the axial stress can be calculated as

$$\sigma = \frac{4F}{\pi D^2} \quad (2.9)$$

where F = applied/measured axial load
 D = diameter of the solid-bar specimen

The engineering axial and shear stresses for tubular specimens can be calculated as

$$\sigma = \frac{4F}{\pi(D_o^2 - D_i^2)} \quad (2.10)$$
$$\tau = \frac{16T}{\pi(D_o - D_i)(D_o + D_i)^2}$$

where D_o = outer diameter of the tubular specimen
 D_i = inner diameter of the tubular specimen
 T = applied/measured torque

2.3.2 Cyclic Properties

Cyclic properties are determined through strain-controlled CAL experiments. The cyclic stress–strain curve is commonly represented by the Ramberg–Osgood equation, which can be written for axial loading in the following form:

$$\varepsilon_a = \varepsilon_a^e + \varepsilon_a^p = \frac{\sigma_a}{E} + \left(\frac{\sigma_a}{K'}\right)^{\frac{1}{n'}} \quad (2.11)$$

where

- K' = strength coefficient
- n' = strain hardening exponent
- E = elastic modulus
- ε_a = strain amplitude
- σ_a = stress amplitude
- ε_a^e = elastic strain amplitude
- ε_a^p = plastic strain amplitude

The Ramberg–Osgood coefficients (K' & n') can be calculated by plotting the true plastic strain amplitudes against the true stress amplitudes in a log–log scale and fitting a line through the data points. The stress intercept at $\varepsilon_a^p=1$ represents the strength coefficient, and the slope of the line represents the strain hardening exponent, as shown in Figure 2.7.

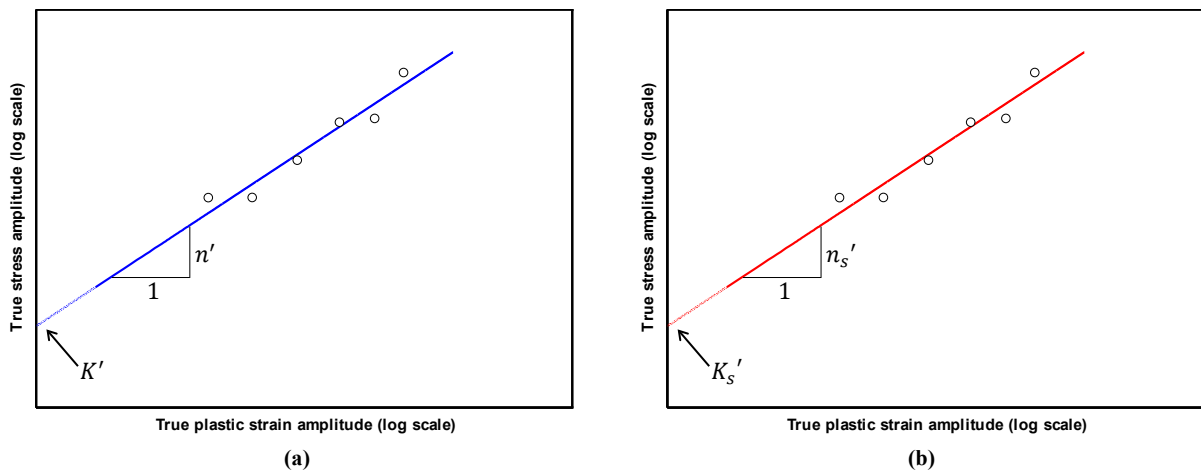


Figure 2.7: Coefficients of cyclic stress–strain curve: (a) axial; (b) shear

The plastic strain amplitudes can be calculated as

$$\varepsilon_a^p = \varepsilon_a - \varepsilon_a^e = \varepsilon_a - \frac{\sigma_a}{E} \quad (2.12)$$

For the calculation of pure torsion loading, Equations (2.11) and (2.12) are applied after the axial parameters have been replaced with the shear parameters.

2.3.3 Fatigue Properties

Depending on whether the damage fatigue model employed is stress-based, strain-based, or energy-based, a number of fatigue properties can be calculated. For stress-based models, the axial stress–life curve can be represented in the form

$$\varepsilon_a = \frac{\sigma_f'}{E} (2N_f)^b \quad (2.13)$$

where σ_f' = fatigue strength coefficient
 b = fatigue strength exponent
 $2N_f$ = number of reversals to failure

Stress-based fatigue properties (σ_f' & b) can be determined by plotting the stress amplitudes against the fatigue life reversals in a log–log scale and then fitting a line through the data points. The fatigue strength coefficient and the fatigue strength exponent are derived from the stress amplitude intercept at $2N_f = 1$ and from the slope of the line, respectively. For pure torsion loading, Equation (2.13) is applied after the replacement of the axial fatigue parameters with the shear parameters. The stress-based fatigue properties are shown schematically in Figure 2.8.

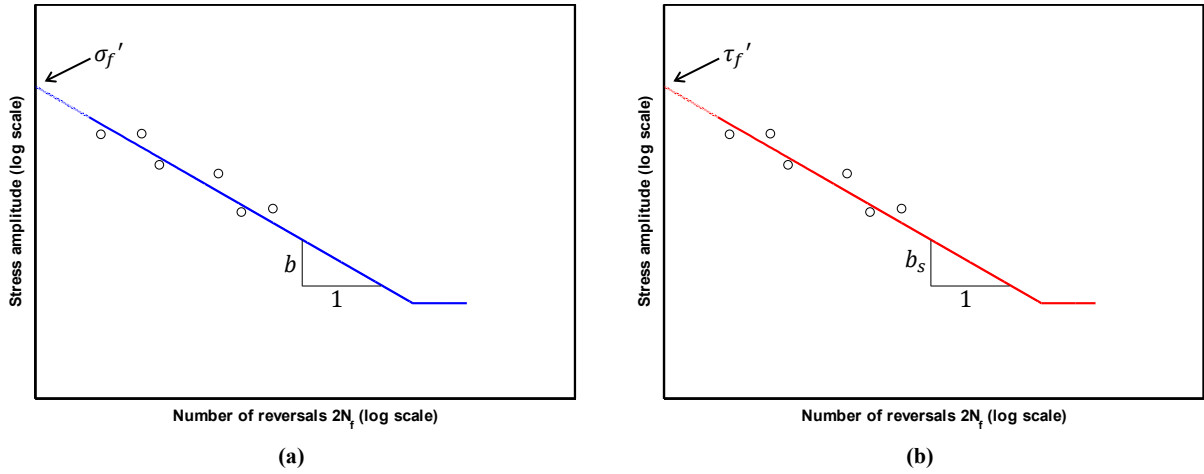


Figure 2.8: Stress–life curve: (a) axial curve; (b) shear curve

In strain-based approaches, the strain–life curve, also known as the Coffin–Manson curve, is used for predicting fatigue life. The Coffin–Manson fatigue life equation for axial loading can be written as

$$\varepsilon_a = \frac{\sigma_f'}{E} (2N_f)^b + \varepsilon_f' (2N_f)^c \quad (2.14)$$

where

- σ_f' = fatigue strength coefficient
- b = fatigue strength exponent
- ε_f' = fatigue ductility coefficient
- c = fatigue ductility exponent
- $2N_f$ = number of reversals to failure

Strain-based fatigue parameters (σ_f' , b , ε_f' & c) can be obtained by plotting the elastic and plastic strain amplitudes against the fatigue life reversals in a log–log scale and then fitting a straight line through each set of points. The intercepts of the elastic and plastic strain lines at $2N_f = 1$ represent σ_f'/E and ε_f' , respectively. The fatigue strength and fatigue ductility exponents are calculated from the slopes of the elastic and plastic strain lines, respectively. For pure torsion loading, Equation (2.14) is applied after the axial fatigue parameters have been replaced with the shear parameters. Figure 2.9 shows a schematic of the strain–life curve.

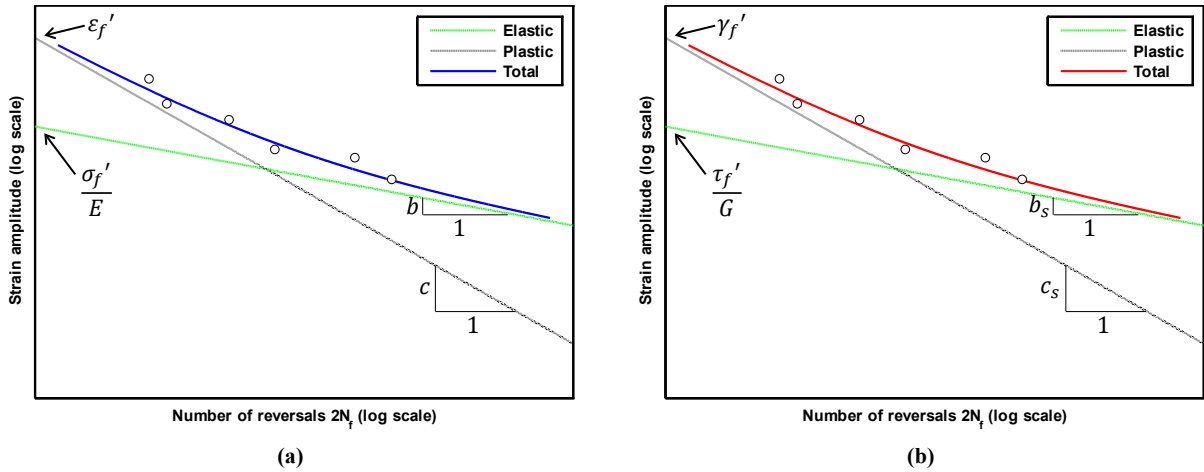


Figure 2.9: Strain–life curve: (a) axial curve; (b) shear curve

The energy-based fatigue life prediction model employed is based on the total energy density ($\Delta E_t = \Delta E_p + \Delta E_e^+$) as the damage-controlling factor. As in the Coffin–Manson equation, the total energy–life curve for axial loading can be written as

$$\Delta E_A = E'_e (2N_A)^B + E'_f (2N_A)^C \quad (2.15)$$

where ΔE_A = total strain energy density
 E'_e = fatigue strength coefficient
 B = fatigue strength exponent
 E'_f = fatigue toughness
 C = fatigue toughness exponent
 $2N_A$ = number of reversals to failure

Energy-based fatigue parameters (E'_e , B , E'_f & C) are calculated in the same manner as the Coffin–Manson parameters. The fatigue strength coefficient is calculated from the intercept of the positive elastic energy line, and the fatigue strength toughness is derived from the intercept of the plastic energy line at the first reversal, respectively. The slopes of the positive elastic and plastic energy lines represent the fatigue strength and the fatigue toughness exponents, respectively. For pure torsion loading, Equation (2.15) is applied after the replacement of the axial fatigue parameters with the shear parameters. Figure 2.10 shows a schematic of the energy-based fatigue properties.

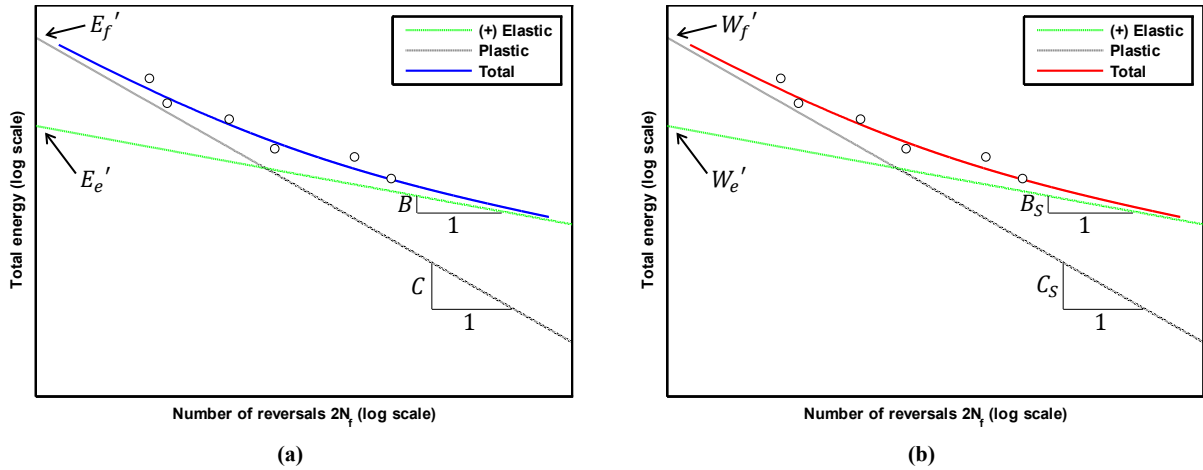


Figure 2.10: Total energy–life curve: (a) axial curve; (b) shear curve

2.4 Fatigue Life Prediction Models

Several methods have been developed and categorized for determining fatigue failure, including stress-based, strain-based, and energy-based approaches. Stress-based approaches, which are the simplest and were the earliest developed, have been established for low loading levels (HCF regime). One of the stress-based approaches commonly used is the maximum equivalent stress parameter [4], in which the von Mises equivalent stress is the damage-controlling factor. The von Mises equivalent stress for tension–torsion loading can be given as [3]

$$\sigma_{eq} = \sqrt{\sigma^2 + 3\tau^2} \quad (2.16)$$

where σ = axial stress component
 τ = shear stress component

For higher applied loads (LCF regime), such as stresses localized at notches, the relation between stress and strain is no longer linear, an observation that has led to the development of strain-based fatigue life prediction approaches, in which the applied strain is split into elastic and plastic components (Equation (2.12)). An example of a strain-based approach is the maximum equivalent strain parameter [4] in which the von Mises equivalent strain is the factor that controls fatigue damage. The von Mises equivalent strain for tension–torsion loading may be expressed as [3]

$$\varepsilon_{eq} = \sqrt{\varepsilon^2 + \frac{\gamma^2}{3}} \quad (2.17)$$

where ε = axial strain component
 γ = shear strain component

An explanation of fatigue life prediction based on the previously mentioned maximum equivalent stress and maximum equivalent strain parameters for 30CrNiMo8HH steel under uniaxial and multiaxial loading is available in [2].

A third generation of fatigue life prediction models combines stress and strain components so that the material deformation behaviour is incorporated into the damage models. These fatigue damage models can be classified as energy-based models, including the subset known as critical plane approaches. Fatigue life predictions provided by energy-based models are generally more acceptable than those resulting from stress-based and strain-based models, especially for multiaxial loading conditions [4]. In the work conducted for this thesis, three energy-based models were employed for estimating fatigue life under VAL conditions. A brief description of each model follows.

2.4.1 Smith–Watson–Topper Model

The Smith–Watson–Topper (SWT) model [30], also known as the SWT parameter, is a critical plane fatigue model that includes consideration of the plane of maximum axial strain as the failure plane. This model was first proposed as a means of incorporating the effects of mean stress through the maximum normal stress on the critical plane, but it can also be used for predicting fatigue life under multiaxial loading [31]. The SWT parameter can be written as

$$\sigma_{n,max} \frac{\Delta\varepsilon_1}{2} = \frac{\sigma_f'^2}{E} (2N_f)^{2b} + \sigma_f' \varepsilon_f' (2N_f)^{b+c} \quad (2.18)$$

where $\sigma_{n,max}$ = maximum normal stress on the maximum axial strain plane
 $\Delta\varepsilon_1$ = maximum principal strain range
 σ_f' = axial fatigue strength coefficient
 b = axial fatigue strength exponent
 ε_f' = axial fatigue ductility coefficient
 c = axial fatigue ductility exponent
 $2N_f$ = number of reversals to failure

2.4.2 Fatemi–Socie Model

The second fatigue life prediction model considered in this research is the critical plane model proposed by Fatemi and Socie (FS) [32], which is a modified version of the previously proposed Brown–Miller model [33]. Fatemi and Socie suggested that the critical plane is the plane at which the shear strain and normal stress are both at their maximum values. The FS model can be expressed as

$$\gamma_{max} \left(1 + k \frac{\sigma_{n,max}}{\sigma_y} \right) = \frac{\tau'_f}{G} (2N_f)^{b_s} + \gamma'_f (2N_f)^{c_s} \quad (2.19)$$

where $\sigma_{n,max}$ = maximum normal stress on the maximum shear strain plane

γ_{max} = maximum shear strain

σ_y = yield strength

k = constant

τ'_f = shear fatigue strength coefficient

b_s = shear fatigue strength exponent

γ'_f = shear fatigue ductility coefficient

c_s = shear fatigue ductility exponent

$2N_f$ = number of reversals to failure

The constant k can be obtained by fitting the uniaxial data against the pure torsion data, and it can also be estimated from the formula in [34] as

$$k = \left[\frac{\frac{\tau'_f}{G} (2N_f)^{b_s} + \gamma'_f (2N_f)^{c_s}}{1.3 \frac{\sigma'_f}{E} (2N_f)^b + 1.5 \varepsilon'_f (2N_f)^c} - 1 \right] \frac{K' (0.002)^{n'}}{\sigma'_f (2N_f)^b} \quad (2.20)$$

where K' and n' are the Ramberg–Osgood coefficients discussed in subsection 2.3.2.

2.4.3 Jahed–Varvani Model

Unlike the fatigue life equations for SWT and FS models, the expression of fatigue life proposed by Jahed and Varvani (JV) [35] includes both axial and shear energy-based fatigue properties. The damage controlling factor in the JV model is the total energy density, which includes both plastic and positive elastic energy densities, as shown in Figure 2.11. This definition of total energy density as a damage parameter was first proposed by Golos and Ellyin [36, 37].

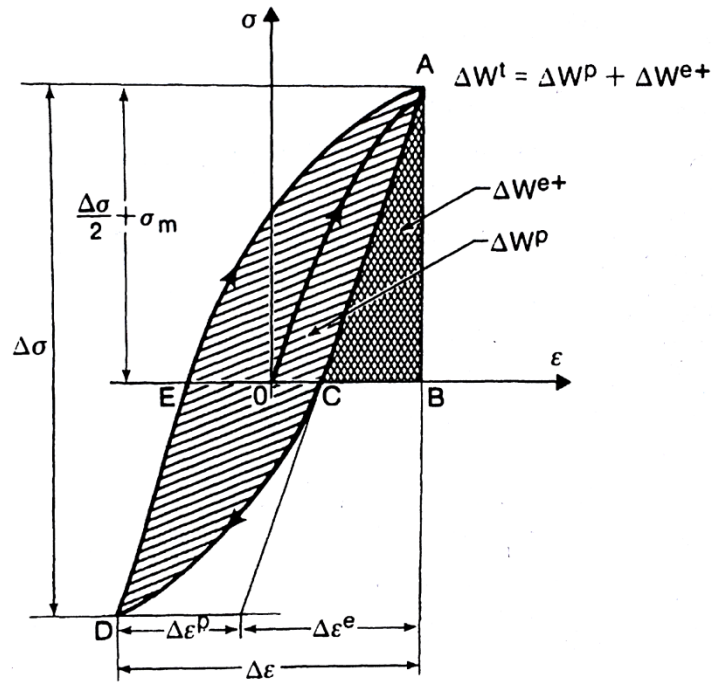


Figure 2.11: Plastic and positive elastic energy densities [22]

The JV fatigue life equation can be expressed as

$$N_f = \frac{\Delta E_A}{\Delta E} N_A + \frac{\Delta E_T}{\Delta E} N_T \quad (2.21)$$

where

- ΔE_A = total energy density due to purely axial loading
- ΔE_T = total energy density due to purely torsion loading
- $\Delta E = \Delta E_A + \Delta E_T$
- N_A = fatigue life obtained under purely axial loading
- N_T = fatigue life obtained under purely torsion loading

The fatigue life values (N_A & N_T) are obtained from the total energy–fatigue life curves discussed in subsection (2.3.3):

$$\begin{aligned}\Delta E_A &= E'_e(2N_A)^B + E'_f(2N_A)^C \\ \Delta E_T &= W'_e(2N_T)^{B_s} + W'_f(2N_T)^{C_s}\end{aligned}\tag{2.22}$$

where

- E'_e = axial fatigue strength coefficient
- B = axial fatigue strength exponent
- E'_f = axial fatigue toughness
- C = axial fatigue toughness exponent
- W'_e = shear fatigue strength coefficient
- B_s = shear fatigue strength exponent
- W'_f = shear fatigue toughness
- C_s = shear fatigue toughness exponent

Plastic energy, also known as cyclic energy, can be calculated based on the hysteresis loop area using trapezoidal integration, whereas positive elastic energy is calculated as

$$\Delta E_e^+ = \frac{\sigma_{max}^2}{2E}\tag{2.23}$$

where σ_{max} is the maximum hysteresis loop stress.

2.4.3.1 Plastic Energy Estimation

Depending on the behaviour of the material, a variety of approaches have been proposed for the estimation of plastic energy density. For Masing materials [38] (Figure 2.12), in which hysteresis loops can be approximated by doubling the cyclic stress–strain curve, the plastic energy density can be computed as [39]

$$\Delta W^p = \left(\frac{1 - n'}{1 + n'} \right) \Delta\sigma \Delta\varepsilon^p\tag{2.24}$$

where

- $\Delta\sigma$ = axial stress range
- $\Delta\varepsilon^p$ = axial plastic strain range
- n' = strain hardening exponent (subsection 2.3.2)

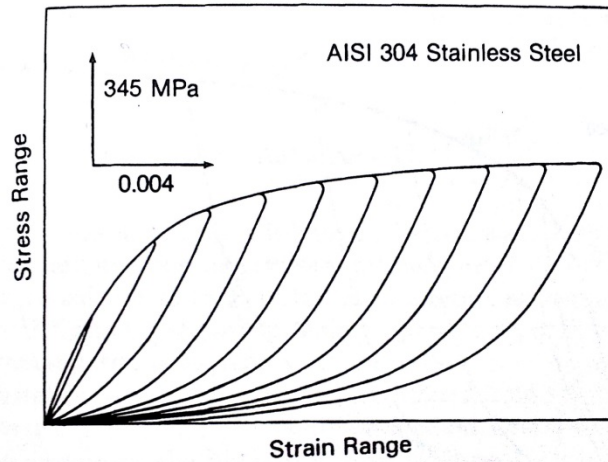
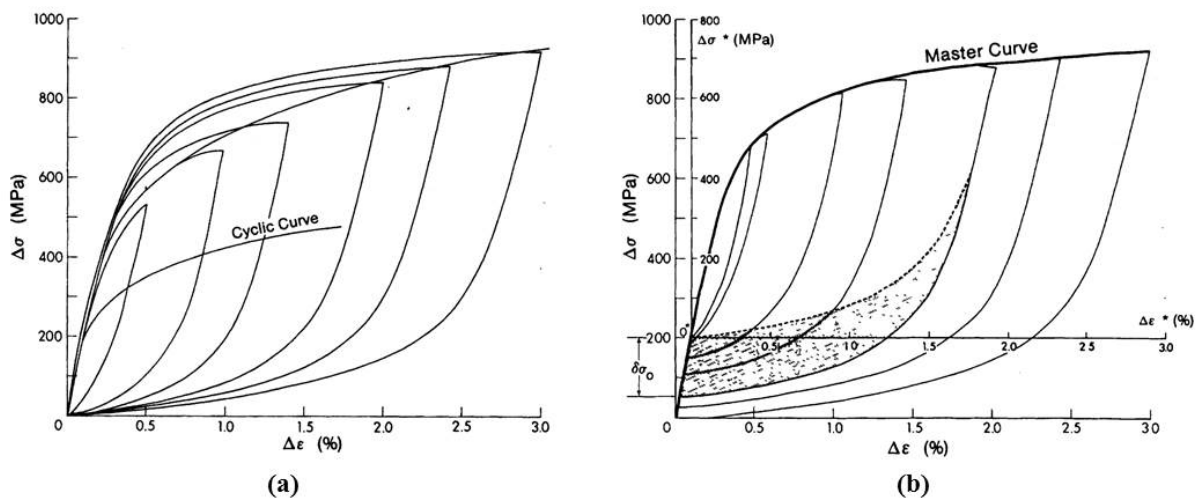


Figure 2.12: Behaviour of Masing materials [22]

For non-Masing materials (Figure 2.13 (a)), Lefebvre and Ellyin [40] proposed a method for estimating plastic energy density. Their approach is based on a new cyclic stress–strain curve (master curve) that contains all of the loading branches of the hysteresis loops at different strain amplitudes (Figure 2.13 (b)). This master curve can be obtained by changing the location of the hysteresis loops so that all the linear portions and the upper branches are matched. A new coordinate system is then established, with its origin located at the lowest point of the smallest hysteresis loop, as shown in Figure 2.13 (b).



**Figure 2.13: Estimation of plastic energy for non-Masing materials:
(a) non-Masing material; (b) master curve [22]**

After the new coordinate system has been established, new cyclic stress–strain properties for the master curve are calculated based on its origin. Hence, the master curve equation, which is a doubled Ramberg–Osgood equation, can be written as

$$\Delta\varepsilon^* = \frac{\Delta\sigma^*}{E} + 2 \left(\frac{\Delta\sigma^*}{2K^*} \right)^{\frac{1}{n^*}} \quad (2.25)$$

where all asterisk superscripts indicate that those values are related to the new coordinate system. K^* and n^* are calculated as explained in subsection 2.3.2.

The Lefebvre–Ellyin method for estimating plastic energy density can then be expressed as

$$\Delta W^p = \left(\frac{1 - n^*}{1 + n^*} \right) \Delta\sigma \Delta\varepsilon^p + \frac{2n^*}{1 + n^*} \delta\sigma_0 \Delta\varepsilon^p \quad (2.26)$$

where

- $\delta\sigma_0$ = increase in the proportional limit (Figure 2.13 (b))
- n^* = strain hardening exponent (new coordinate system)
- $\Delta\sigma$ = axial stress range (original coordinate system)
- $\Delta\varepsilon^p$ = axial plastic strain range (original coordinate system)

The increase in the proportional limit $\delta\sigma_0$ is dependent on the applied strain amplitude and can be calculated as

$$\delta\sigma_0 = \Delta\sigma - \Delta\sigma^* = \Delta\sigma - 2K^* \left(\frac{\Delta\varepsilon^p}{2} \right)^{n^*} \quad (2.27)$$

Another method of estimating plastic energy is through the use of a cyclic plasticity model for approximating the elasto–plastic response of the material. Noban et al. [2] employed the two plasticity models developed by Mroz [41] and Chaboche [42] in order to model the cyclic behaviour of 30CrNiMo8HH steel, and they concluded that the estimation produced by the Chaboche model is more appropriate under multiaxial loading conditions. For this research, another method of estimating total energy density under uniaxial loading is discussed in section 4.4.

2.5 Previous Studies of Variable Amplitude Loading

A number of studies have been conducted with respect to the prediction of fatigue life under VAL. Bannantine and Socie [43, 44] proposed a method for the estimation of fatigue life under multiaxial VAL. Their approach was based on the application of the SWT and FS critical plane models, and they applied the linear damage rule for damage accumulation. Depending on the fatigue model employed, the rainflow counting method was used to determine either the axial or shear cycles. Łagoda and Macha [45] examined the fatigue life of 30CrNiMo8 steel under bending-torsion VAL. They employed the rainflow counting method and Miner's rule and concluded that the most satisfactory fatigue life correlation was obtained based on the maximum shear and normal stresses on the fracture plane. A new method that requires no cycle counting was suggested by Tchankov and Esselinov [46]. They considered an incremental dissipated energy measurement as the damage-controlling factor, with the suggestion that failure would occur if this dissipated energy reaches a critical level. The application of the Tchankov–Esselinov approach to random loading conditions, however, requires additional VAL experiments. For S45C steel under multiaxial VAL, Kim and Park [47] applied two shear-based multiaxial fatigue parameters: Kandil–Brown–Miller [48] and FS. They reported adequate fatigue life estimations from both parameters provided that the rainflow method is used for counting the cycles obtained from the shear strain history and that the linear damage rule is applied for damage summation. Another method of counting the cycles for a multiaxial VAL was proposed by Lee et al. [49]. Their suggestion was to count the cycles from both normal and shear histories and to adopt the one that produces the higher damage value. Colin and Fatemi [50] successfully applied the SWT parameter along with the rainflow counting method and the linear damage rule in order to predict the fatigue life of stainless steel 304L and aluminum 7075-T6 under VAL.

In most of the VAL studies available, the effect of load sequence on fatigue life is often ignored because of the application of the linear damage rule for computing the accumulated damage. The work conducted for this thesis has shed additional light on the effect of load sequence through the application of a variety of damage accumulation methods that include consideration of load sequence.

Chapter 3

Experimental Program

3.1 Introduction

This chapter provides detailed information about the material under investigation, the testing equipment, and the experimental results. Section 3.2 explains the hardness, chemical composition, and specimen geometry of the material. The testing machine and the extensometers utilized, along with their capacities, are presented in section 3.3. Section 3.4 describes the testing program and the experimental results, including those produced by the monotonic, constant amplitude loading (CAL), two-step, mean strain, and variable amplitude loading (VAL) experiments. The monotonic, cyclic, and fatigue properties are discussed in subsections 3.4.1 and 3.4.2.

3.2 Material and Specimens

The material investigated is 30CrNiMo8HH steel alloy with a Vickers hardness number (VHN) and chemical composition as presented in Table 3.1 and Table 3.2, respectively. All two-step, mean strain, and VAL experiments were performed on tubular specimens with the geometry shown in Figure 3.1. The monotonic and CAL experiments had already been conducted during previous studies of the same material [1, 2]. The monotonic and axial fatigue experiments were performed on solid-bar specimens, whereas the pure torsion tests were performed on the same tubular specimens used for the previous tests, as shown in Figure 3.1.

Table 3.1: Vickers hardness number of 30CrNiMo8HH steel

| Test | Test Average | Overall Average |
|------|--------------|-----------------|
| SP29 | 266.0 | |
| SP57 | 261.6 | 262.5± (4.6) |
| SP58 | 259.8 | |

Table 3.2: Chemical composition of 30CrNiMo8HH steel [1]

| | C | Cr | Ni | Mo | Si | Mn | P | S | Fe |
|-----|-----------|---------|---------|---------|------|------|--------|--------|---------|
| wt% | 0.26–0.33 | 1.8–2.2 | 1.8–2.2 | 0.3–0.5 | <0.4 | <0.6 | <0.035 | <0.035 | Balance |

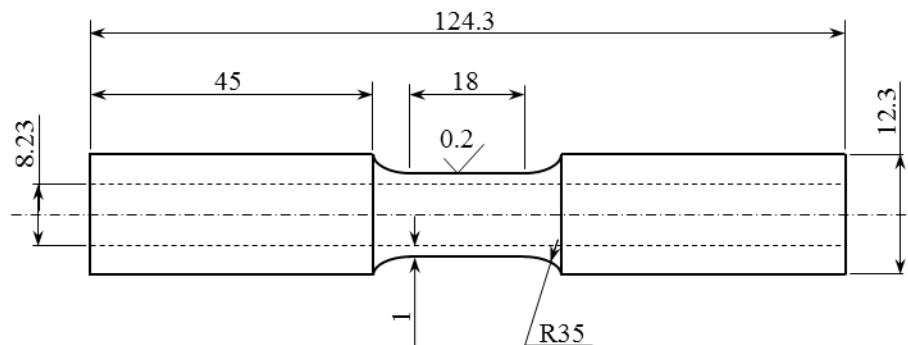


Figure 3.1: Specimen geometry [mm]

3.3 Testing Equipment and Standards

All tests were performed on an Instron 8874 Axial–Torsion Fatigue Testing System with axial and torsional capacities of up to 25 KN and 100 Nm, respectively, and V-grooved jaw faces were used for gripping the tubular specimens. The frequencies for all tests ranged from 0.5 Hz to 1.0 Hz, and the cyclic axial and biaxial tests were performed based on ASTM-E606 [51] and ASTM-E2207 [52], respectively. Figure 3.2 shows the biaxial testing machine.



Figure 3.2: Testing machine

Two uniaxial and biaxial extensometers were used for controlling the strain in all tests, with Instron’s uniaxial extensometer (Figure 3.3 (a)) for control of the strain in the axial two-step and axial mean strain tests. For the torsional two-step, torsional mean strain, and VAL tests, the strain was controlled with Epsilon’s axial–torsion extensometer (Figure 3.3 (b)). The uniaxial extensometer has a 10 mm gage length and a ± 1.0 mm axial extension capacity, whereas the biaxial extensometer gage length is 20 mm and its axial extension and rotational capacities are ± 1.0 mm and $\pm 3.0^\circ$, respectively. Vishay M-Coat D was used to protect the surfaces of the specimens at the contact points and to help hold the extensometers.

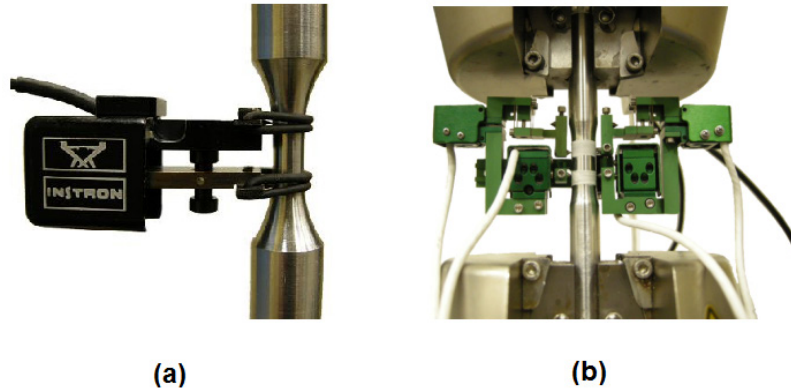


Figure 3.3: Extensometers employed: (a) uniaxial; (b) biaxial

3.4 Experimental Results and Material Properties

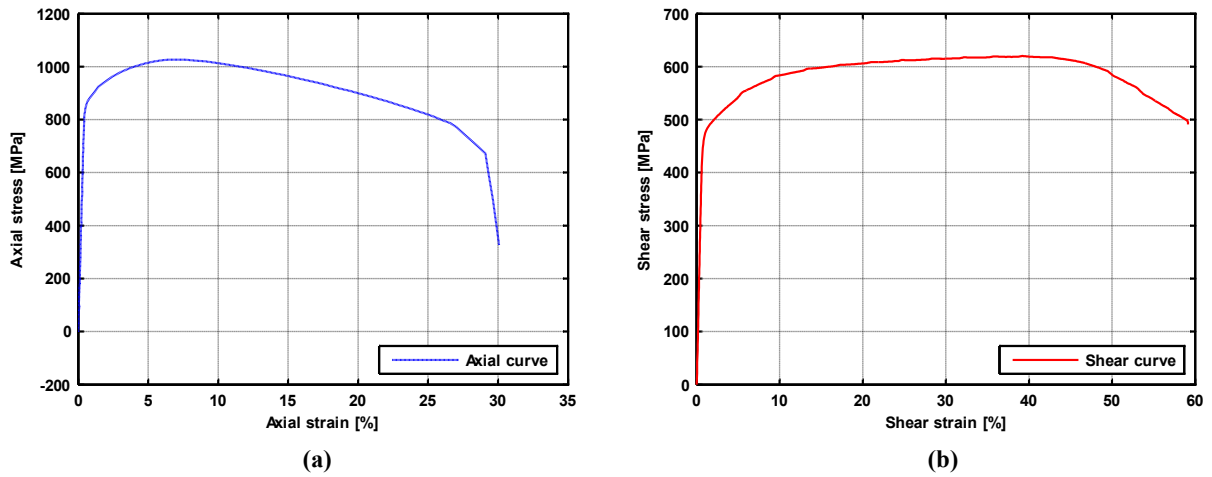
The objective of this research was to estimate the fatigue life of 30CrNiMo8HH steel alloy under VAL by taking into account the VAL components (section 2.2). For this research, the monotonic behaviour and the CAL fatigue data for the material under investigation were already available based on previous studies [1, 2]. To examine the effects of load sequence and mean stress on fatigue life, two sets of strain-controlled two-step and non-zero mean strain axial and pure torsion loading experiments were conducted. A set of VAL experiments were then performed in order to evaluate the procedure for estimating fatigue life. The failure criterion for all cyclic tests was considered to be 20 % load or torque drop.

3.4.1 Monotonic Tests

Solid-bar and tubular specimens were used for tensile and torsional monotonic tests, respectively. The geometry of the solid-bar specimens is available in [1], and that of the tubular specimens is shown in Figure 3.1. The tensile tests were performed under strain-controlled loading for which the applied strain rate was within 0.015 ± 0.006 mm/mm/min, as recommended by ASTM standard [28], whereas the torsion monotonic test was performed under rotation-controlled loading. The monotonic properties of the material obtained from the tests were tabulated as shown in Table 3.3, and the axial and shear monotonic stress–strain curves are depicted in Figure 3.4.

Table 3.3: Monotonic properties

| Axial | σ_y [MPa] | σ_{ult} [MPa] | E [GPa] |
|-------|------------------|----------------------|---------------|
| | 895.345 | 1027.860 | 195.382 |
| | $\pm (8.094)$ | $\pm (10.523)$ | $\pm (7.977)$ |
| Shear | τ_y [MPa] | τ_{ult} [MPa] | G [GPa] |
| | 443.499 | 613.743 | 71.615 |
| | $\pm (27.576)$ | $\pm (9.536)$ | $\pm (0.544)$ |

**Figure 3.4: Monotonic stress-strain curves: (a) axial curve; (b) shear curve**

3.4.2 Constant Amplitude Loading Tests

All CAL fatigue experiments were performed under strain-controlled fully reversed loading, at standard laboratory temperature and humidity levels. Most of the tests were conducted in the low-cycle fatigue (LCF) regime, in which the strain amplitudes ranged from 0.34 % to 1 % and 0.69 % to 1.39 % for the cyclic tension–compression and the cyclic shear experiments, respectively. In addition to the fully reversed axial and pure torsion data, a set of multiaxial proportional and nonproportional fatigue data are available in [1, 2]. The CAL experimental data (Table 3.4) were used in order to calculate the cyclic curve parameters as well as the strain-based and energy-based fatigue properties.

Table 3.4: Fully reversed CAL experimental results [2]

| Test | ε_a (%) [mm/mm] | γ_a (%) [rad] | σ_a [MPa] | τ_a [MPa] | N_f [cycles] |
|-------|--------------------------------|-------------------------|---------------------|-------------------|-------------------|
| Axial | 0.71 | 0 | 703 | 0 | 1221 |
| Axial | 0.72 | 0 | 708.80 | 0 | 1649 |
| Axial | 0.46 | 0 | 652 | 0 | 3064 |
| Axial | 0.51 | 0 | 654.5 | 0 | 2191 |
| Axial | 0.40 | 0 | 624 | 0 | 12732 |
| Axial | 0.34 | 0 | 624 | 0 | 25686 |
| Axial | 0.42 | 0 | 634 | 0 | 11484 |
| Axial | 1.00 | 0 | 720 | 0 | 500 |
| Shear | 0 | 1.06 | 0 | 372.01 | 1414 |
| Shear | 0 | 1.06 | 0 | 372.78 | 1833 |
| Shear | 0 | 1.06 | 0 | 377.62 | 2341 |
| Shear | 0 | 0.79 | 0 | 357.17 | 5200 |
| Shear | 0 | 0.80 | 0 | 359.88 | 5500 |
| Shear | 0 | 1.39 | 0 | 401.69 | 793 |
| Shear | 0 | 1.38 | 0 | 407.48 | 1100 |
| Shear | 0 | 0.69 | 0 | 341.11 | 13748 |

The cyclic curve can be represented by the Ramberg–Osgood equation (Equation (2.11)):

$$\varepsilon_a = \varepsilon_a^e + \varepsilon_a^p = \frac{\sigma_a}{E} + \left(\frac{\sigma_a}{K'}\right)^{\frac{1}{n'}} \quad (3.1)$$

For 30CrNiMo8HH steel, the Ramberg–Osgood parameters, namely, the strength coefficients and the strain hardening exponents, were calculated and tabulated as shown in Table 3.5, and the cyclic axial and shear experimental data as well as the cyclic curves are shown in Figure 3.5.

Table 3.5: Cyclic stress–strain parameters

| | | |
|-------|--------------|--------|
| Axial | K' [MPa] | n' |
| | 925.356 | 0.052 |
| Shear | K'_s [MPa] | n'_s |
| | 722.400 | 0.125 |

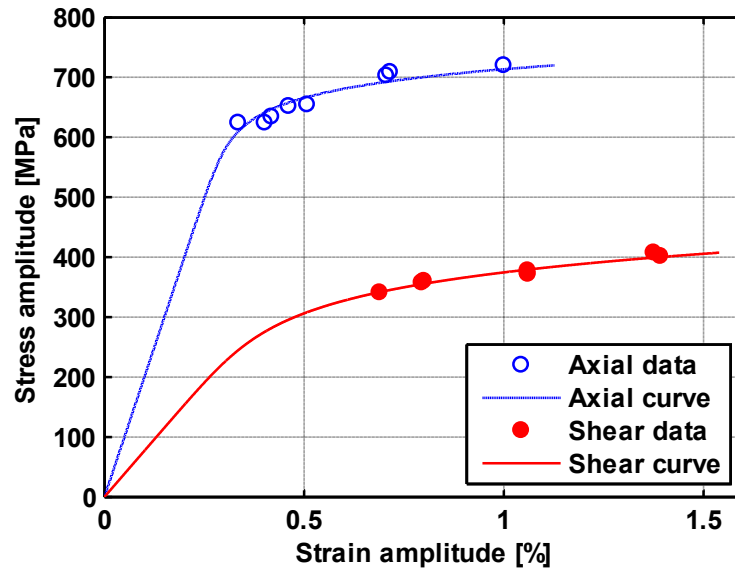


Figure 3.5: Cyclic stress–strain curves

The strain–life curve is commonly represented by the Coffin–Manson curve (Equation (2.14)):

$$\varepsilon_a = \frac{\sigma'_f}{E} (2N_f)^b + \varepsilon'_f (2N_f)^c \quad (3.2)$$

The strain-based fatigue properties and the strain-life curves for 30CrNiMo8HH steel are available in Table 3.6 and Figure 3.6, respectively.

Table 3.6: Strain-based fatigue parameters

| Axial | σ'_f [MPa] | ε'_f | b | c |
|-------|-------------------|------------------|--------|--------|
| | 951.160 | 1.064 | -0.041 | -0.733 |
| Shear | τ'_f [MPa] | γ'_f | b_s | c_s |
| | 608.063 | 0.277 | -0.057 | -0.470 |

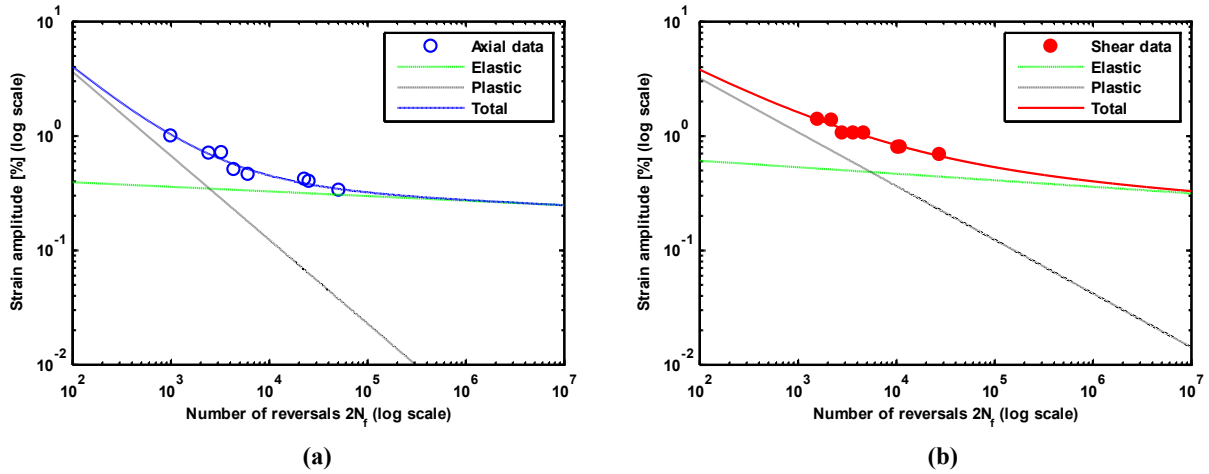


Figure 3.6: Strain–life curves: (a) axial curve; (b) shear curve

As with the strain–life curve, based on Equation (2.15), the total energy–life curve can be expressed as

$$\Delta E_A = E'_e(2N_A)^B + E'_f(2N_A)^C \quad (3.3)$$

The energy-based fatigue properties of 30CrNiMo8HH steel were calculated and are presented in Table 3.7, and the energy–life curves, together with the experimental results, are shown in Figure 3.7.

Table 3.7: Energy-based fatigue parameters

| Axial | E'_e [MJ/m ³] | E'_p [MJ/m ³] | B | C |
|-------|-----------------------------|-----------------------------|--------|--------|
| | 2.262 | 3651.153 | -0.081 | -0.774 |
| Shear | W'_e [MJ/m ³] | W'_p [MJ/m ³] | B_s | C_s |
| | 2.734 | 1353.355 | -0.132 | -0.647 |

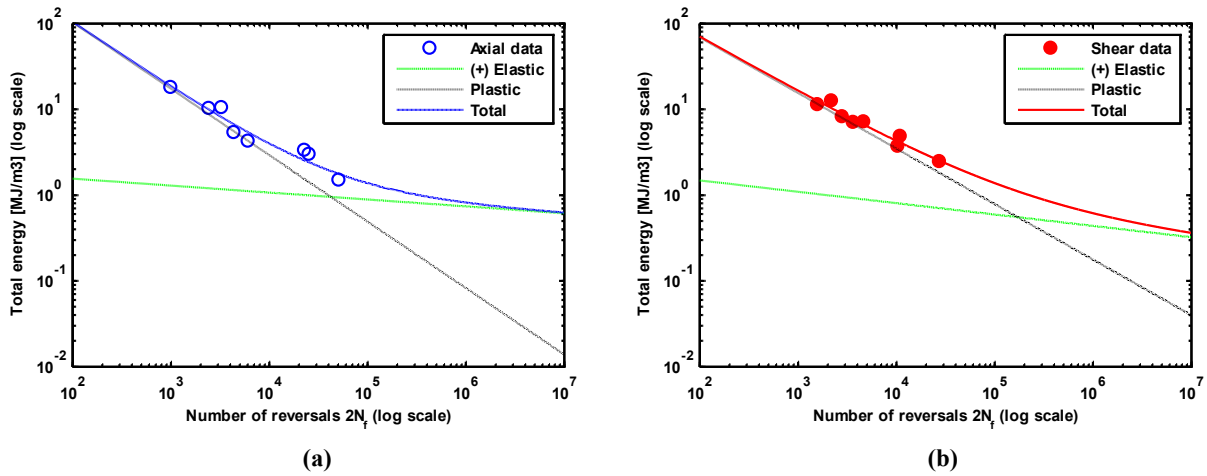


Figure 3.7: Total energy–life curves: (a) axial curve; (b) shear curve

3.4.3 Two-Step Loading Tests

The load sequence effect is one of the factors that must be considered with respect to the estimation of fatigue life under VAL. To this end, several strain-controlled axial and pure torsion two-step loading experiments were conducted at different strain amplitudes, as shown schematically in Figure 3.8. The high-low (HL) tests (Figure 3.8 (a)) were conducted first with pre-specified n_1 cycles for the first step and then continued at the second step until failure. The low-high (LH) experiments (Figure 3.8 (b)) were then performed, with the number of cycles for the first step, n_1 , being equal, in most cases, to the n_2 values obtained from the HL tests. A comparison of the fatigue life results of the HL and LH tests reveals the load sequence effect.

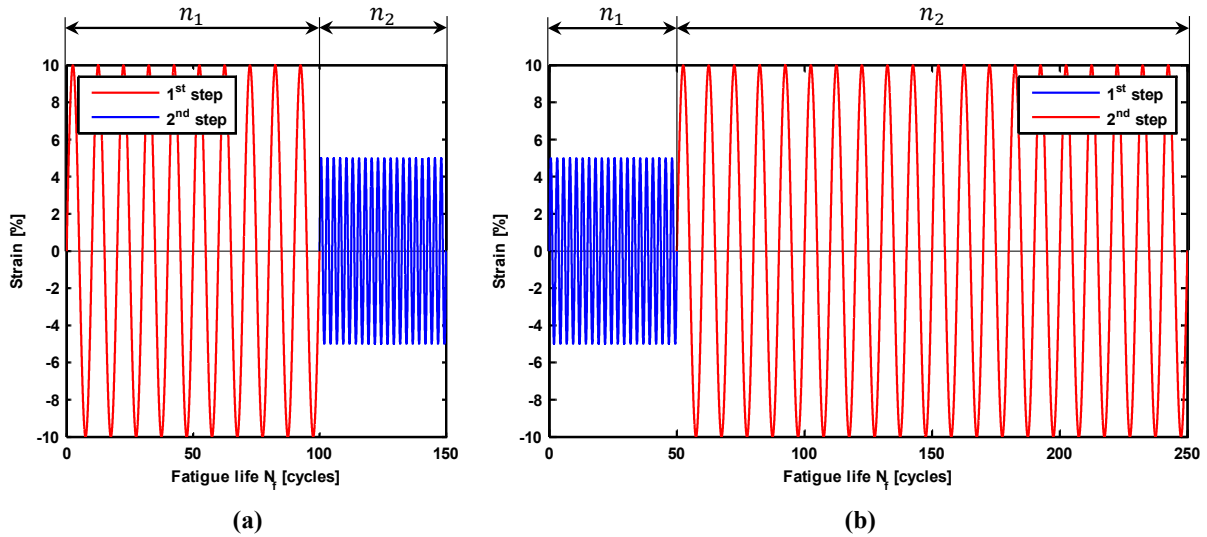


Figure 3.8: Two-step experiments: (a) HL test; (b) LH test

3.4.3.1 Axial Two-Step Tests

A set of strain-controlled HL and LH experiments were performed in order to investigate the effect of load sequence on fatigue life under axial loading. Different strain amplitudes were applied for the first and second steps, with the number of pre-specified cycles for the HL first steps differing according to the applied strain amplitudes. The applied strain amplitudes were 0.45 % to 0.50 % and 0.25 % to 0.33 % for the high step and low step, respectively. The axial two-step experimental results are presented in Table 3.8, and a sample of the hysteresis loops for the two steps is shown in Figure 3.9 (Appendix A includes the hysteresis loops for the other tests).

Table 3.8: Axial two-step experimental results

| Test | 1 st step | 2 nd step | 1 st step | 2 nd step | 1 st step | 2 nd step | N_f [cycles] |
|---------|--------------------------------|--------------------------------|----------------------|----------------------|----------------------|----------------------|-------------------|
| | ε_a (%) [mm/mm] | ε_a (%) [mm/mm] | σ_a [MPa] | σ_a [MPa] | n_1 [cycles] | n_2 [cycles] | |
| SP7-HL | 0.50 | 0.25 | 623.73 | 451.03 | 1000 | 20480 | 21480 |
| SP8-LH | 0.25 | 0.50 | 493.61 | 603.52 | 20500 | 2034 | 22534 |
| SP9-HL | 0.45 | 0.30 | 605.63 | 496.69 | 2000 | 13130 | 15130 |
| SP10-LH | 0.30 | 0.45 | 566.97 | 597.18 | 13000 | 4105 | 17105 |
| SP5-LH | 0.33 | 0.45 | 571.50 | 626.97 | 8500 | 664 | 9164 |

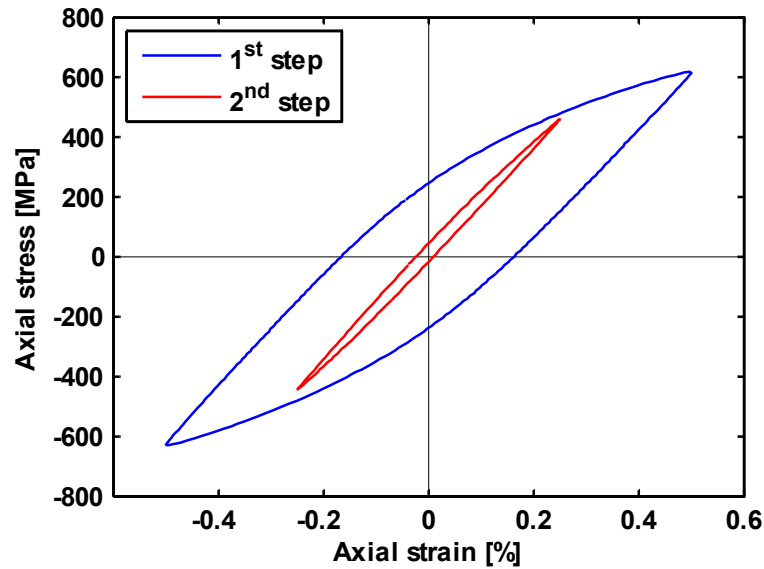


Figure 3.9: SP7-HL hysteresis loops:
 $[\epsilon_{a_high} = 0.50\% ; \epsilon_{a_low} = 0.25\%]$

A comparison of the experimental results for tests SP7 and SP8 (Table 3.8) reveals that the number of cycles at the higher step is doubled in the LH test, and the same effect can be observed when the SP9 and SP10 results are compared. The overall fatigue life results produced by the LH experiments could have been even higher if the number of cycles at the lower step had been increased. The fatigue life results of the axial two-step experiments show that load sequence does have an influence on fatigue life and that it should be taken into account when VAL conditions are present.

3.4.3.2 Shear Two-Step Tests

A similar procedure was used for the examination of the effect of load sequence on fatigue life under pure torsion loading. The amplitudes for the shear two-step experiments ranged from 1 % to 1.35 % for the higher step and from 0.50 % to 0.67 % for the lower step. A combination of a variety of strain amplitude steps and the associated fatigue life values observed were tabulated as shown in Table 3.9. A sample of the half-life hysteresis loops is depicted in Figure 3.10, and illustrations of additional loops are included in Appendix A.

Table 3.9: Torsional two-step experimental results

| Test | 1 st step | 2 nd step | 1 st step | 2 nd step | 1 st step | 2 nd step | N_f [cycles] |
|---------|---------------------------|---------------------------|----------------------|----------------------|----------------------|----------------------|-------------------|
| | γ_a (%) [mm/mm] | γ_a (%) [mm/mm] | τ_a [MPa] | τ_a [MPa] | n_1 [cycles] | n_2 [cycles] | |
| SP22-HL | 1.35 | 0.67 | 378.69 | 306.90 | 1033 | 3344 | 4377 |
| SP25-LH | 0.68 | 1.35 | 341.99 | 380.07 | 2975 | 1461 | 4436 |
| SP26-HL | 1.18 | 0.59 | 376.66 | 299.15 | 1000 | 4632 | 5632 |
| SP27-LH | 0.59 | 1.18 | 337.71 | 370.30 | 5631 | 1642 | 7273 |
| SP19-HL | 1.00 | 0.50 | 372.92 | 282.61 | 1003 | 32731 | 33734 |

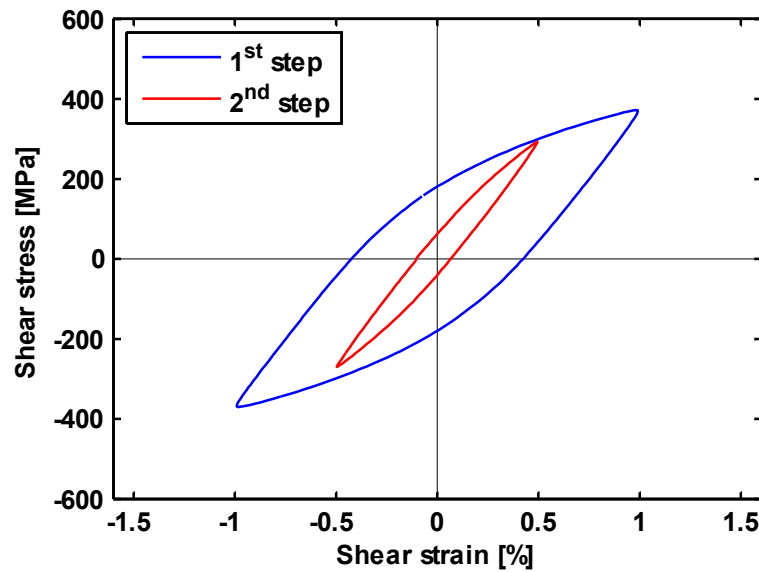


Figure 3.10: SP19-HL hysteresis loops:
 $[\gamma_{a_high} = 1.00\% ; \gamma_{a_low} = 0.50\%]$

As with the axial loading, the load sequence under torsional loading can be observed when SP22 is compared with SP25 and when SP26 is compared with SP27. Although the number of cycles of the lower step in the HL and LH experiments is not identical, the number of cycles resulting at the higher step is greater from the LH experiments. The influence of load sequence is thus important with respect to both axial and pure torsion loading and should therefore be taken into account in the design of components subjected to VAL.

3.4.4 Mean Strain Loading Tests

Mean stress is another factor likely to be present in a VAL scenario, which should thus also be accounted for in an estimation of fatigue life. A set of non-zero mean strain experiments were performed in order to quantify the effect of mean stress on fatigue life. To distinguish between the effect on fatigue life of strain amplitude and that of mean strain, a two-level factorial design [53] was employed for the testing procedure. A brief description of this experimental design follows, and the experimental results are presented in the next subsections.

In the two-level factorial design, for each factor under investigation, namely the strain amplitude (ϵ_a) and the mean strain (ϵ_m), two levels (high and low) were selected and combined to form a set of four tests. It was assumed that the change in each factor is linear over the range of the levels selected. To eliminate any misleading interaction relations between the effects of the two factors under investigation, coded values (-1 & $+1$) were chosen for the statistical analysis. The results of the four experiments that resulted from the combination of the applied strain amplitudes and mean strains for the axial experiment are shown schematically in Figure 3.1, and the coded values were calculated based on Equation (3.4).

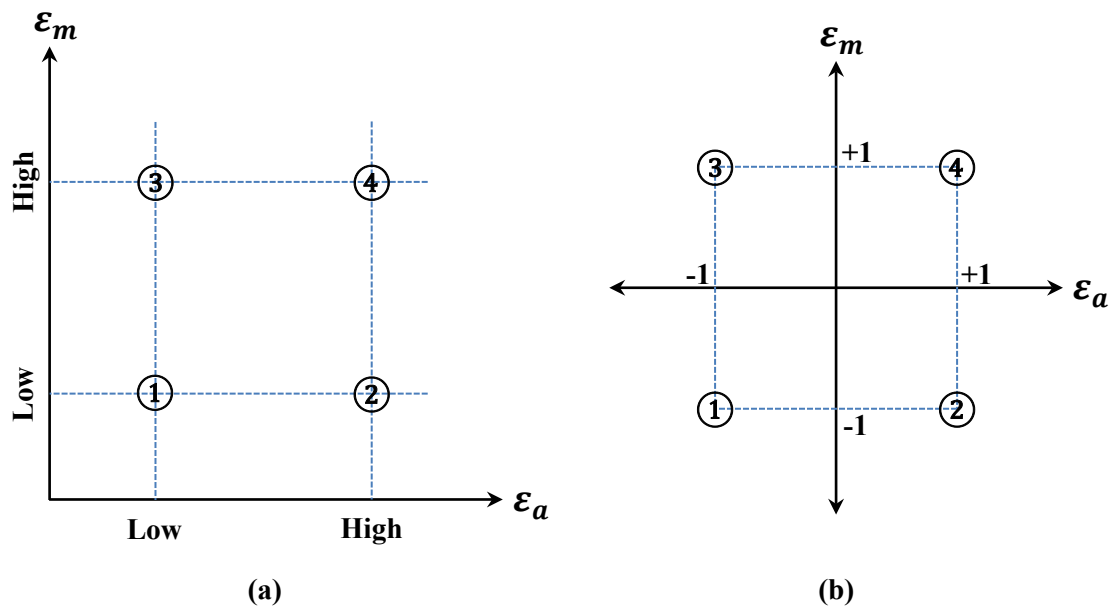


Figure 3.11: Two-level factorial experiments at intersections of (a) uncoded values and (b) coded values

$$\varepsilon_{coded} = \frac{2(\varepsilon - \varepsilon_{ave})}{(\varepsilon_{high} - \varepsilon_{low})} \quad (3.4)$$

where ε = uncoded value of strain amplitude or mean strain
 ε_{ave} = average value of the two levels selected
 ε_{high} = higher level of strain amplitude or mean strain
 ε_{low} = lower level of strain amplitude or mean strain

The underlying regression model for the two-level factorial design for axial loading can be written in the polynomial form

$$N_f = \beta_0 + \beta_1 \varepsilon_a + \beta_2 \varepsilon_m + \beta_{12} \varepsilon_a \varepsilon_m + e_1 \quad (3.5)$$

where β_i = parameters to be determined
 ε_a = coded values of the strain amplitude
 ε_m = coded values of the mean strain
 $\varepsilon_a \varepsilon_m$ = term refers to the interaction effect of the two factors under investigation
 e_1 = term refers to a random error

The purpose of the two-level factorial design employed for this study was to determine an empirical relation that relates the applied strain amplitude and the mean strain to the fatigue life observed. The same procedure can also be used for an estimation of the level of plastic energy density based on the applied strain amplitude and the mean strain. The experimental results obtained from the axial and torsional mean strain experiments are summarized in the following subsections.

3.4.4.1 Axial Mean Strain Test Results

Several axial mean strain experiments were performed in order to investigate the effect of mean stress on fatigue life. The set was comprised of the four factorial design experiments described above (Figure 3.11) along with additional tests at different levels of mean strain and strain amplitude, including a zero mean strain test. The applied strain amplitudes and mean strains for all of these experiments ranged from 0.30 % to 0.50 % and from 0.15 % to 0.25 %, respectively. The experimental results from the mean strain experiments are summarized in Table 3.10, in which the boldfaced rows represent the four factorial design experiments. Initial and half-life hysteresis loop samples are shown in Figure 3.12, and additional samples are included in Appendix A.

Table 3.10: Axial mean strain experimental results

| Test | Uncoded values | | Coded values | | σ_a [MPa] | σ_m [MPa] | $\Delta E_p \times 10^{-2}$ [MJ/m ³] | N_f [cycles] |
|-------------|--------------------------------|--------------------------------|-----------------|-----------------|---------------------|---------------------|---|-------------------|
| | ε_a (%) [mm/mm] | ε_m (%) [mm/mm] | ε_a | ε_m | | | | |
| SP4 | 0.30 | 0.15 | -1 | -1 | 540.06 | 71.54 | 33.35 | 24045 |
| SP12 | 0.40 | 0.15 | 1 | -1 | 579.89 | -2.56 | 149.10 | 4538 |
| SP15 | 0.30 | 0.25 | -1 | 1 | 538.27 | 133.59 | 24.58 | 25869 |
| SP13 | 0.40 | 0.25 | 1 | 1 | 571.87 | 12.58 | 146.48 | 6826 |
| SP3 | 0.33 | 0.20 | -0.34 | 0.13 | 561.91 | 98.33 | 45.85 | 11151 |
| SP6 | 0.40 | 0.20 | 1 | 0.13 | 572.63 | 13.43 | 141.00 | 10376 |
| SP11* | 0.40 | 0.25 | 1 | 1 | 580.39 | 5.57 | 203.36 | 5525 |
| SP14 | 0.50 | 0.25 | 2.55 | 1 | 622.78 | -10.19 | 405.31 | 1932 |
| SP16* | 0.30 | 0.15 | -1 | -1 | 553.71 | 32.20 | 66.98 | 15633 |
| SP55 | 0.30 | 0 | -1 | -4 | 574.01 | -31.38 | 27.49 | 41122 |

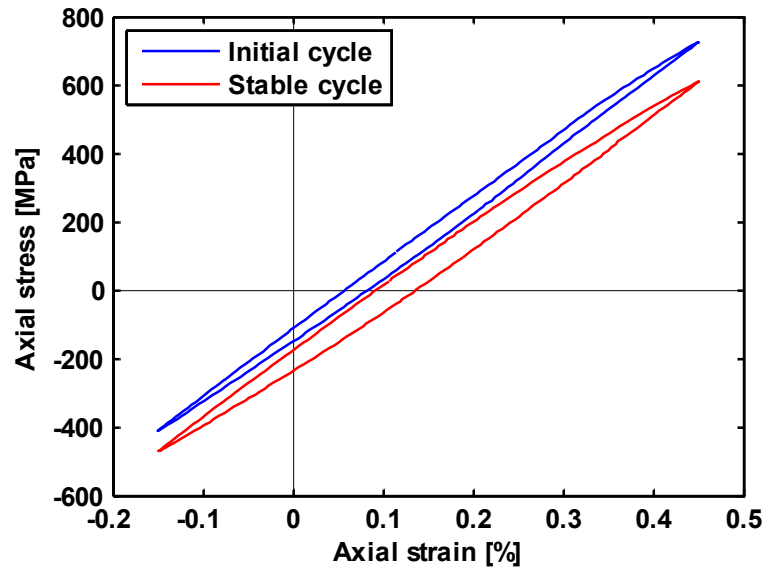


Figure 3.12: SP4 hysteresis loops:
[$\varepsilon_a = 0.30$ %; $\varepsilon_m = 0.15$ %]

Since the correlation between the applied strain amplitude and fatigue life is commonly represented by a power law function, a logarithmic transformation was incorporated into Equation (3.5), from which the parameters β_i can be found through linear regression.

* Replicated tests

The first four rows in Table 3.10 can be written in the form

$$\begin{aligned}
\beta_0 - \beta_1 - \beta_2 + \beta_{12} + e_1 &= \log_{10}(24045) \\
\beta_0 + \beta_1 - \beta_2 - \beta_{12} + e_2 &= \log_{10}(4538) \\
\beta_0 - \beta_1 + \beta_2 - \beta_{12} + e_3 &= \log_{10}(25869) \\
\beta_0 + \beta_1 + \beta_2 + \beta_{12} + e_4 &= \log_{10}(6826)
\end{aligned}
\tag{3.6}$$

which can be presented in the matrix form

$$\underline{X}\underline{\beta} + \underline{e} = \underline{y} \tag{3.7}$$

The parameters β_i must be estimated such that the sum of squared errors (L) is minimized, where

$$L = \sum_{i=1}^4 e_i^2 = \underline{e}^t \underline{e} = (\underline{y} - \underline{X}\underline{\beta})' (\underline{y} - \underline{X}\underline{\beta}) \tag{3.8}$$

The partial derivative $\frac{\partial L}{\partial \underline{\beta}} = 0$ results in

$$\underline{\beta} = (\underline{X}^t \underline{X})^{-1} \underline{X}^t \underline{y} \tag{3.9}$$

The derivation of Equation (3.9) is explained in greater detail in [53], section 10.3.

The same procedure was used to relate plastic energy to the applied strain amplitudes and the mean strains. Both empirical formulations are as follows:

$$\begin{aligned}
\log_{10}(N_f) &= 4.0712 - 0.3257\varepsilon_a + 0.0523\varepsilon_m + 0.0364\varepsilon_a\varepsilon_m \\
\log_{10}(W_p) &= -0.1867 + 0.3564\varepsilon_a - 0.0350\varepsilon_m + 0.0312\varepsilon_a\varepsilon_m
\end{aligned}
\tag{3.10}$$

Based on the analysis of variance (ANOVA) table and the residual plots (error in fatigue life prediction) [53], the interaction terms ($\varepsilon_a\varepsilon_m$) in Equations (3.10) are insignificant and can be omitted. On the other hand, the mean strain term cannot be omitted because the residual plots, which should show random error distributions, will instead indicate a decreasing trend (Figure 3.13 (b)) after the removal of those terms. Thus,

$$\begin{aligned}
\log_{10}(N_f) &= 4.0712 - 0.3257\varepsilon_a + 0.0523\varepsilon_m \\
\log_{10}(W_p) &= -0.1867 + 0.3564\varepsilon_a - 0.0350\varepsilon_m
\end{aligned}
\tag{3.11}$$

where ε_a and ε_m are the coded values of the axial strain amplitude and mean strain, respectively.

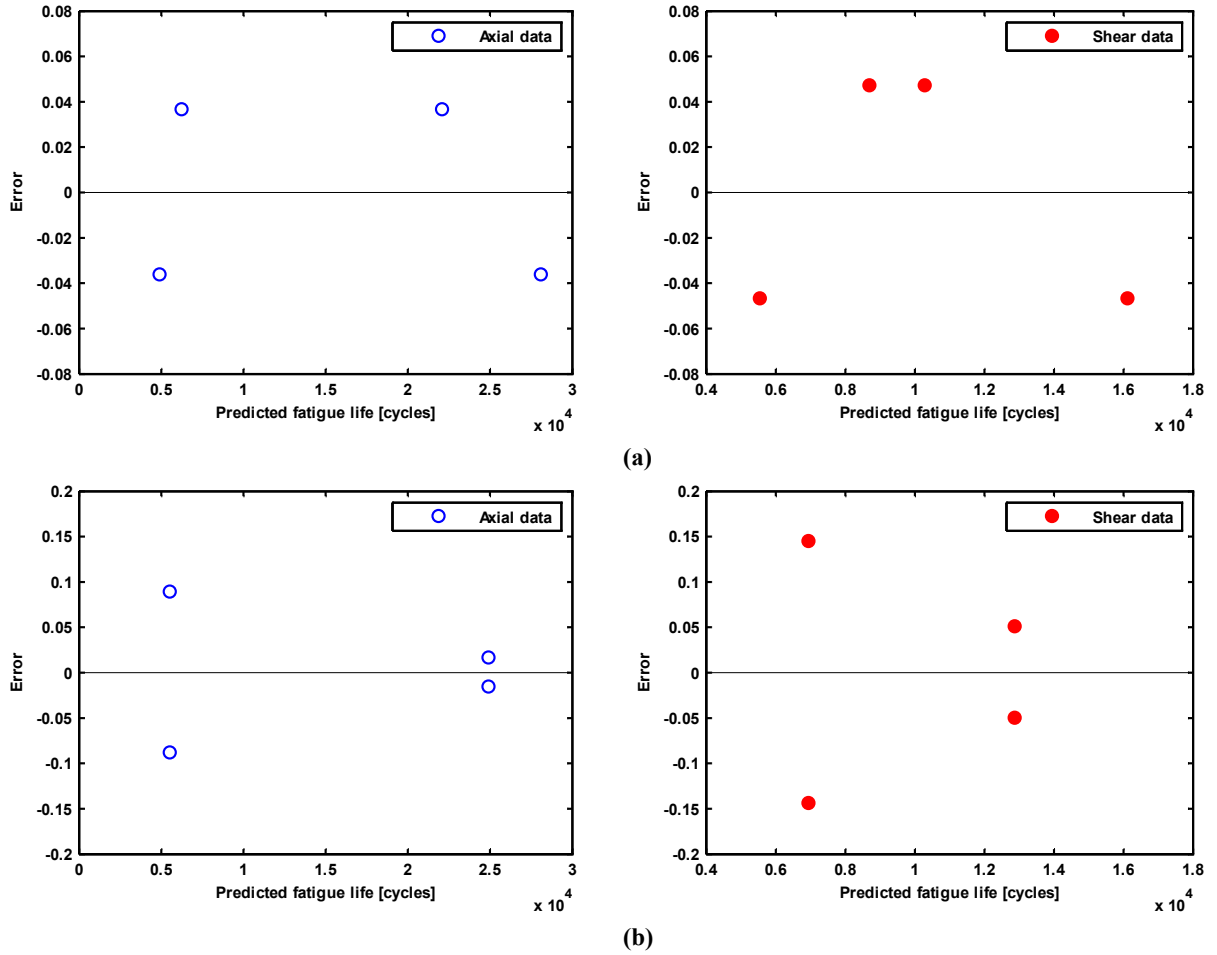


Figure 3.13: Residual plots: (a) including the ϵ_m term; (b) excluding the ϵ_m term

The logarithmic transformation was not applied with respect to the mean strain, so the empirical formulas can be used for zero mean strains as well. The coded values for strain amplitudes and the mean strain can hence be calculated as

$$\epsilon_a = \frac{2 \left[\log_{10}(\epsilon_{a_uncoded}) - \frac{\log_{10}(0.003 \times 0.004)}{2} \right]}{\log_{10} \left(\frac{0.004}{0.003} \right)} \quad (3.12)$$

$$\epsilon_m = \frac{2 \left[\epsilon_{m_uncoded} - \left(\frac{0.0015 + 0.0025}{2} \right) \right]}{0.0025 - 0.0015} \quad (3.13)$$

The experimental data shown in normal font in Table 3.10 were used as a means of evaluating the empirical relations presented in the Equation (3.11) formulas. The fatigue life and plastic energy density predictions based on the empirical relations were within a factor of 2 of the results from the mean strain tests (Figure 3.14 (a)). For the zero mean strain experiments, however, the fatigue life and plastic strain predictions were less satisfactory (Figure 3.14 (b)). These findings imply that the Equation (3.11) formulas cannot be used for a determination of the zero mean strain loading.

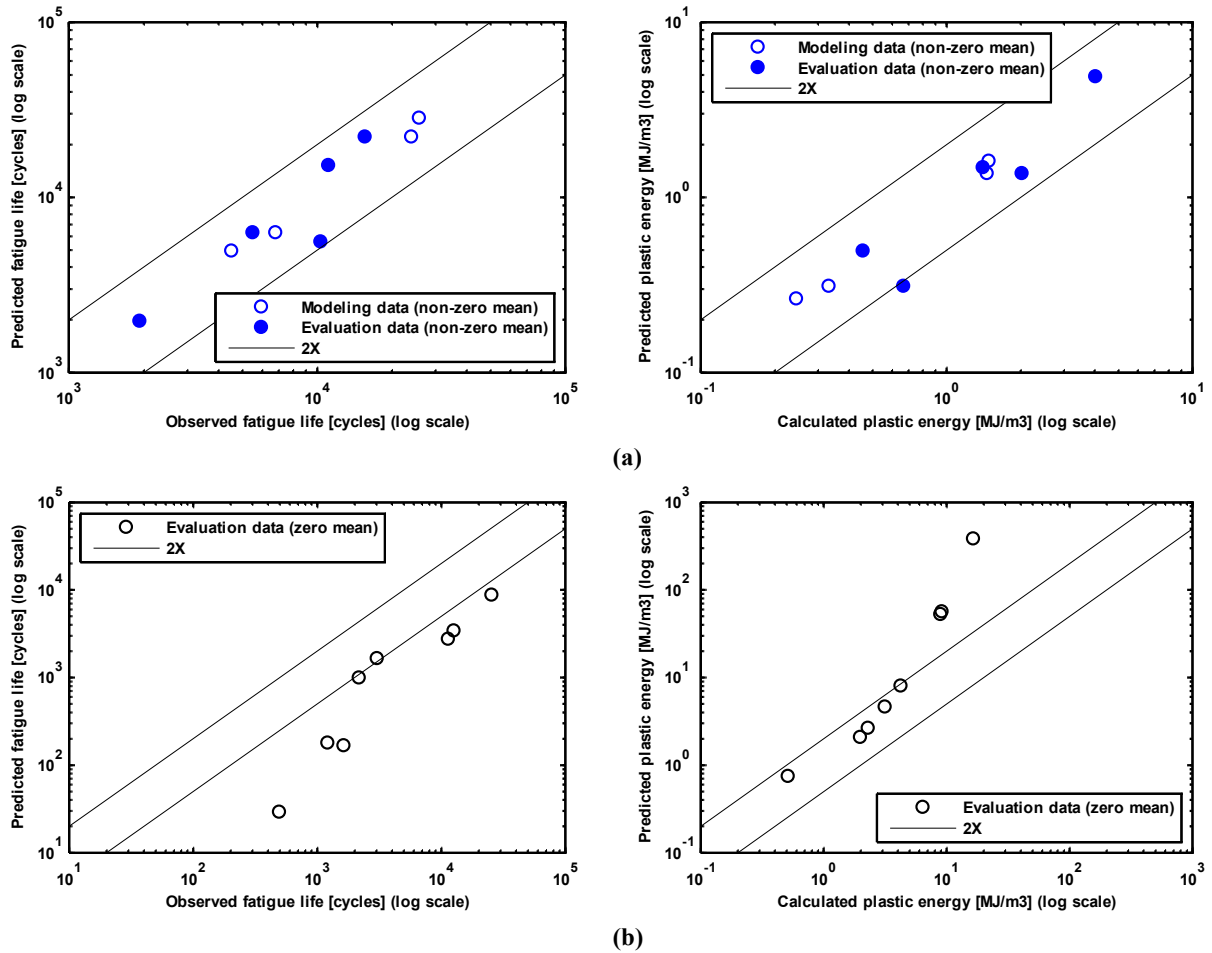


Figure 3.14: Predictions of fatigue life and plastic strain based on the axial empirical relations: (a) non-zero mean strain tests; (b) zero mean strain tests

3.4.4.2 Shear Mean Strain Test Results

As with axial loading, some shear mean strain tests were performed in order to study the effect of mean stress on fatigue life. The test parameters ranged from 0.60 % to 0.80 % for the applied shear strain amplitudes and from 0.25 % to 0.50 % for the shear mean strains. A zero mean strain test was also included. The experimental results for the shear mean strain tests were tabulated as shown in Table 3.11, in which the first four rows represent the experiments suggested based on the factorial design (as in Figure 3.11). Figure 3.15 shows an example of the stress–strain responses resulting from the shear mean strain experiments. Appendix A includes the stress–strain responses for the other tests.

Table 3.11: Shear mean strain experimental results

| Test | Uncoded values | | Coded values | | τ_a [MPa] | τ_m [MPa] | $\Delta W_p \times 10^{-2}$ [MJ/m ³] | N_f [cycles] |
|------|-------------------------|-------------------------|--------------|------------|-------------------|-------------------|---|-------------------|
| | γ_a (%) [rad] | γ_m (%) [rad] | γ_a | γ_m | | | | |
| SP30 | 0.60 | 0.25 | -1 | -1 | 325.52 | 14.62 | 96.52 | 14485 |
| SP31 | 0.80 | 0.25 | 1 | -1 | 343.43 | 1.31 | 276.70 | 9705 |
| SP34 | 0.60 | 0.50 | -1 | 1 | 320.20 | 15.97 | 111.04 | 11480 |
| SP33 | 0.80 | 0.50 | 1 | 1 | 345.67 | 5.67 | 271.77 | 4993 |
| SP29 | 0.40 | 0.25 | -3.82 | -1 | 286.32 | 75.80 | 16.57 | 42786 |
| SP56 | 0.60 | 0 | -1 | -3 | 329.33 | -1.29 | 147.60 | 17827 |

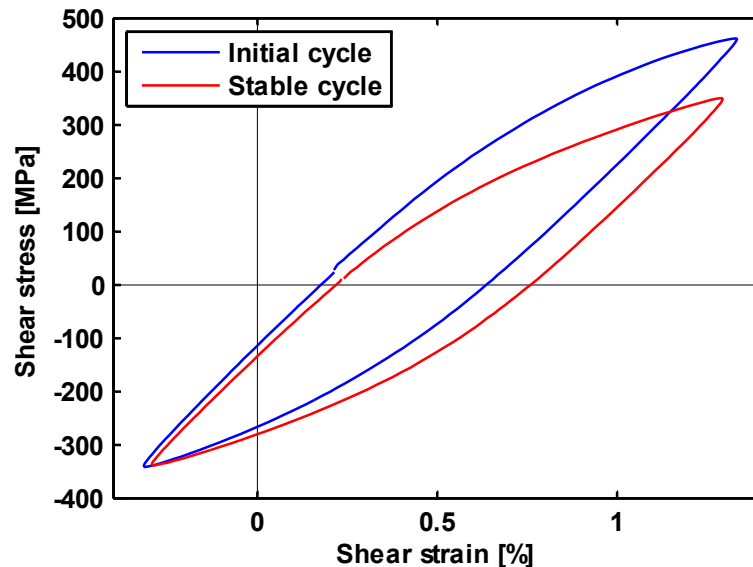


**Figure 3.15: SP33 hysteresis loops:
[$\gamma_a = 0.80$ %; $\gamma_m = 0.50$ %]**

The empirical relations that indicate the links between fatigue life and plastic strain density on one hand and the applied strain amplitude and mean strain on the other can be derived based on the same procedure used for axial mean strain (Equations (3.6) to (3.13)). After the regression parameters have been determined and the interaction terms omitted, the two formulas can be written as

$$\begin{aligned}\log_{10}(N_f) &= 3.9766 - 0.1339\gamma_a - 0.0974\gamma_m \\ \log_{10}(W_p) &= 0.2266 + 0.2115\gamma_a + 0.0133\gamma_m\end{aligned}\tag{3.14}$$

Good fatigue life and plastic energy density correlations were calculated from the above equations for the experiments involving non-zero mean strain. However, for pure shear loading with zero mean strain, the fatigue life was overestimated, as shown in Figure 3.16 (b).

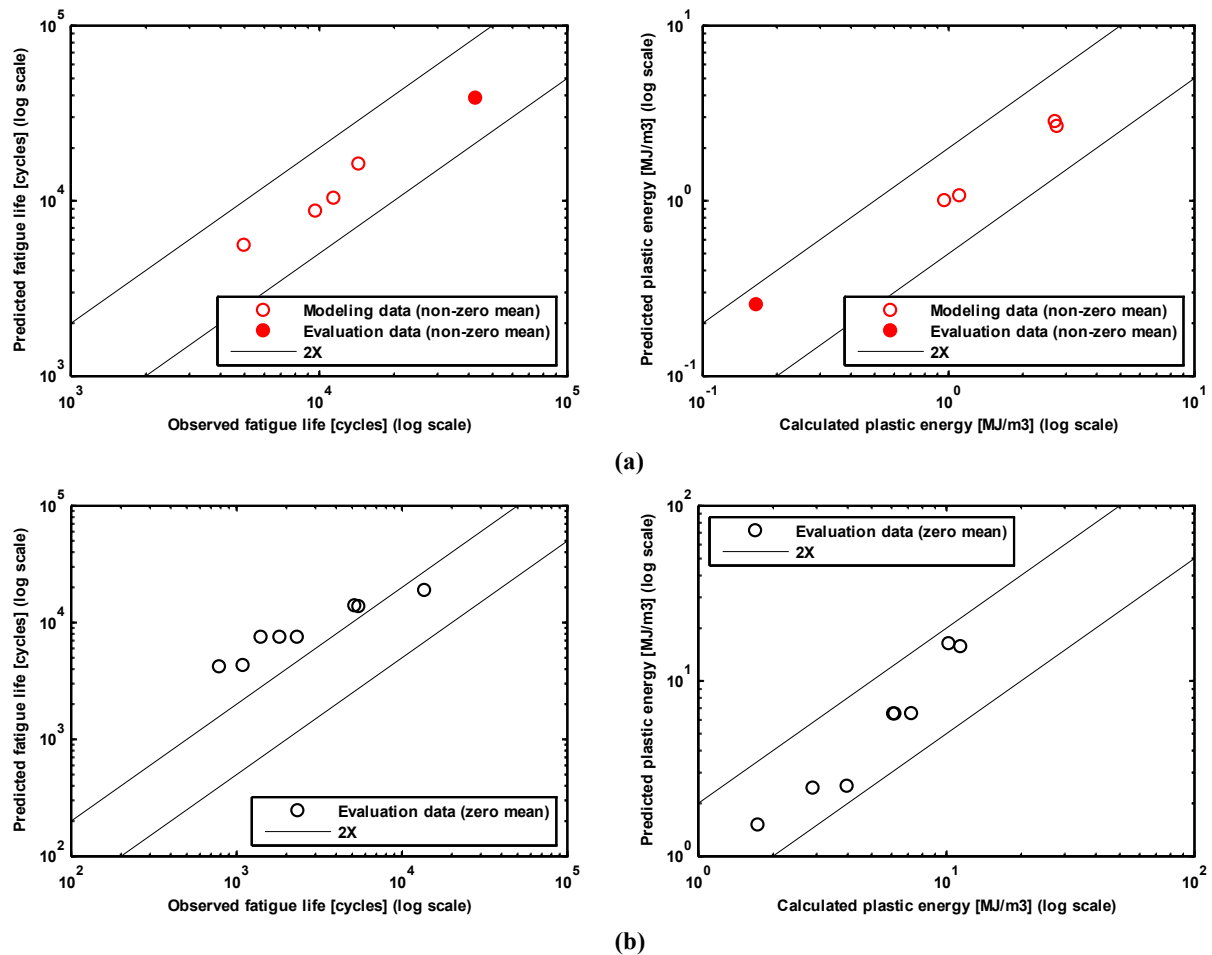


Figure 3.16: Predictions of fatigue life and plastic strain based on the shear empirical relations: (a) non-zero mean strain tests; (b) zero mean strain tests

3.4.4.3 Mean Strain Observations

The two-level factorial design employed facilitated a comparison of the independent effects of strain amplitude and mean strain. The effects of strain amplitude on fatigue life can be seen when the results of the experiments with the same mean strain are matched against those of the experiments involving different strain amplitudes, i.e., SP12 versus SP4 and SP13 versus SP15 in Table 3.10, and SP31 versus SP30 and SP33 and SP34 in Table 3.11. As expected, the fatigue life decreases at higher strain amplitudes, as shown in Figure 3.17.

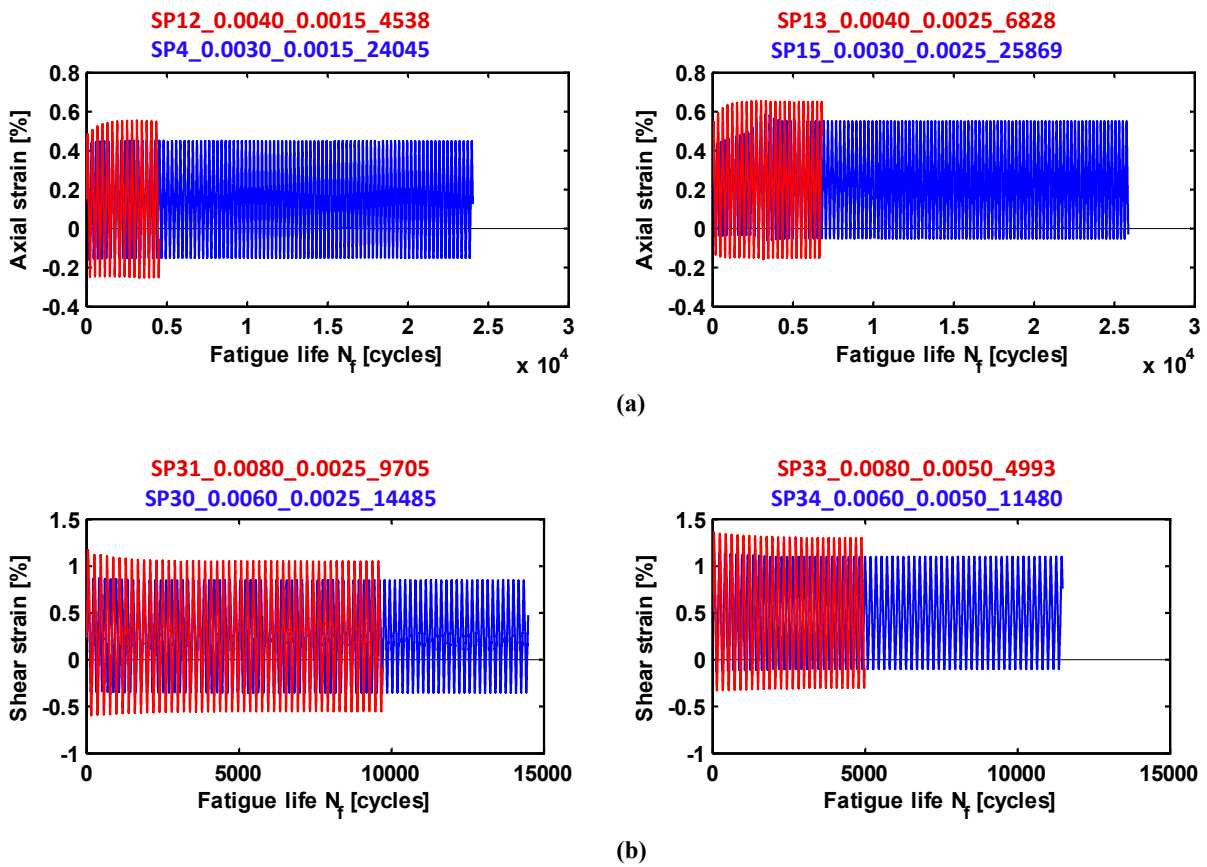
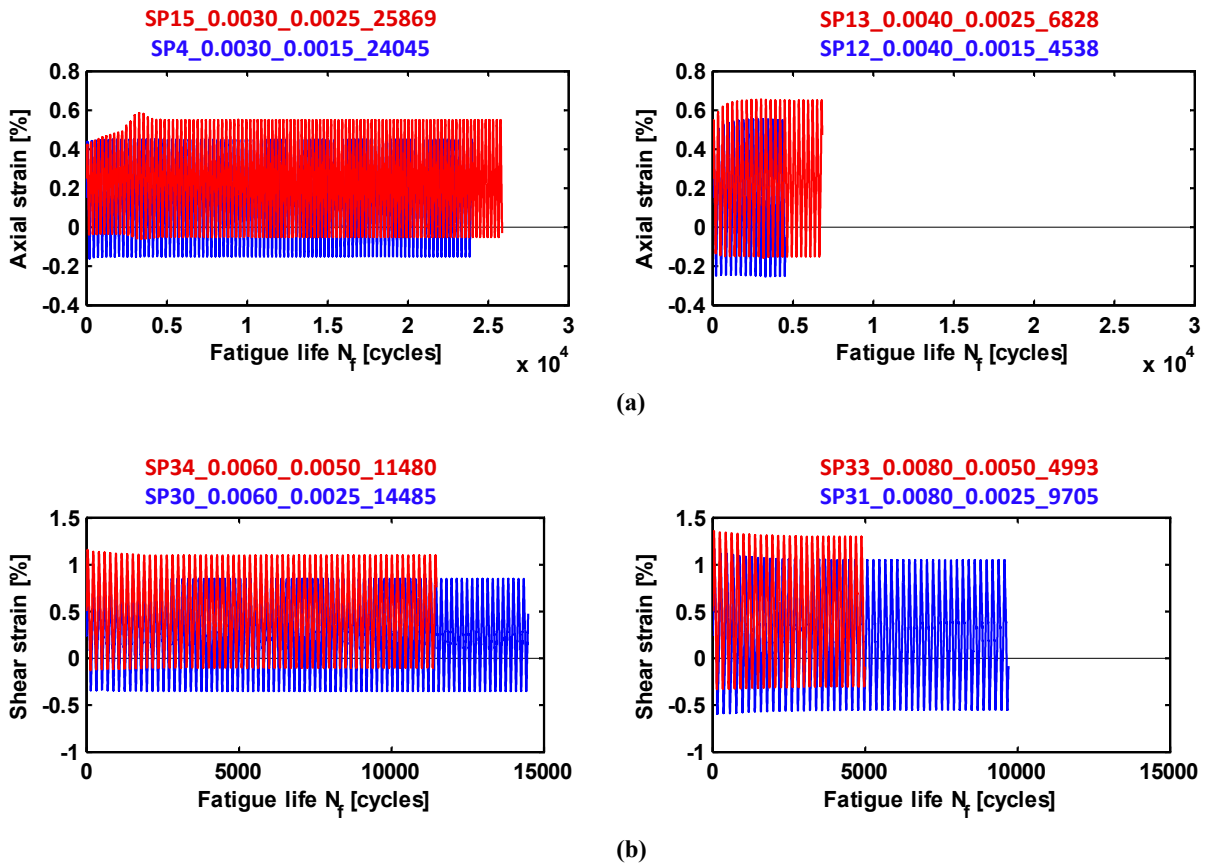


Figure 3.17: Effects of strain amplitude on fatigue life:
(a) pure axial loading; (b) pure torsion loading

Similarly, the effect of the applied mean strain on fatigue life can be seen when the test results for the same strain amplitudes are compared with those for different mean strains. In the axial loading experiments, the effect of mean strain on fatigue life can be observed from an examination of SP15 versus SP4 and SP13 versus SP12, whereas in the pure torsion loading experiments, the mean strain effect is evident from a comparison of SP34 versus SP30 and SP33 versus SP31. Figure below shows the comparison of the axial and shear mean strain test data.



**Figure 3.18: Effects of mean strain on fatigue life:
(a) pure axial loading; (b) pure torsion loading**

Since it is believed that tensile mean stress is detrimental with respect to fatigue life, it was expected that higher levels of tensile mean strain would result in lower fatigue life values. However, as can be seen from Figure 3.18 (a), the fatigue life increased slightly at higher positive mean strains. On the other hand, the fatigue life values observed based on the pure shear loading experiments were unsurprisingly lower at higher levels of mean strain (Figure 3.18 (b)).

In an attempt to explain the unexpected observations at higher levels of tensile mean strain, a number of factors, including maximum stress, mean stress, stress amplitude, and plastic energy, were compared. At higher fatigue life values (SP13, SP15), both the maximum and mean stresses were found to be also higher (Figure 3.19 (a) & (b)), which fails to account for the improvement in fatigue life. On the other hand, the stress amplitudes for the same tests are smaller than those at lower mean strains (Figure 3.19 (c)). This difference means that, for the mean strain ranges applied, the effect of the mean strain can be attributed to the stress amplitude rather than to the mean strain. The fact that higher stress amplitudes can be observed at lower mean strain levels can be attributed to the dependency of the level of cyclic softening on the strain amplitude and the mean strain levels.

Stabilized plastic strain energy densities listed in Table 3.10 (areas of hysteresis loops) were compared to the fatigue life observations. A comparison of SP4 versus SP15 and SP12 versus SP13 in Table 3.12 reveals that the plastic energy densities calculated at higher mean strains are less than those at lower mean strains. In other words, plastic energy can be considered an additional parameter that explains the slight improvement in fatigue life at higher tensile mean strain values.

Table 3.12: Comparison of plastic energy in mean strain experiments

| Test | ε_a (%) [mm/mm] | ε_m (%) [mm/mm] | N_f [cycles] | $E_p \times 10^{-2}$ [MJ/m ³] |
|-------------|--------------------------------|--------------------------------|-------------------|--|
| SP4 | 0.30 | 0.15 | 24045 | 33.35 |
| SP12 | 0.40 | 0.15 | 4538 | 149.10 |
| SP15 | 0.30 | 0.25 | 25869 | 24.58 |
| SP13 | 0.40 | 0.25 | 6826 | 146.48 |

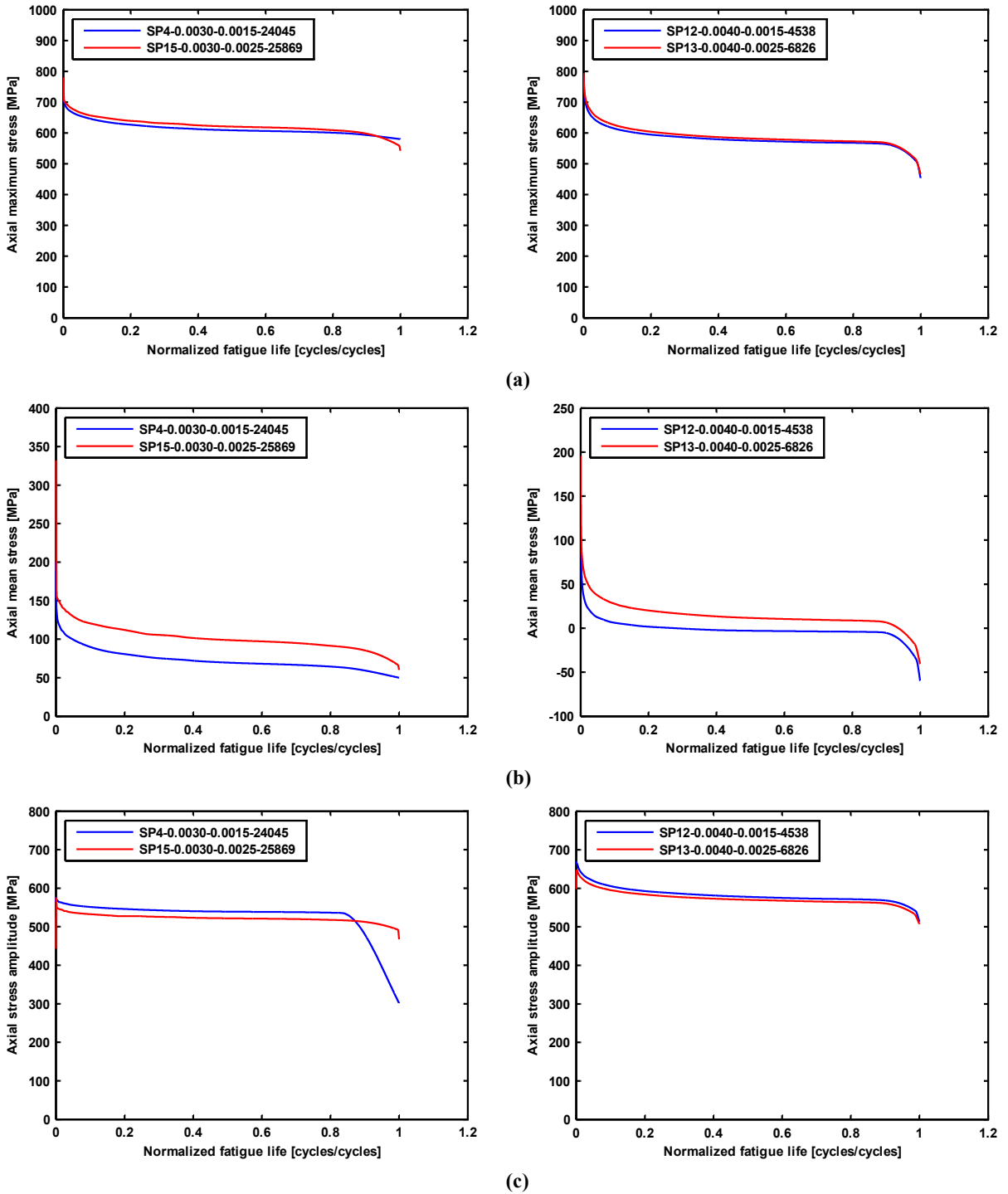
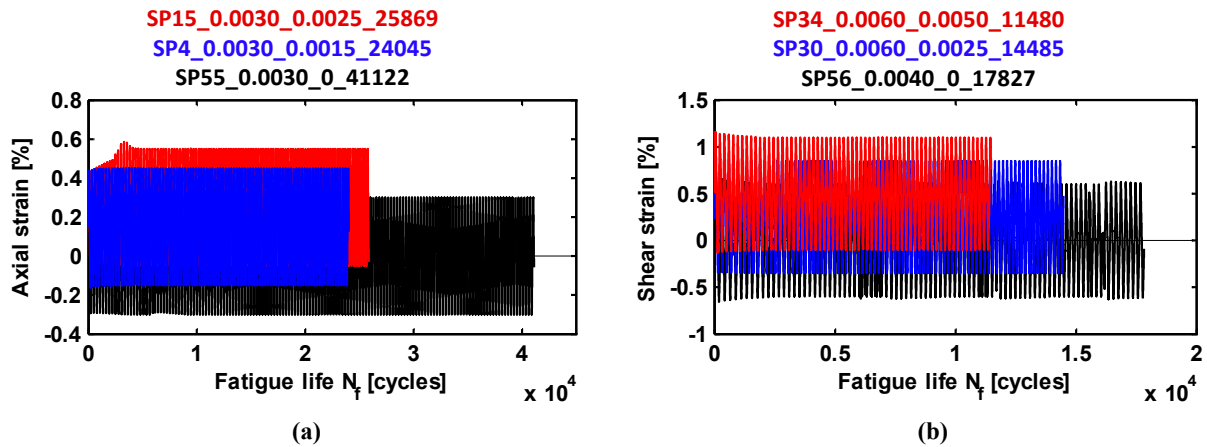


Figure 3.19: Comparison of stress levels in mean strain experiments:
(a) maximum stress; (b) mean stress; (c) stress amplitude

Despite the arguments discussed above, the improvement in fatigue life at higher tensile mean strains cannot be generalized for all mean strain levels. This premise was confirmed through axial and shear zero mean strain tests, the results of which were compared with those of the non-zero mean strain tests, as shown in Figure below



**Figure 3.20: Effect of mean strain on fatigue life, including zero-mean strain tests:
(a) pure axial loading; (b) pure torsion loading**

3.4.5 Variable Amplitude Loading Tests

Following a study of the parameters involved in most service loading histories, a series of strain-controlled axial and pure torsion VAL tests were performed. To incorporate variable amplitudes using the Instron MAX software, random numbers were generated between maximum and minimum points and then used as the applied strain values for each loading block. Depending on the length of the loading block, the time was specified so that the frequency ranged from 0.5 Hz to 1.0 Hz. The block was then repeated over time until the point of failure. As with the CAL sinusoidal wave, the first loading block begins with zero strain and progresses until the end of the block is reached, but each subsequent block starts from the point of the last strain value in the previous block and continues to the last point. Figure 3.21 shows a sample of a VAL block used for the pure shear loading tests.

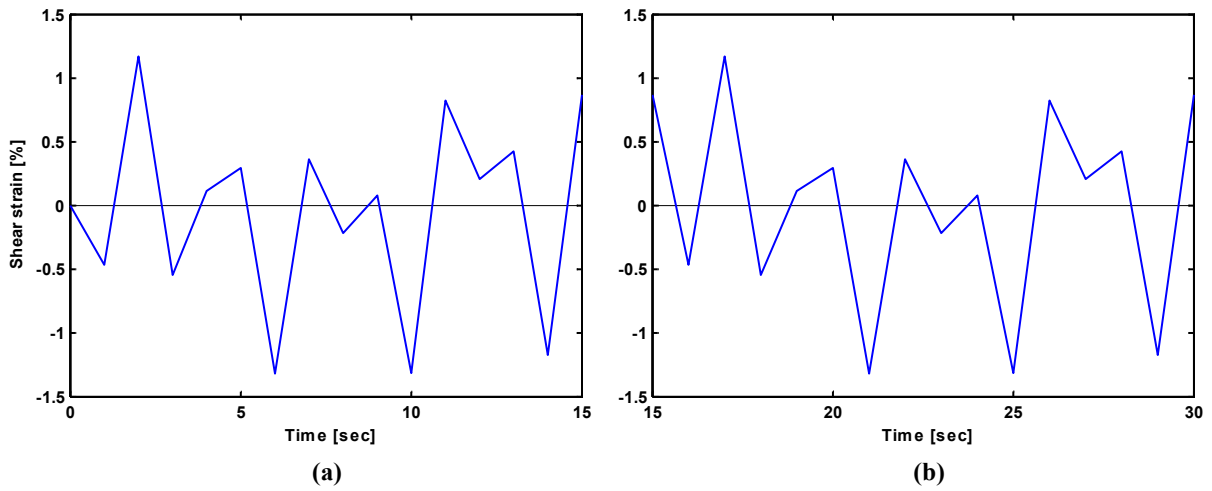


Figure 3.21: SP28 loading blocks: (a) first block; (b) subsequent blocks

Other VAL blocks of a different type were generated with repeated cycles within each block (SP57 and SP58). These loading blocks were obtained from the SP28 and SP17 randomly generated blocks by repeating each cycle counted (section 4.2) 50 times within each block. Figure 3.22 shows the loading history for the SP57 test.

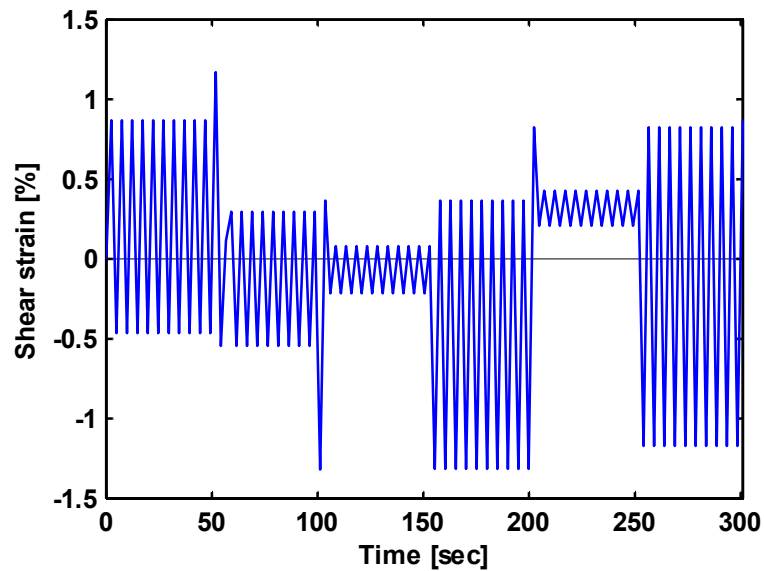


Figure 3.22: SP57 Loading block

For all VAL experiments, the maximum applied strain amplitudes for the axial and shear strain tests were 0.37 % and 1.24 %, respectively. Table 3.13 shows the experimental results obtained from the VAL histories, and Figure 3.23 shows a sample of the hysteresis loops obtained from one VAL test. Additional results are included in Appendix A.

Table 3.13: VAL experimental results

| Test | Max ϵ_a (%) [mm/mm] | Max γ_m (%) [rad] | N_f (no. of blocks) [cycles] |
|------|---------------------------------|-----------------------------|-----------------------------------|
| SP17 | 0.37 | 0 | 3903 |
| SP18 | 0.30 | 0 | 12616 |
| SP28 | 0 | 1.24 | 439 |
| SP57 | 0 | 1.24 | 7 |
| SP58 | 0.27 | 0 | 229 |

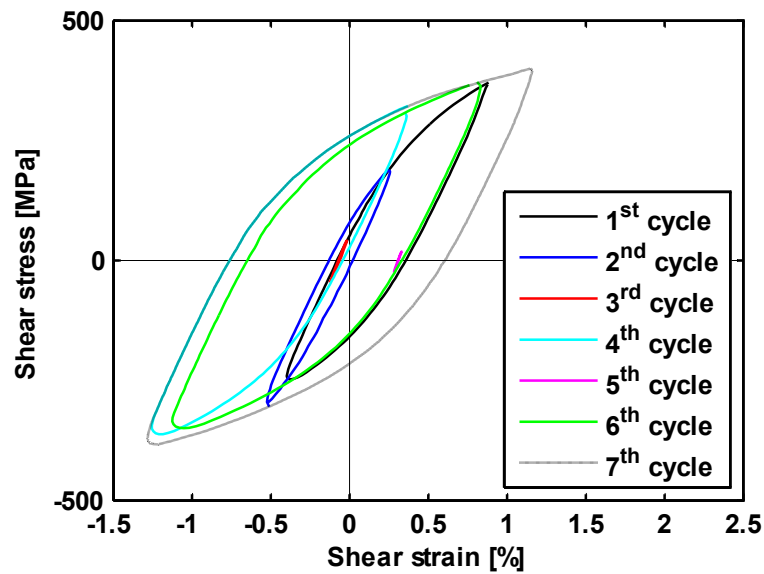


Figure 3.23: SP28 hysteresis loops

As the figure indicates, based on the VAL test, due to the variability in strain amplitudes within the loading block, the stress–strain response consists of a number of intersecting loops. To enable the use of the CAL fatigue parameters in order to estimate fatigue life for VAL tests, a proper cycle counting technique is required, as discussed in section 4.2.

Chapter 4

Fatigue Life Prediction

4.1 Introduction

This chapter presents the methods suggested and analysis used for predicting fatigue life. Section 4.2 provides details about the cycle counting method employed, including a flow chart and a sample of the counting results. Proposed modifications to damage accumulation methods are explained in section 4.3, along with their application to Manson's approach and the Marco–Starkey theory. A description and evaluation of an enhanced energy estimation method for the Jahed–Varvani (JV) model are included in section 4.4. Section 4.5 concludes the chapter with the presentation and discussion of the fatigue life estimation results for the constant amplitude loading (CAL), two-step, mean strain, and variable amplitude loading (VAL) experiments.

4.2 Cycle Counting Method

One of the primary factors under investigation in this study was the effect of load sequence on fatigue life. Since the stress–strain response of the material under VAL consists of several overlapping hysteresis loops (Figure 3.23), an appropriate cycle counting method that retains the applied strain sequence was required. Although the rainflow counting procedure suggested in ASTM standard [10] is commonly used, it requires that the applied VAL history be rearranged.

To examine the effect of load sequence on fatigue life, a rainflow counting procedure with no rearrangement of the loading history was employed. Figure 4.1 illustrates the flow chart that explains the counting of the cycles, which is performed through the following steps:

1. Read the loading block (repeated block) and count the number of data points in the block.
2. Provided that the first point in the block is zero, start the counting from the second point.
3. Count the cycle if the second strain range is equal to or greater than the previous range, and also if the signs of the two slopes differ.
4. Calculate the maximum strain, minimum strain, strain amplitude, and mean strain for each cycle counted.
5. Remove the counted cycle from the VAL history and begin counting again.
6. If the last point in the loading block is reached, end the counting process (loop).
7. From the lowest point to the highest point, add the last (largest) cycle that encompasses all previously counted cycles.

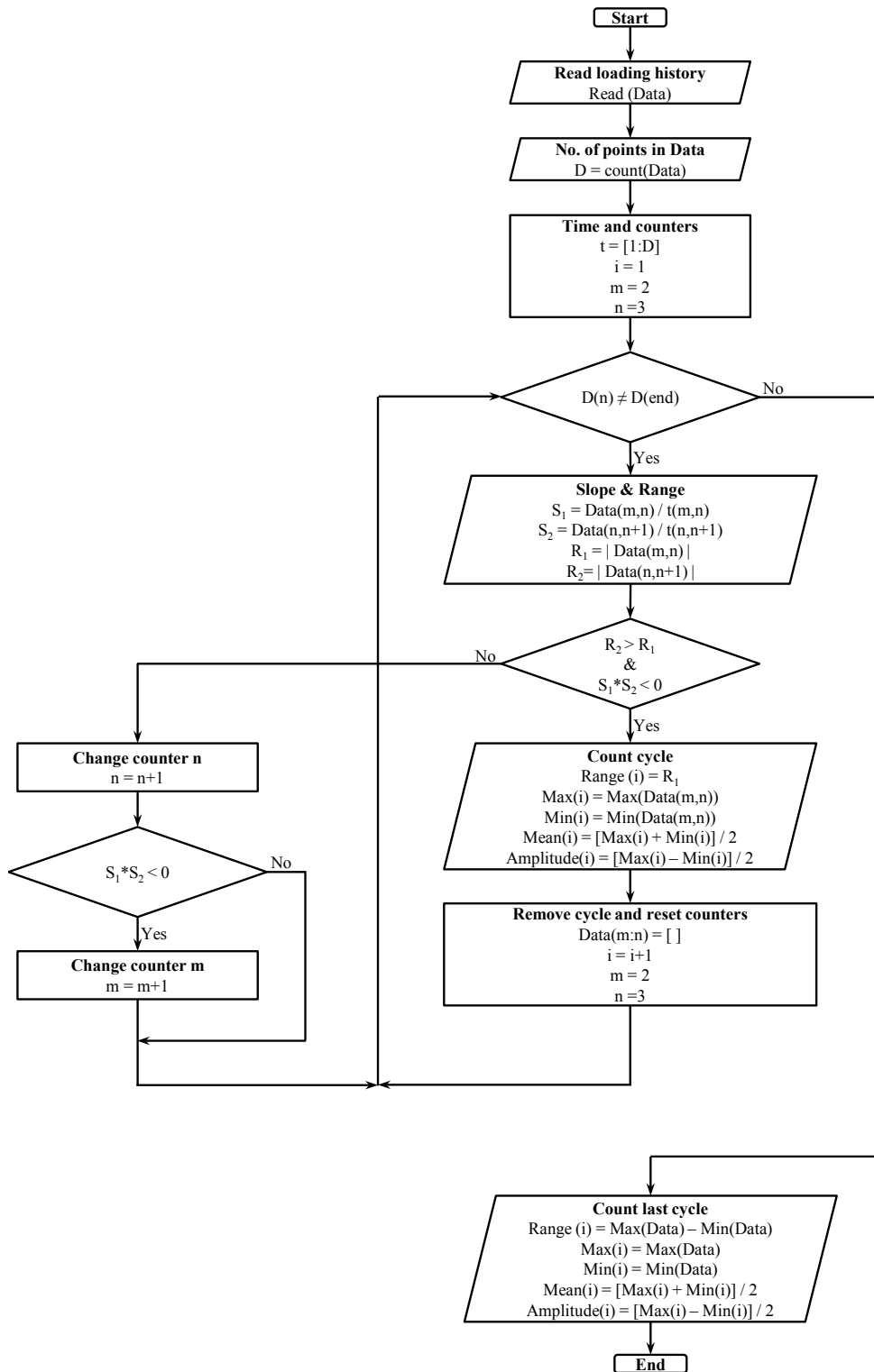


Figure 4.1: Rainflow counting flow chart

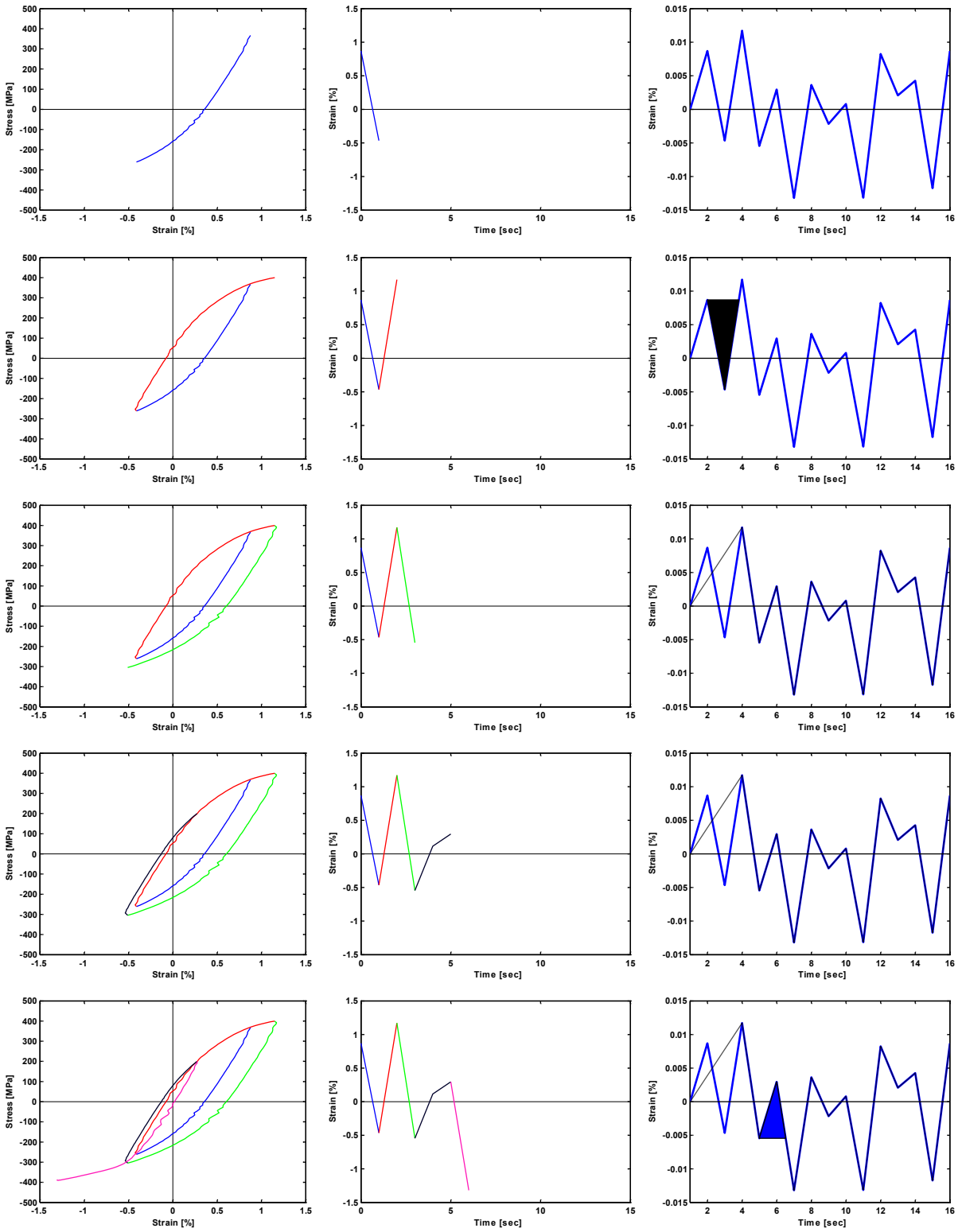


Figure 4.2: SP28 cycle counting steps

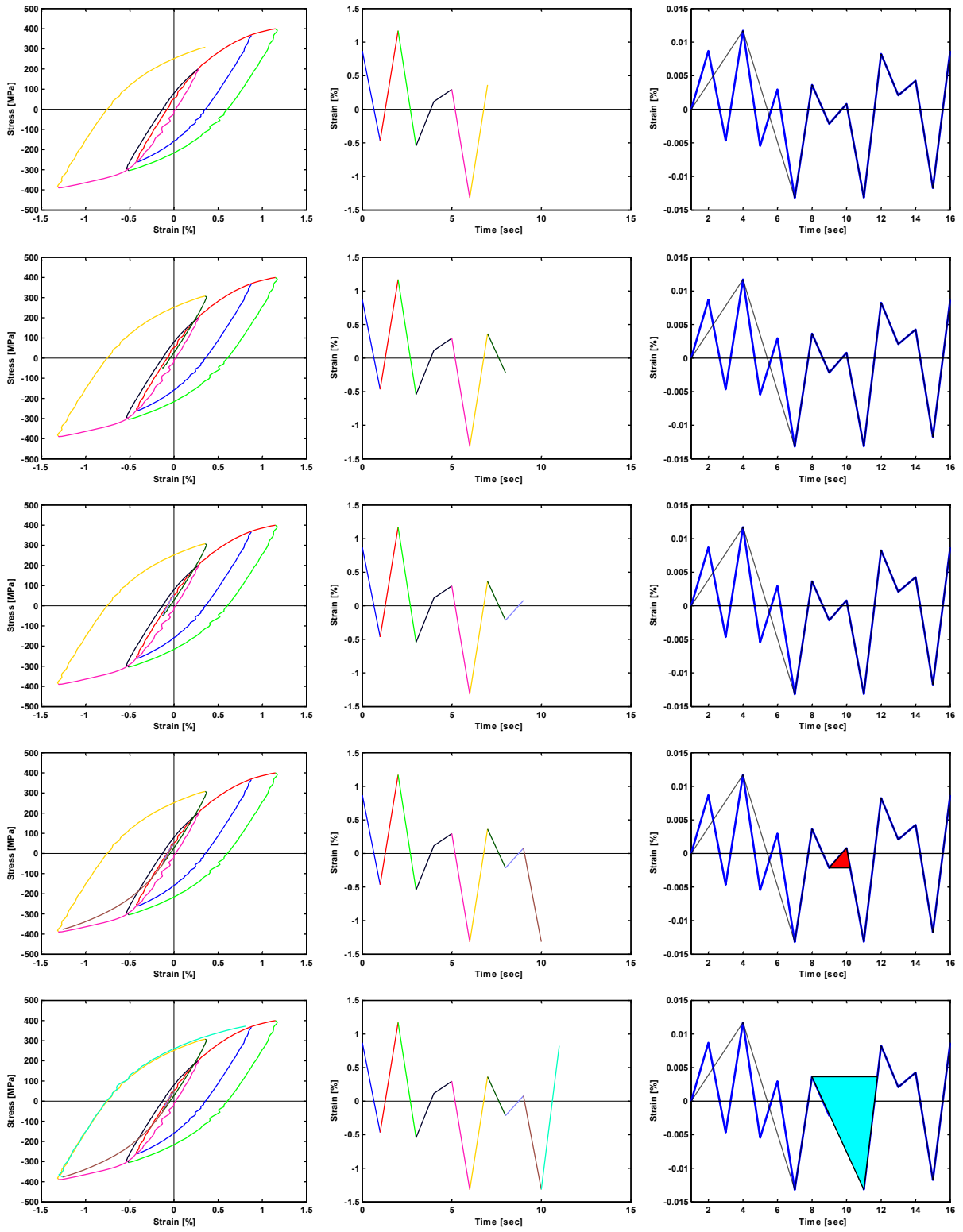


Figure 4.2: SP28 cycle counting steps (continued)

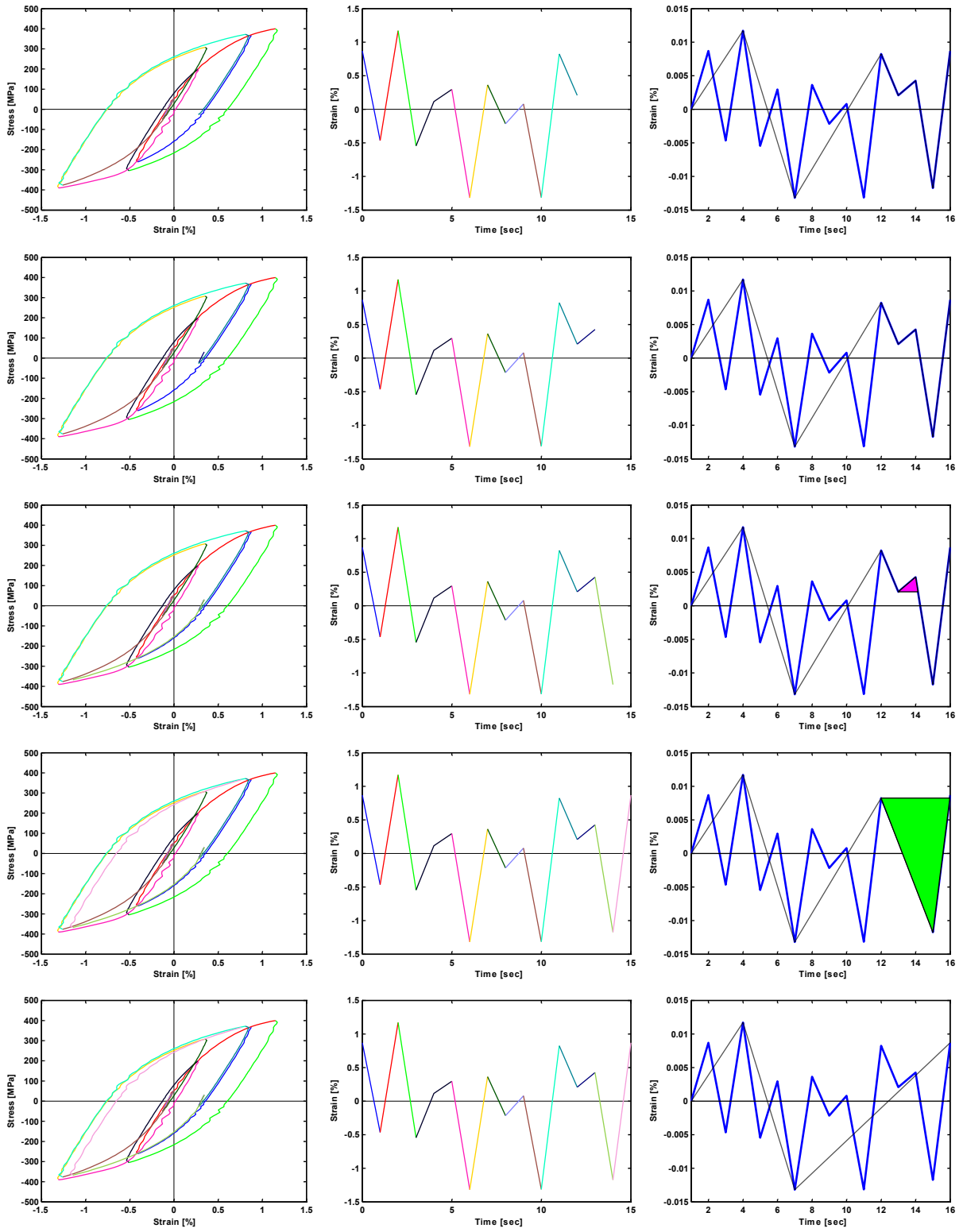


Figure 4.2: SP28 cycle counting steps (continued)

As can be seen from Figure 4.2, the counting method employed corresponds to the formation of closed hysteresis loops under VAL conditions. The code for counting the VAL cycles was developed in MATLAB and is included in Appendix B, and the cycle counting results for the SP28 shear test are listed in Table 4.1.

Table 4.1: SP28 cycle counting results

| Cycles counted | γ_a (%) [rad] | γ_{max} (%) [rad] | γ_{min} (%) [rad] | γ_{mean} (%) [rad] | $\Delta\gamma$ (%) [rad] |
|----------------|-------------------------|-----------------------------|-----------------------------|------------------------------|-----------------------------|
| 1 | 0.67 | 0.87 | -0.46 | 0.20 | 1.33 |
| 2 | 0.42 | 0.30 | -0.54 | -0.12 | 0.84 |
| 3 | 0.15 | 0.08 | -0.22 | -0.07 | 0.30 |
| 4 | 0.84 | 0.36 | -1.31 | -0.48 | 1.68 |
| 5 | 0.11 | 0.43 | 0.21 | 0.32 | 0.22 |
| 6 | 1.00 | 0.82 | -1.17 | -0.17 | 2.00 |
| 7 | 1.24 | 1.17 | -1.32 | -0.07 | 2.49 |

4.3 Damage Accumulation Method

Three damage accumulation methods were applied for the two-step and VAL experiments. The first method was the widely used Miner's rule, which does not account for the effect of load sequence on fatigue life. The other two methods were modified versions of Manson's approach and the Marco–Starkey theory. The three methods are discussed in detail in subsection 2.2.2, and the modifications applied to Manson's approach and the Marco–Starkey theory are explained below.

In Manson's approach, the convergence point (point A) is considered to be a material constant that must be obtained experimentally. This point is located on the virgin curve, with a suggested range from 10^2 to 10^3 cycles on the fatigue life axis [17, 18]. However, fatigue life predictions based on Miner's rule (as discussed later in section 4.5.2) imply that the effect of load sequence under pure shear loading is negligible compared to its effect under axial loading. The proposal was therefore to relate the number of reversals at point A to the number of reversals at point B. As can be seen from Figure 4.3, decreasing the distance between point A and point B increases the rotation angle between the virgin and the damaged curves. The most satisfactory fatigue life correlations were obtained when the number of reversals at point A was considered equal to 90 % of the number of reversals at point B for axial loading and 10% of the number of reversals at point B for shear loading.

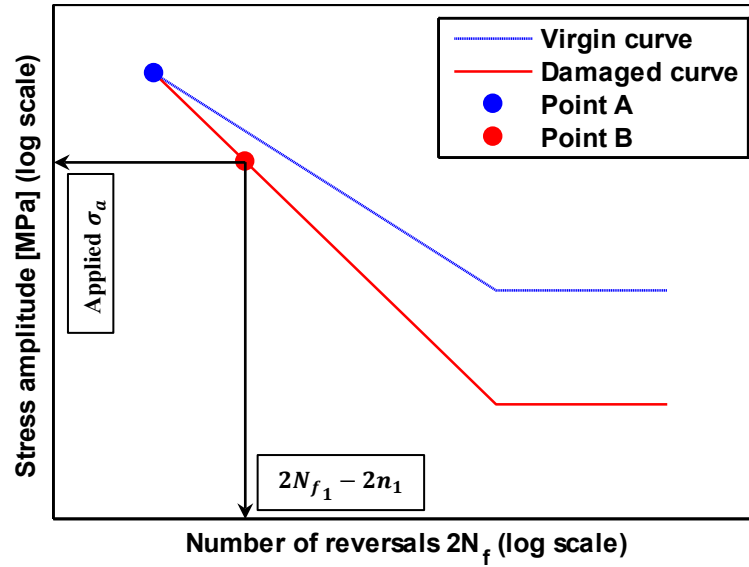


Figure 4.3: Applying Manson's approach to two-step loading (S-2N_f curve)

For the $S-2N_f$ curve shown in Figure 4.3, the damaged curve can be obtained from the line passing from point A through point B to the point corresponding to 10^6 cycles. Two coordinates are required for points A and B, which, for axial loading, can be obtained as

$$\text{Point B } (x) = 2N_{f_1} - 2n_1 \quad (4.1)$$

$$\text{Point B } (y) = \sigma_1$$

where $2N_{f_1}$ = number of reversals to failure at the 1st step stress amplitude

$2n_1$ = number of reversals applied at the 1st step

σ_1 = applied stress amplitude at the 1st step

$$\text{Point A } (x) = 90\% \text{ Point B } (x) \quad (4.2)$$

$$\text{Point A } (y) = \sigma_f'(\text{Point A } (x))^b$$

For shear loading, Equations (4.1) and (4.2) are applied after the axial fatigue parameters are replaced with the shear parameters and after the number of reversals at point A is changed ($\text{Point A } (x) = 10\% \text{ Point B } (x)$).

For the Smith–Watson–Topper (SWT), Fatemi–Socie (FS), and JV models employed in this study, the damaged fatigue life curve shown in Figure 4.4 can also be obtained from two points, each of which has three coordinates: elastic, plastic, and number of reversals. The number of reversals (x-coordinate) at point B and point A are defined as in Equations (4.1) and (4.2). However, the elastic and plastic coordinates at the two points are dependent on the fatigue life curve and are defined according to Equations (4.3), (4.4), and (4.5).

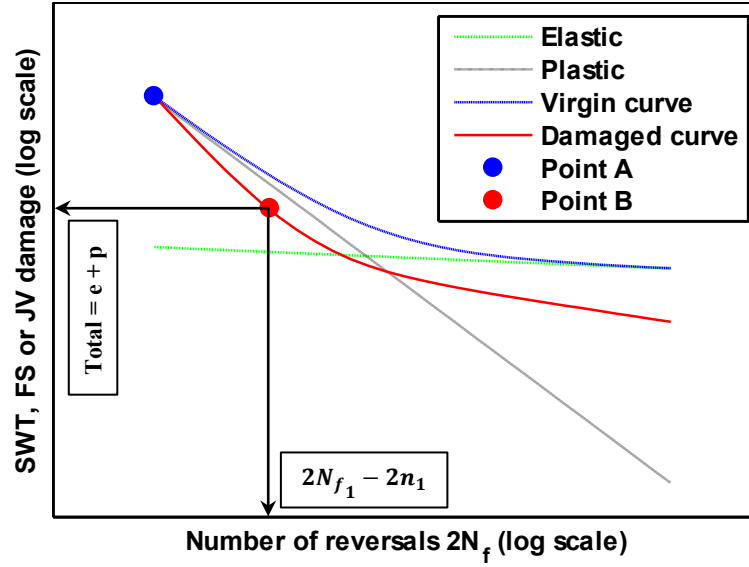


Figure 4.4: Applying Manson’s approach for two-step loading
 $(\epsilon_a-2N_f ; \gamma_a-2N_f ; \Delta E_{AX}-2N_f ; \Delta E_{SH}-2N_f$ curves)

$$\begin{aligned}
 \text{Point } B_{SWT} (y_e) &= \frac{\sigma_f'^2}{E} (2N_{f_1})^{2b} \\
 \text{Point } B_{SWT} (y_p) &= \sigma_f' \epsilon_f' (2N_{f_1})^{b+c} \\
 \text{Point } A_{SWT} (y_e) &= \frac{\sigma_f'^2}{E} (\text{Point } A (x))^{2b} \\
 \text{Point } A_{SWT} (y_p) &= \sigma_f' \epsilon_f' (\text{Point } A (x))^{b+c}
 \end{aligned}
 \tag{4.3}$$

$$\begin{aligned}
\text{Point } B_{FS} (y_e) &= \frac{\tau'_f}{G} (2N_{f_1})^{b_s} \\
\text{Point } B_{FS} (y_p) &= \gamma'_f (2N_{f_1})^{c_s}
\end{aligned} \tag{4.4}$$

$$\begin{aligned}
\text{Point } A_{FS} (y_e) &= \frac{\tau'_f}{G} (\text{Point } A (x))^{b_s} \\
\text{Point } A_{FS} (y_p) &= \gamma'_f (\text{Point } A (x))^{c_s}
\end{aligned}$$

$$\begin{aligned}
\text{Point } B_{JV} (y_e) &= E'_e (2N_{A_1})^B \\
\text{Point } B_{JV} (y_p) &= E'_p (2N_{A_1})^C
\end{aligned} \tag{4.5}$$

$$\begin{aligned}
\text{Point } A_{JV} (y_e) &= E'_e (\text{Point } A (x))^B \\
\text{Point } A_{JV} (y_p) &= E'_p (\text{Point } A (x))^C
\end{aligned}$$

where $2N_{A_1}$ is number of reversals predicted at the 1st step due to purely axial loading.

For shear loading, Equation (4.5) is applied after the axial fatigue parameters have been replaced with the shear parameters based on the fatigue life predicted due to purely torsional loading, N_{T_1} .

The Marco–Starkey theory [19] is based on a determination of a technique for calculating a critical value at which failure occurs. In Miner’s rule, this critical value is equal to one. However, for two-step loading, the critical value was found to be less than one for high-low (HL) tests and greater than one for low-high (LH) tests [3]. The nonlinear damage theory proposed by Marco and Starkey can be expressed as the following power relationship previously provided as Equation (2.4):

$$D = \sum \left(\frac{n_i}{N_{f_i}} \right)^{x_i} \tag{4.6}$$

where x_i is a quantity related to the i^{th} loading level (obtained experimentally).

Determining the value of the exponents x_i through numerous experiments could be costly and time-consuming. In this research, the proposal was to relate the nonlinear exponents to the predicted fatigue life values rather than to the applied strain amplitudes, with no additional experiments needed in order to obtain the values for the nonlinear exponents. The suggested method can be expressed as

$$D = \sum \left(\frac{n_i}{N_{f_i}} \right)^{1/x_i} \quad (4.7)$$

- where
- $x_i = 1$ for the shortest predicted life (highest applied strain)
 - $x_i = 0.1$ for the longest predicted life (lowest applied strain), with infinite lives ignored
 - $0.1 < x_i < 1$ for the predicted fatigue life values between the shortest and longest fatigue life values

Associating the exponent $x_i = 1$ with the highest level of the loading block makes this method applicable for CAL conditions. The change in the values of x_i from 0.1 to 1 can be a linear, exponential, logarithmic, or power-law function. The closest correlations between the predicted and the observed fatigue life values for the two-step and VAL tests are obtained when a linear trend is assumed, as explained in subsections 4.5.2 and 4.5.4.

Schematic representations of Equation (4.7) at different values for x_i , together with its application for HL, LH, and VAL conditions, are shown in Figure 4.5 and Figure 4.6.

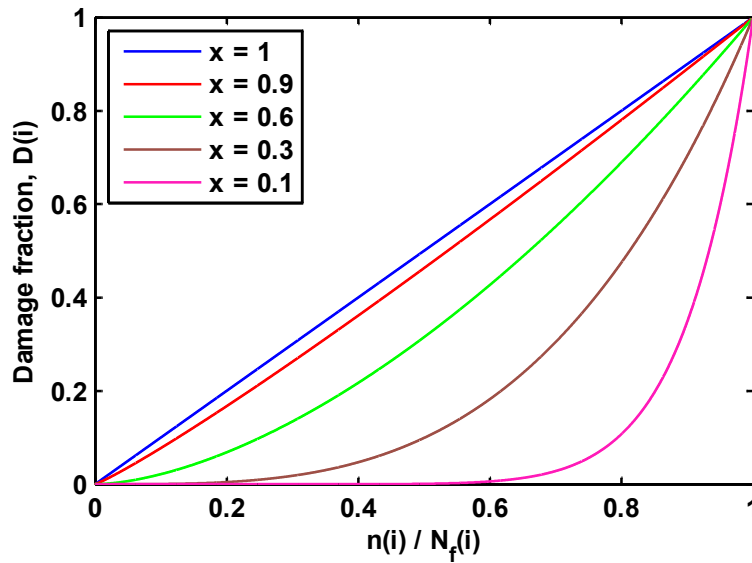


Figure 4.5: Schematic representation of Marco–Starkey damage curves

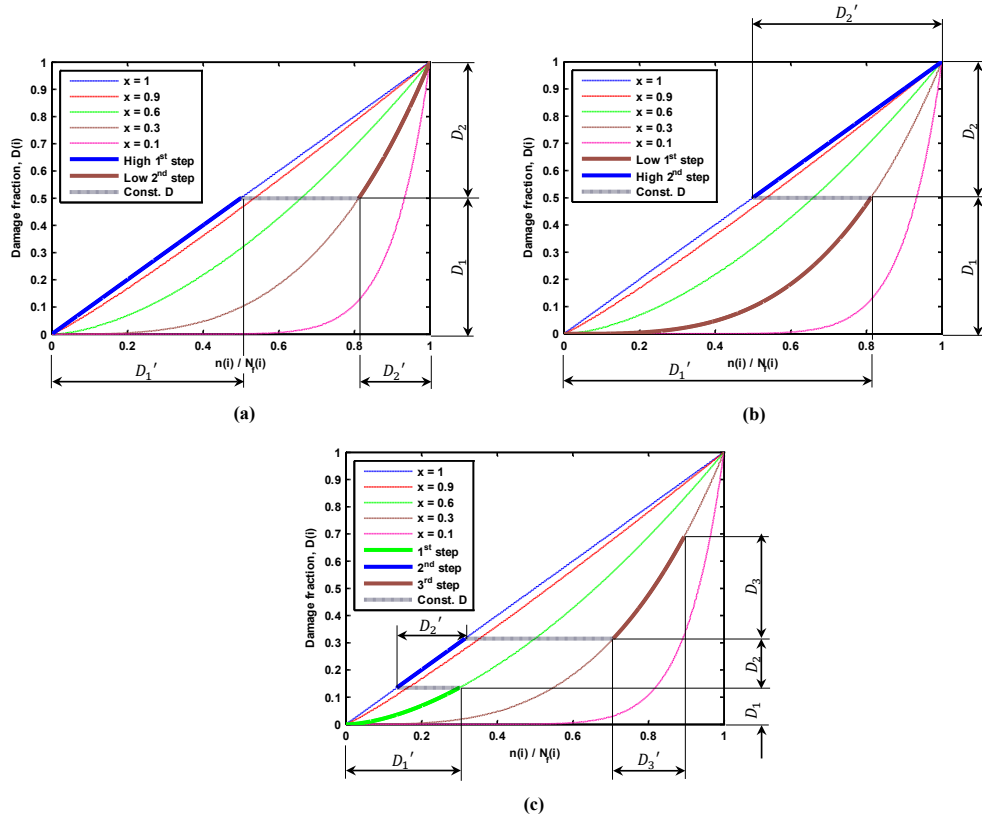


Figure 4.6: Application of the Marco–Starkey theory for (a) HL, (b) LH, (c) VAL

Figure 4.6 shows that $(D_1' + D_2')$ is less than one for the HL loading but greater than one for the LH test, which agrees with the experimental observations. The fatigue life for the two-step experiments can therefore be estimated as

$$N_f = \left[(D_1' + D_2') - \frac{n_1}{N_{f_1}} \right] N_{f_2} + n_1 \quad (4.8)$$

For the VAL history (Figure 4.6 (c)), in which the whole block is repeated until the point of failure, the predicted fatigue life can be calculated as

$$N_f = \frac{D_1' + D_2' + D_3'}{\left(\frac{n_1}{N_{f_1}} + \frac{n_2}{N_{f_2}} + \frac{n_3}{N_{f_3}} \right)} \quad (4.9)$$

4.4 Total Energy Estimation Method

In strain-based approaches, the fatigue life observed is related to the amplitude of the applied strain, whereas in the energy-based JV model, the fatigue life is related to the total energy density ($\Delta E_p + \Delta E_e^+$). Mean stress relaxation and cyclic softening are associated with 30CrNiMo8HH steel, and high levels of mean stress relaxation were observed with negligible half-life mean stress for the majority of the mean strain experiments conducted (excluding SP3, SP4, and SP15 for axial loading, and SP29 for shear loading), as shown in Figure 4.7. The assumption was therefore that the applied mean strain has no significant effect on the total energy density, and a relationship was proposed between the total energy density and the applied strain amplitude, in a manner similar to that employed with a Coffin–Manson curve. Figure 4.8 shows the axial and shear total energy–strain amplitude curves, and the total energy densities were determined based on the applied strain amplitude, as indicated in Equation (4.10).

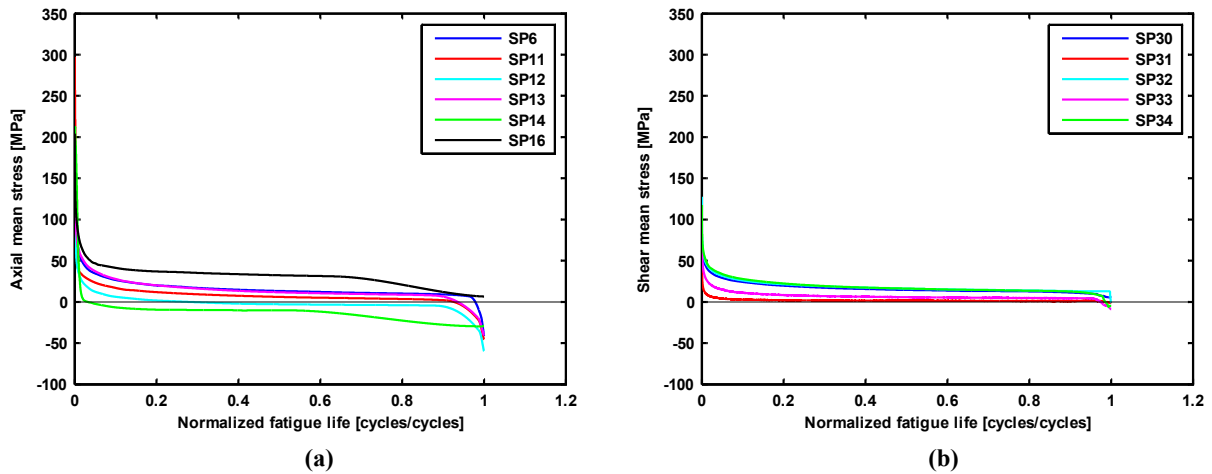
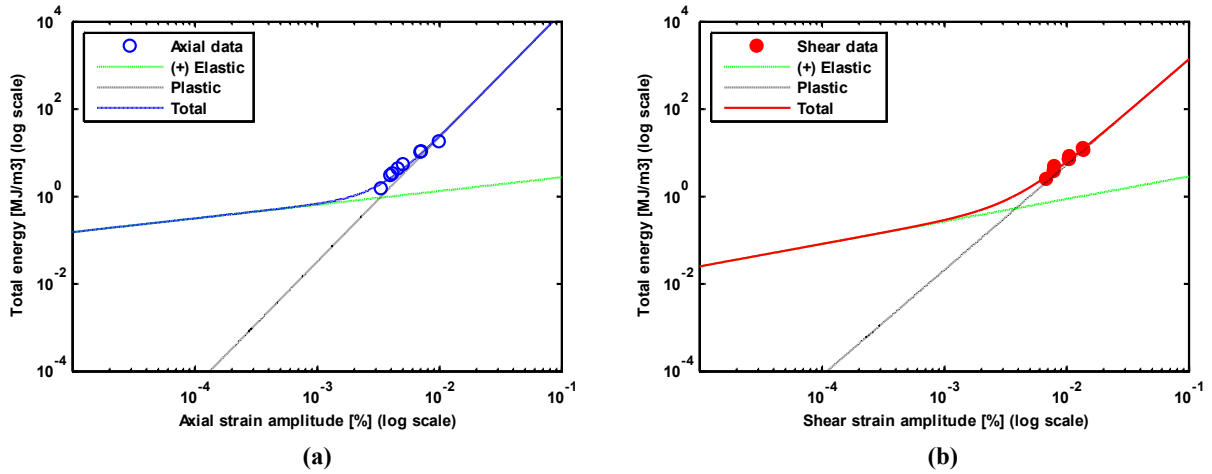


Figure 4.7: Mean stress relaxation: (a) axial loading; (b) shear loading



**Figure 4.8: Total energy–strain amplitude curves:
(a) pure axial loading; (b) pure torsion loading**

$$\begin{aligned}\Delta E_A &= 5.677(\varepsilon_a)^{0.313} + 10^7(\varepsilon_a)^{2.851} \\ \Delta E_T &= 9.398(\gamma_a)^{0.514} + 3.551 \times 10^5(\gamma_a)^{2.411}\end{aligned}\quad (4.10)$$

where ΔE_A = total axial energy density
 ΔE_T = total shear energy density
 ε_a = applied normal strain amplitude
 γ_a = applied shear strain amplitude

The evaluation of these formulas was based on a comparison of the predicted total energy densities with the total energy densities observed (calculated), as shown in Figure 4.9. The figure indicates that the total energy density predictions based on Equations (4.10) are in very good agreement with the values calculated. This formula was therefore employed for subsequent estimations of the total energy density for the counted cycles obtained from the VAL histories.

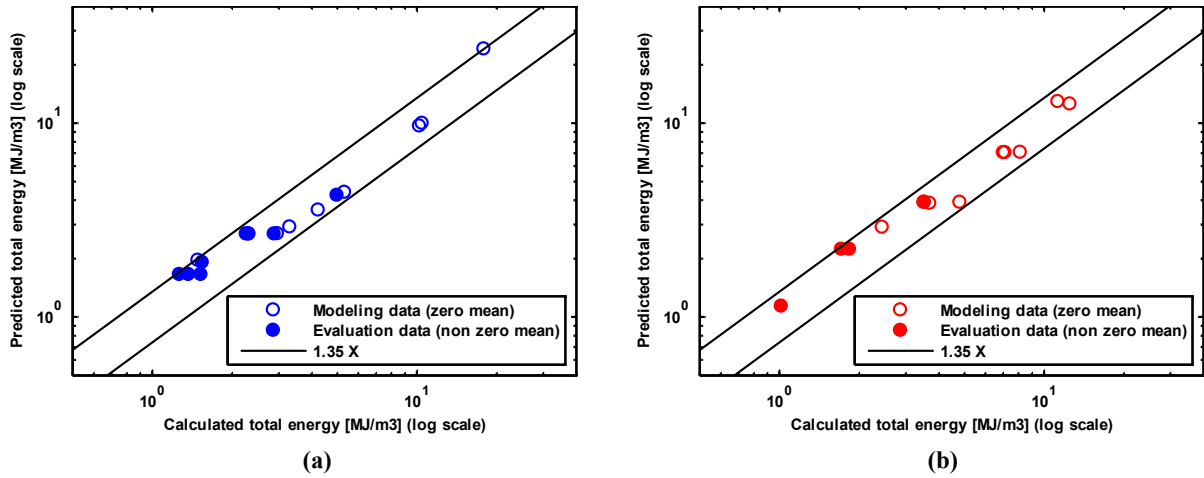


**Figure 4.9: Predicted versus calculated total energy density:
(a) pure axial loading; (b) pure torsion loading**

4.5 Fatigue Life Predictions

This section presents the fatigue life predictions derived from the three fatigue models employed: SWT, FS, and JV, which were discussed in detail in section 2.4. The predictions include those based on CAL, two-step, mean-strain, and VAL tests. To estimate the fatigue life results of two-step and VAL experiments, the three fatigue damage models were combined with the three damage accumulation methods: Miner's rule, the modified Manson's approach, and the modified Marco–Starkey theory. The cycle counting method discussed in section 4.2 was also essential for the VAL tests. For all tests, the fatigue life estimations were then compared with the observed life values.

4.5.1 Constant Amplitude Loading Tests

The axial and shear CAL data for this research were available from previous studies of 30CrNiMo8HH steel alloy [1, 2]. All CAL experiments were strain controlled and primarily in the LCF regime. Table 3.4 lists the CAL experimental results. The fatigue life predictions produced by the SWT, FS, and JV models were compared to the observed values, as shown in Figure below.

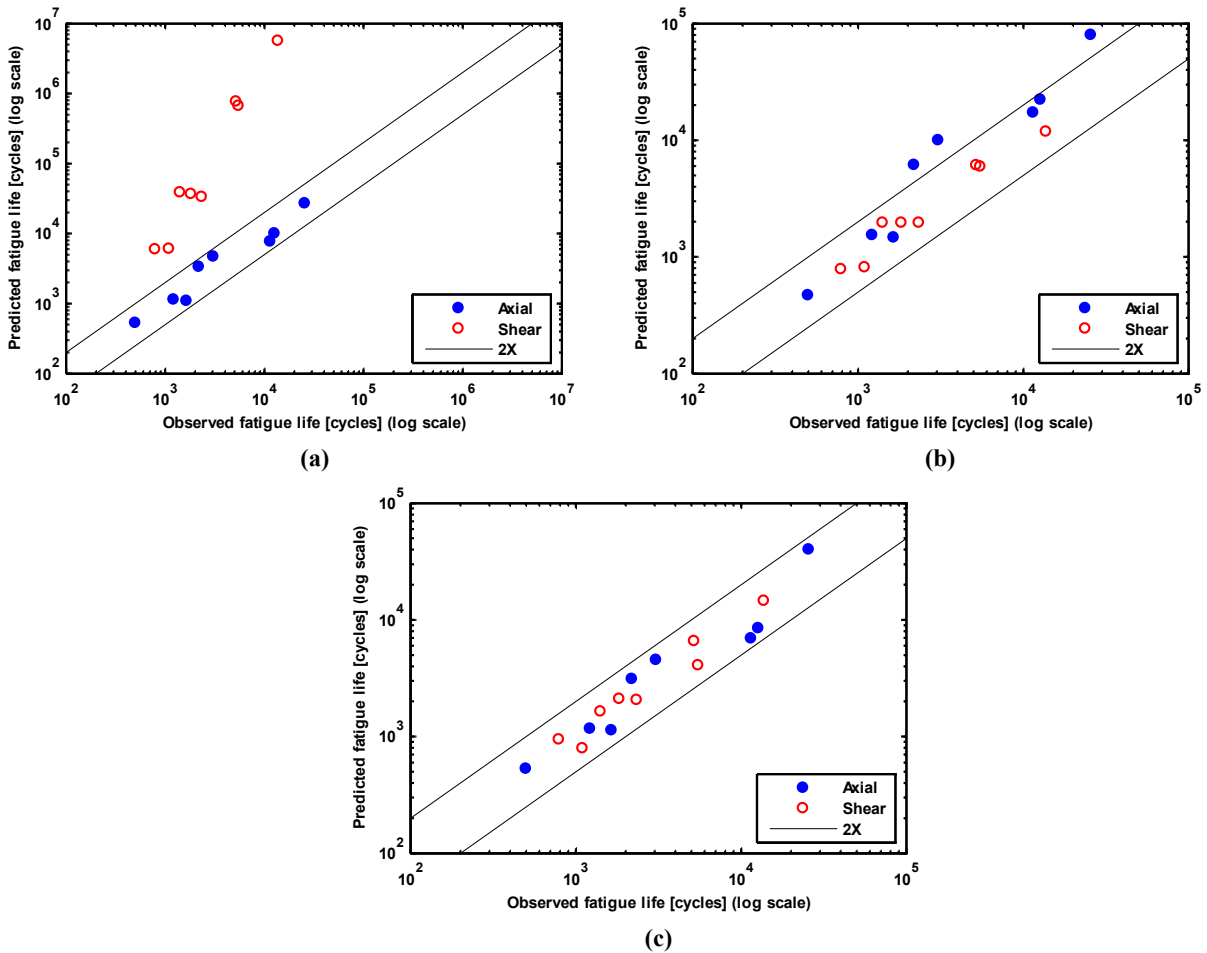


Figure 4.10: Fatigue life predictions for CAL tests: (a) SWT; (b) FS; (c) JV

As can be seen in Figure 4.10 (a), the SWT predictions for axial loading are within a factor of 2 but are overestimated for pure torsion loading because SWT predictions are based on axial fatigue properties with no additional parameters to account for shear loading. Although the FS fatigue damage model predicts fatigue life based only on shear fatigue properties, it also attempts to overcome SWT shortcomings through the use of a constant k , obtained from the fitting of the uniaxial data against the pure torsion data. This method results in improved fatigue life predictions for axial tests (Figure 4.10 (b)). The fatigue life equation proposed by Jahed and Varvani utilizes both axial and shear energy-based fatigue properties and hence produces superior fatigue life correlations, as illustrated in Figure 4.10 (c).

4.5.2 Two-Step Loading Tests

The fatigue life estimations for the HL and LH axial and pure torsion loading experiments required the application of a fatigue damage prediction model in conjunction with the damage accumulation method. The Miner's, Manson's, and Marco–Starkey damage accumulation methods discussed in subsection 2.2.2 and 4.3 were combined with the SWT, FS, and JV fatigue damage prediction models in order to produce the fatigue life estimations for the two-step tests. The experimental results for the axial and shear two-step experiments are shown in Table 3.8 and Table 3.9, respectively.

If load sequence in fact has no effect on fatigue life, the Miner's rule approach would be expected to result in good fatigue life correlations. However, Figure 4.11 shows that the fatigue predictions for the HL axial loading tests (SP7 and SP9) are overestimated compared to those for the LH axial tests. On the other hand, disregarding the SWT fatigue predictions, the fatigue life predictions for the pure torsion two-step loading experiments are satisfactory for both the HL and LH tests. With respect to the applied strain amplitudes, these findings mean that load sequence has a greater effect on axial loading than on shear loading.

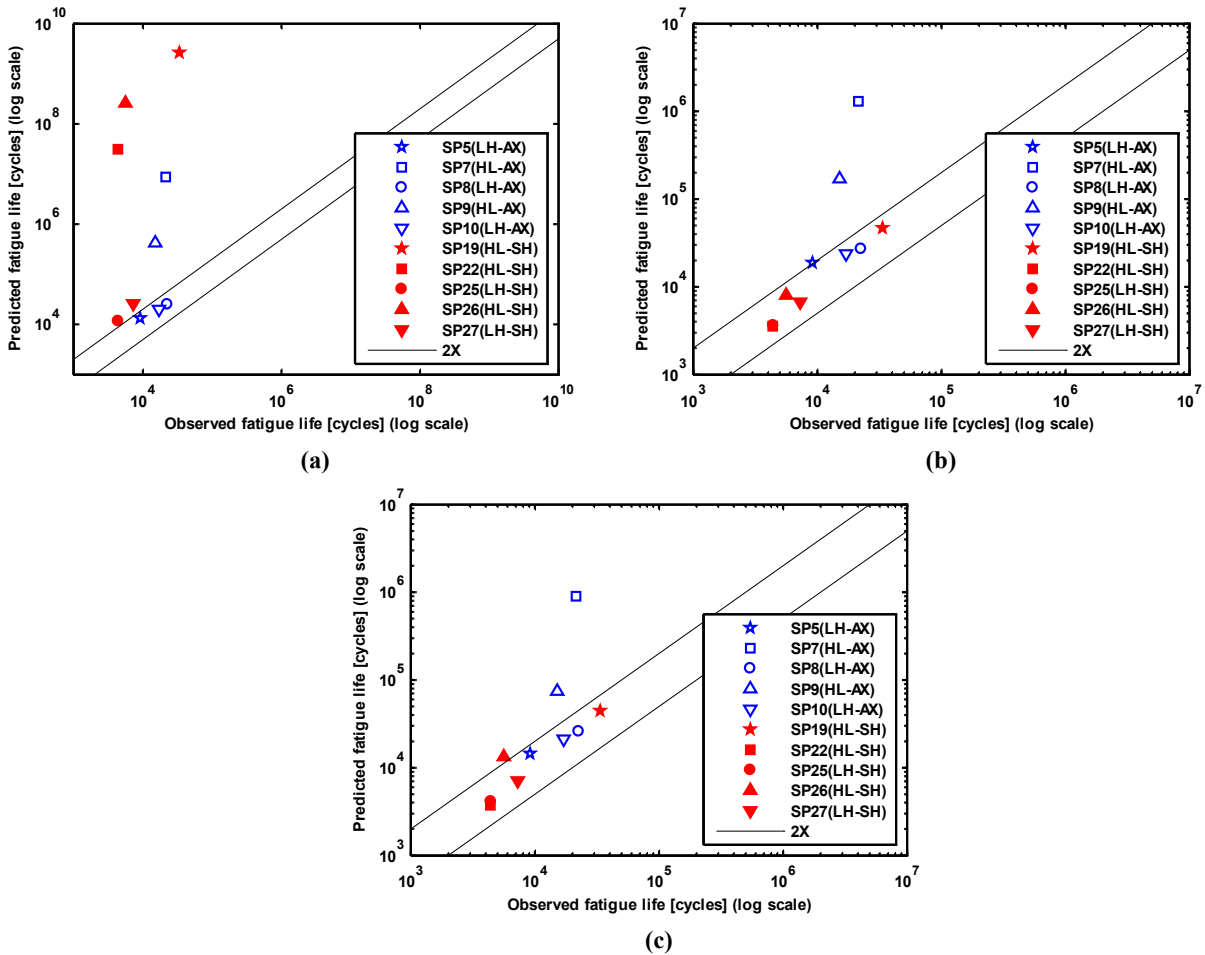


**Figure 4.11: Miner’s rule and fatigue life predictions for two-step loading:
(a) SWT; (b) FS; (c) JV**

In an attempt to overcome the shortcomings of the Miner’s rule approach by accounting for the effect of load sequence on fatigue life, two other damage accumulation methods were considered: a modified version of Manson’s approach and a method based on modifications to the Marco–Starkey theory.

Manson’s approach accounts for the effect of load sequence through a rotation of the fatigue life curve that is dependent on the pre-loading cycles. To avoid any experimentally determined constants, the convergence point between the virgin and the damaged curves was related to the known second point, as explained in section 4.3. Figure 4.12 shows that the application of the modified Manson’s approach improved the fatigue predictions produced for the HL axial tests while maintaining acceptable limits for most of the fatigue life predictions from the other experiments.

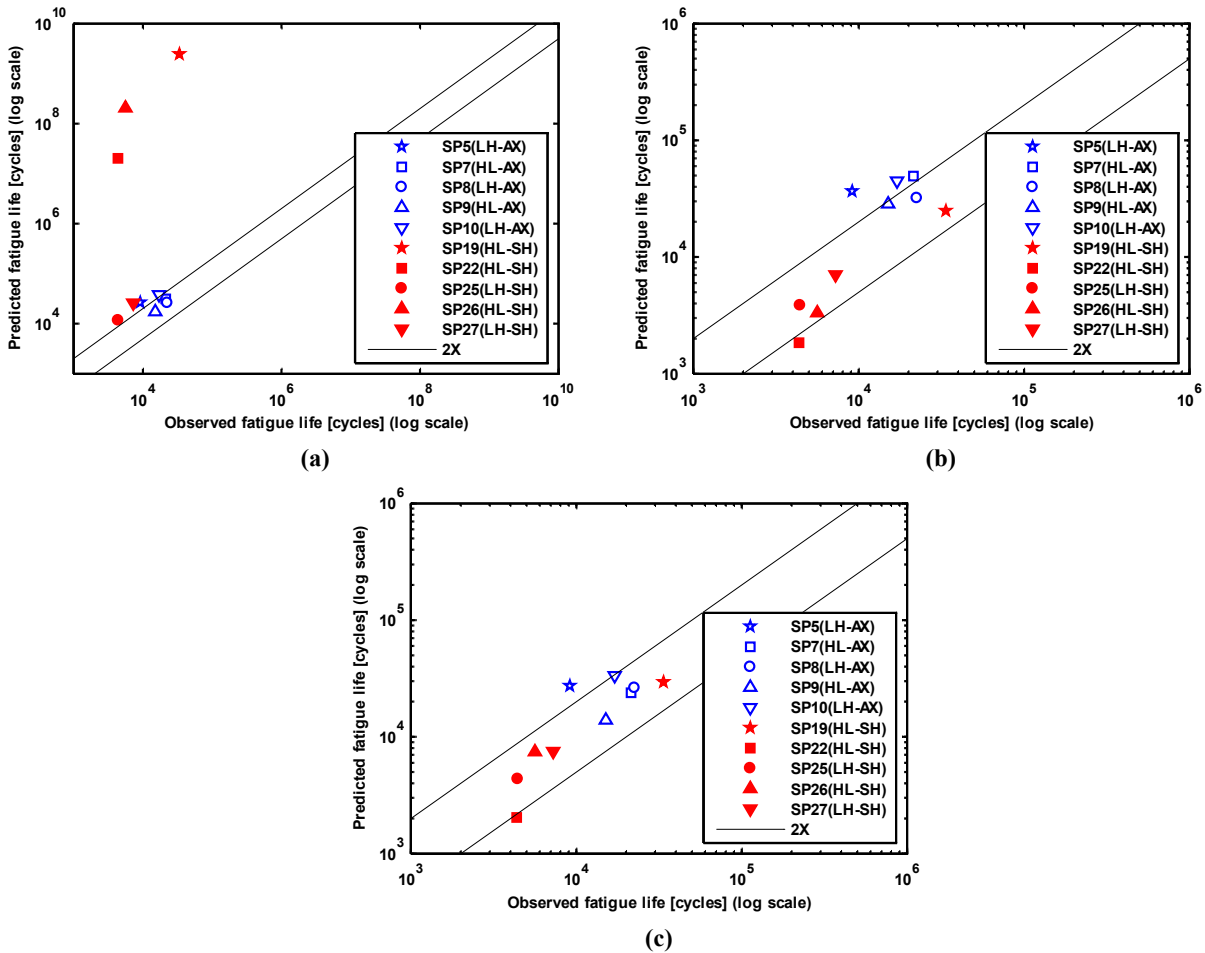


Figure 4.12: Manson’s approach and fatigue life predictions for two-step loading: (a) SWT; (b) FS; (c) JV

The Marco–Starkey theory is another damage accumulation method that takes into account the effect of load sequence on fatigue life through the definition of multiple damage curves (Figure 2.4) that are dependent on the applied strain amplitudes. As explained in section 4.3, this theory was modified by relating the damage curves to the fatigue life predictions, which eliminates the experimentally determined constants required for this method. A slight improvement in the fatigue life predictions produced for the HL axial experiment can be noticed when the modified Marco–Starkey theory is applied, but the fatigue life estimations for some pure torsion two-step loadings were inaccurately underestimated, as shown in Figure 4.13.

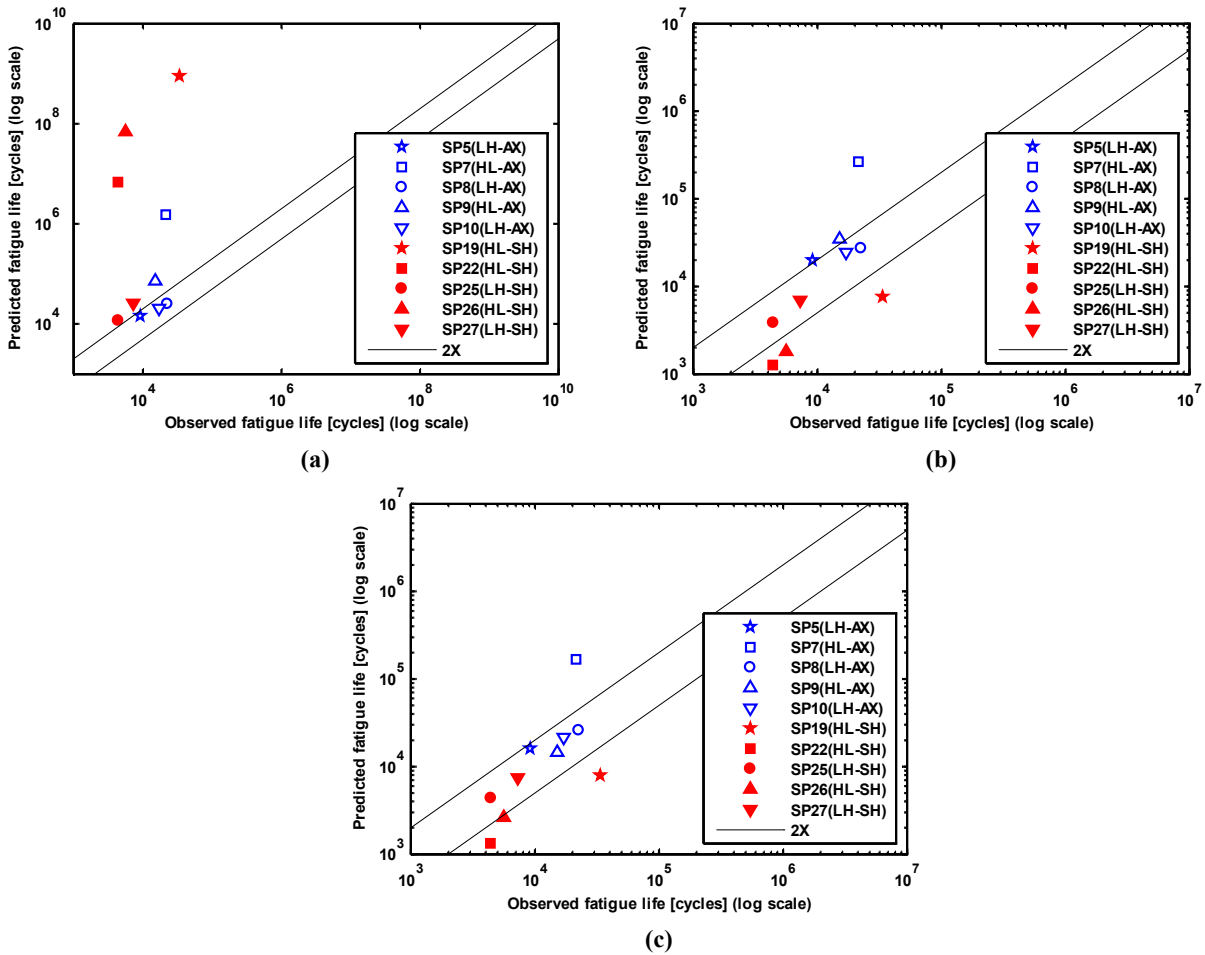
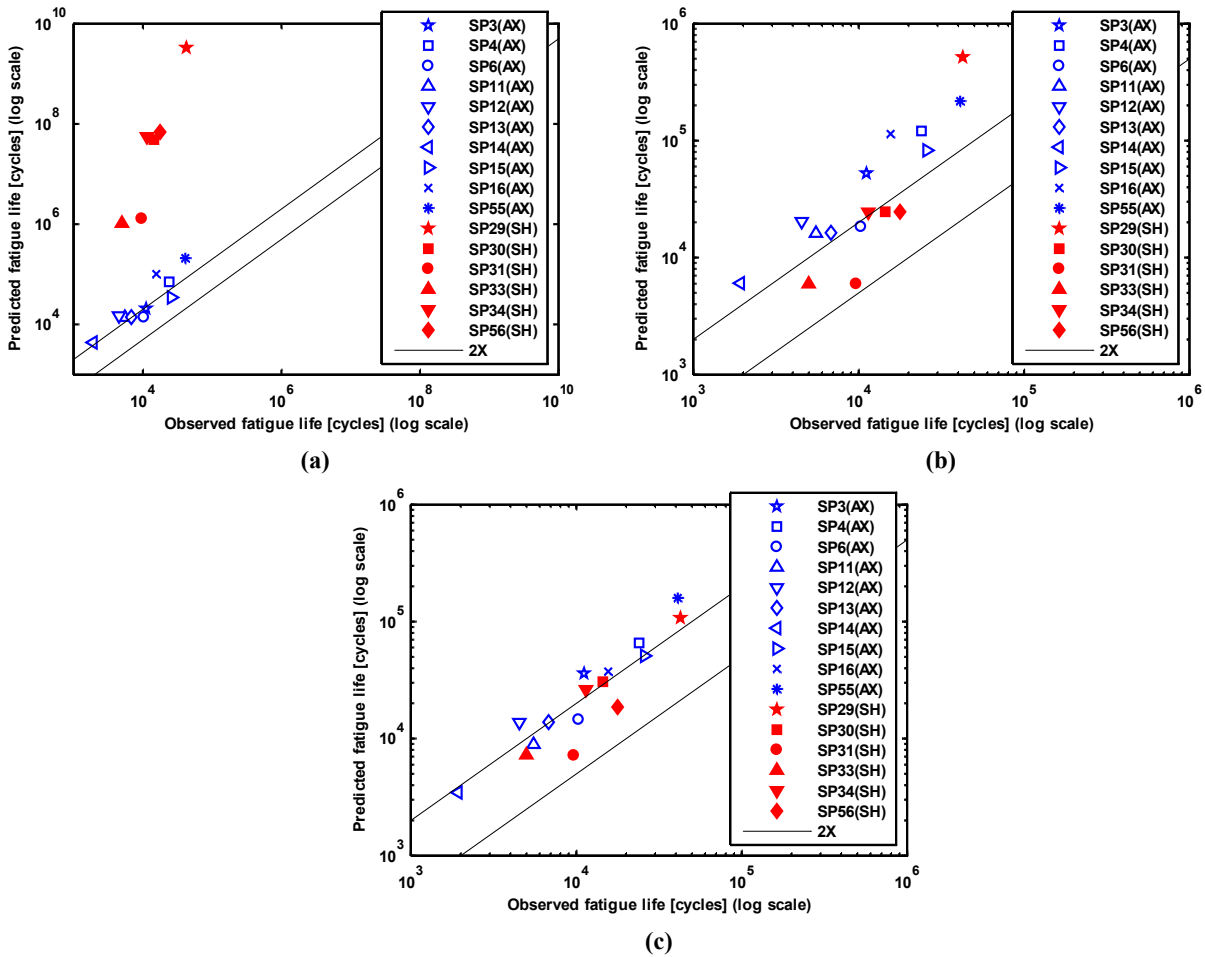


Figure 4.13: Marco–Starkey theory and fatigue life predictions for two-step loading: (a) SWT; (b) FS; (c) JV

4.5.3 Mean Strain Loading Tests

The SWT, FS, and JV fatigue damage models employed were expected to take into account the mean stress effect. In the SWT and FS models, the mean stress effect is incorporated with the normal stress on the critical planes, whereas in JV model it is considered through the positive elastic energy. The results of the axial and shear mean strain experiments are shown in Table 3.10 and Table 3.11, respectively. The fatigue life predictions from the three fatigue damage models employed are shown in Figure 4.14.



**Figure 4.14: Fatigue life predictions for mean strain tests:
(a) SWT; (b) FS; (c) JV**

As can be seen from Figure 4.14, some of the experimental results are correlated within a factor of 2, but others are overestimated. The SWT predictions (ignoring the pure torsion data) are satisfactory for approximately half of the tests, whereas the FS predictions are slightly overestimated for the axial tests. Superior fatigue life predictions for the mean strain data were obtained from the JV model with a narrower scatter band. The fatigue life overestimations can be attributed to the low values of mean stress at the stable hysteresis loops due to the mean stress relation behaviour of the 30CrNiMo8HH steel alloy.

4.5.4 Variable Amplitude Loading Tests

The estimation of fatigue life for the VAL tests required a combination of fatigue damage prediction models, cycle counting, and the damage accumulation method. Since load sequence was one of the factors under investigation, the cycle counting method employed in this research maintains the sequence of the applied cycles, as explained in section 4.2. The stable hysteresis loops used in the SWT and FS models were extracted from the actual VAL history (e.g., Figure 4.2), whereas the total energy density estimations used in the JV model were based on Equation (4.10), as discussed earlier in this chapter. The experimental results obtained from the VAL tests were tabulated as shown in Table 3.13, and the fatigue life estimations produced by the three damage accumulation methods and the three fatigue damage models are discussed below.

The fatigue life estimations based on Miner's rule are shown in Figure 4.15. The fatigue life predictions based on the SWT model are overestimated for all VAL tests, whereas the predictions obtained from the FS model are satisfactory for pure torsion loading but none conservative for axial loading. The fatigue life estimations produced by the JV model are satisfactory for both axial and pure torsion loading.

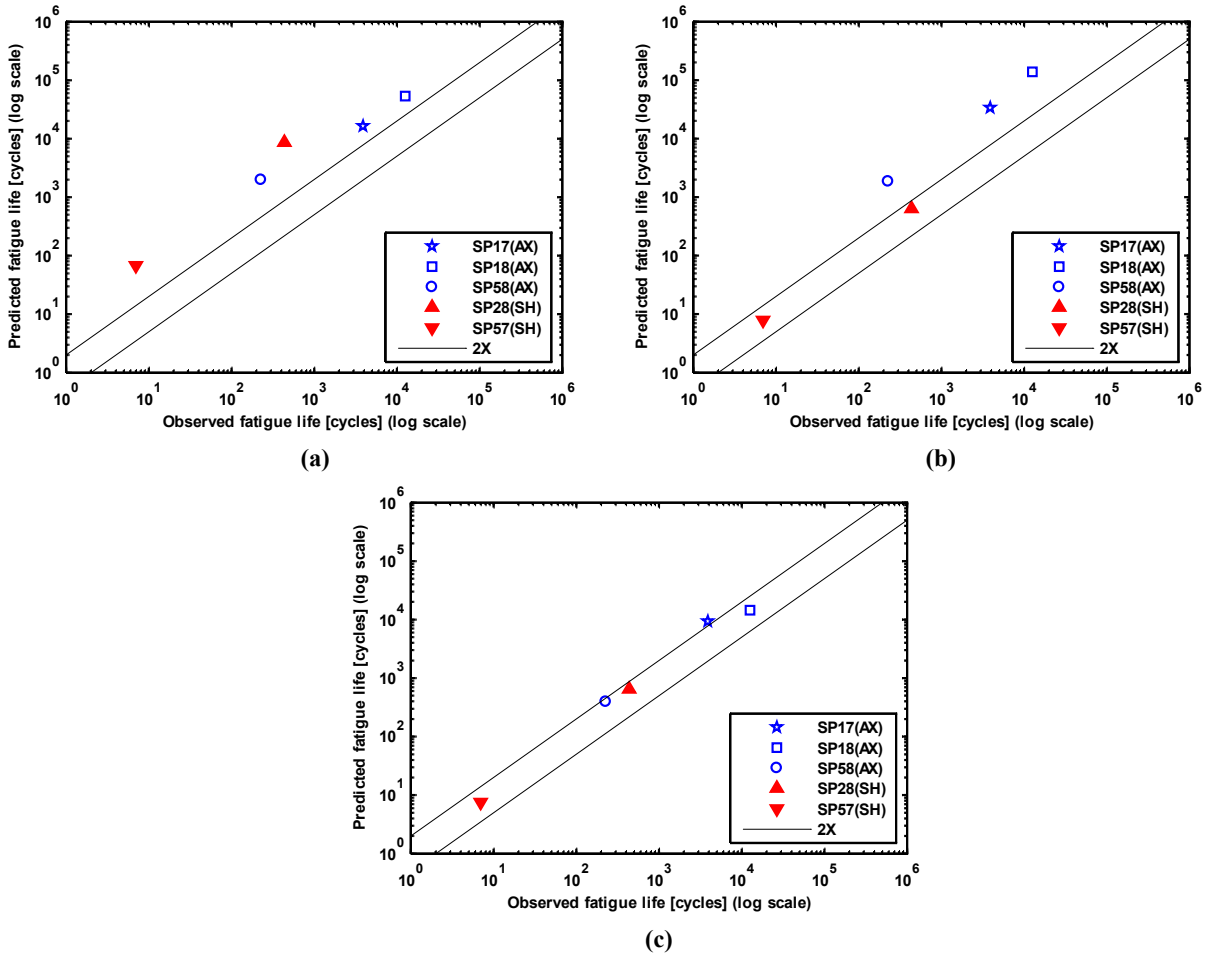


**Figure 4.15: Miner's rule and fatigue life predictions for VAL:
(a) SWT; (b) FS; (c) JV**

The modified Manson's approach was then applied in combination with the three fatigue damage models in order to determine fatigue life predictions for the VAL tests. For experiments SP17, SP18, and SP28, the loading blocks consist of several randomly generated cycles with no repeated cycles within the loading block ($2n_1 = 2$ in Equation (4.1)). Therefore, point B, used for modifying the fatigue life curve, is located approximately on the virgin curve ($2N_{f_1} - 2 \approx 2N_{f_1}$), and hence both point A and point B are on the virgin curve. This circumstance resulted in fatigue life estimations equivalent to those based on Miner's rule, as can be seen from a comparison of Figure 4.15 and Figure 4.16. No significant improvement in fatigue life predictions was noticeable in the results produced for the VAL block with repeated cycles (SP57 and SP58).

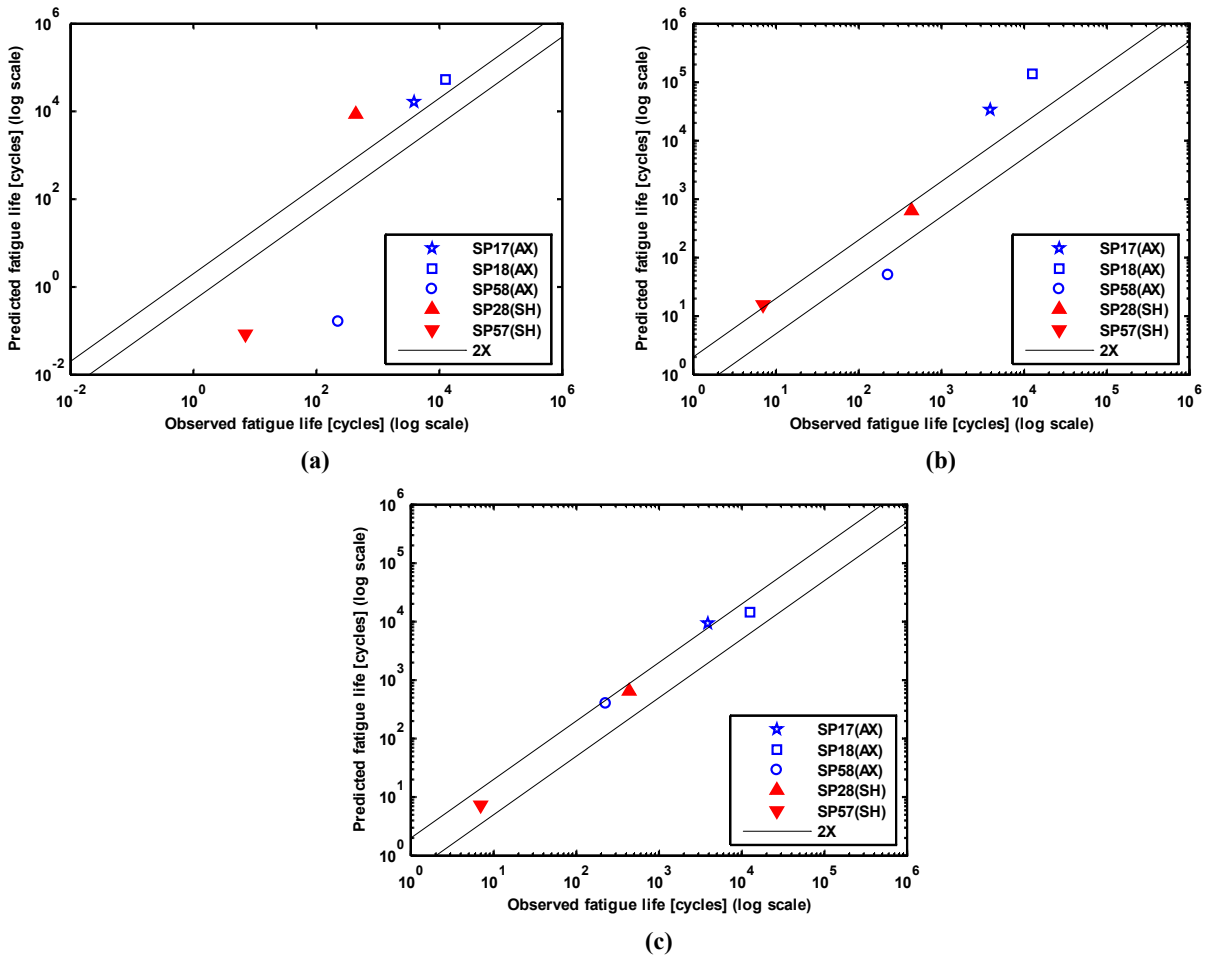


**Figure 4.16: Manson’s approach and fatigue life predictions for VAL:
(a) SWT; (b) FS; (c) JV**

The final step was to use the modified Marco–Starkey theory as the damage accumulation method for predicting the fatigue life for the VAL tests. A detailed discussion of this theory can be found in subsection 2.2.2.3 and section 4.3. Although the fatigue life predictions for the two-step loading experiments based on this damage accumulation method were not promising (Figure 4.13), the modified method based on the Marco–Starkey theory did improve the fatigue life predictions produced by the SWT, FS, and JV models for the VAL tests, as can be seen in Figure below.

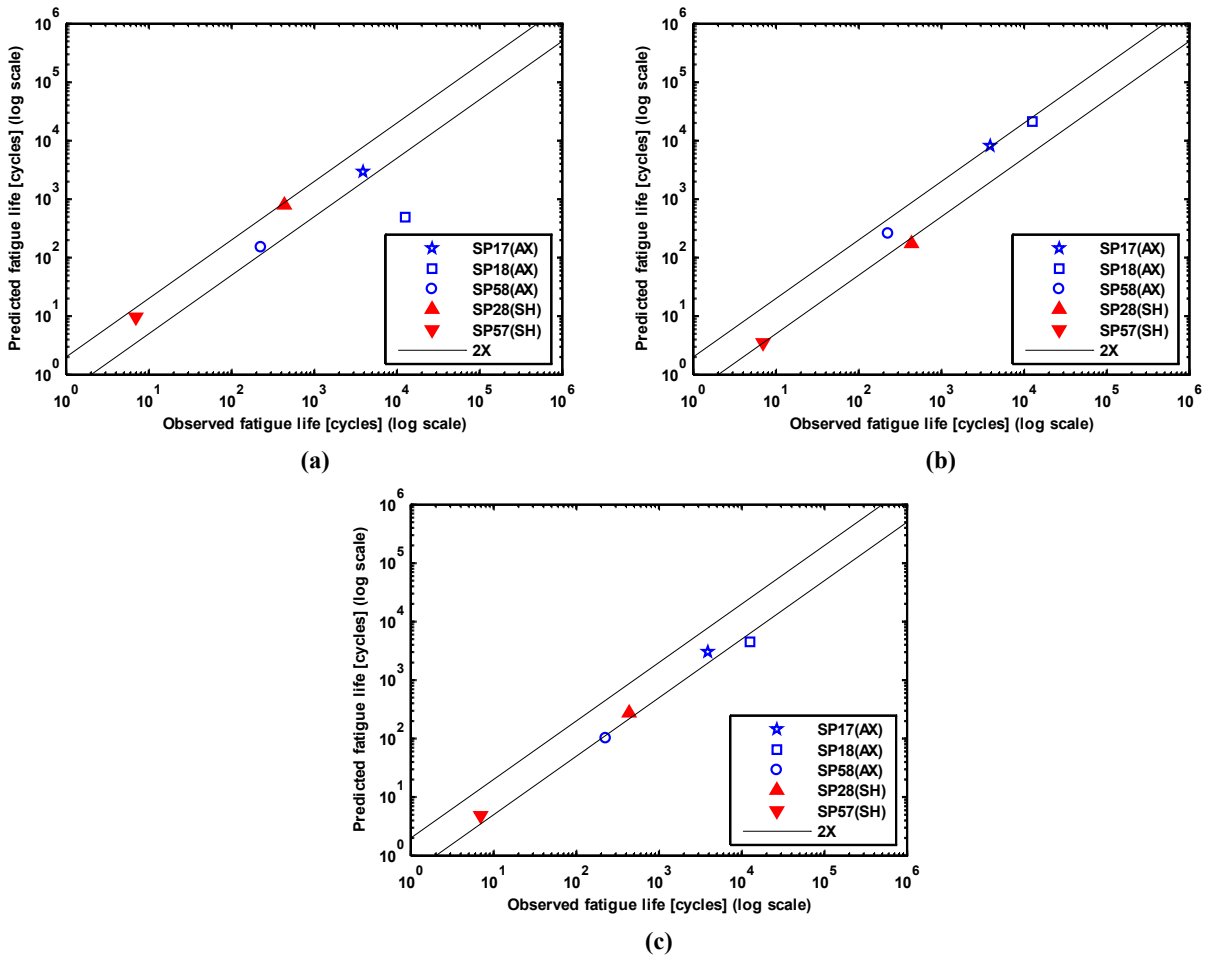


Figure 4.17: Marco–Starkey theory and fatigue life predictions for VAL:
 (a) SWT; (b) FS; (c) JV

Chapter 5

Summary, Conclusions, and Recommendations

5.1 Summary

Accurate estimations of the fatigue life of a component subjected to variable amplitude loading (VAL) require the incorporation of several factors included in VAL histories. This study investigated the effects of load sequence and mean stress on the fatigue life of nickel-chromium-molybdenum 30CrNiMo8HH steel alloy. The monotonic and constant amplitude loading (CAL) data were available from a previous study, and three sets of additional experiments were performed: two-step loading, non-zero mean strain loading, and VAL. Three fatigue life prediction models were also employed: Smith–Watson–Topper (SWT), Fatemi–Socie (FS), and Jahed–Varvani (JV). The fatigue life predictions for the axial CAL data were within the desired scatter band of 2, with the exception of a few overestimated data points predicted by the FS model. With respect to the pure torsion CAL data, only the fatigue life predictions produced by the JV and FS models were satisfactory.

The determination of the effect of load sequence on fatigue life was based on a comparison of the fatigue life results of the two-step high–low (HL) and low–high (LH) tests. The individual damage amounts were summed according to the Miner, Manson, and Marco–Starkey damage accumulation methods. Miner’s rule is considered the simplest method but it fails to account for the effect of load sequence, and hence resulted in overestimated fatigue life predictions for the HL axial loading data. Manson’s approach and the Marco–Starkey theory were modified based on the fatigue life observations from the two-step experiments in order to eliminate the use of empirically determined constants. The application of the modified damage accumulation approaches resulted in all three fatigue models producing improved two-step fatigue life predictions.

A number of non-zero mean strain experiments were performed in order to monitor the effect of mean stress on fatigue life. To help distinguish between the effect of strain amplitude and that of mean strain, a two-level factorial design was used for this set of experiments. The statistical analyses of the non-zero mean strain experiments revealed two empirical relations that correlate the applied strain amplitude and mean strain with fatigue life and plastic energy density. When the empirically derived relations were evaluated, it was concluded that those correlations cannot be generalized for zero mean strain loading, and the effect of mean stress on fatigue life was therefore considered using the three fatigue models employed. With the exception of the SWT prediction for shear data, the fatigue life predictions for the mean strain data ranged from the acceptable limit of ± 2 to values that are slightly overestimated. A narrower scatter band was produced by the JV model.

For the VAL experiments, the cycles were counted using a rainflow counting procedure, which does not change the sequence of the applied strain. This procedure follows exactly the stress–strain response of the material so that the hysteresis loops for the counted cycles can be extracted from the test output. A new method for estimating the total energy density required for the energy-based JV model was developed. This method assumes that the applied mean strain has no significant effect on the total energy density so that the total energy density can therefore be related to the applied strain amplitude. Those correlations resulted in very good agreement between the estimated and the calculated total energy densities, so they were incorporated into the VAL fatigue life predictions based on the JV model. Satisfactory fatigue life estimations were obtained by the SWT and FS models after the application of the modified Marco–Starkey damage accumulation theory. For all the damage accumulation methods employed, the fatigue life predictions produced by the JV model were accurate within a factor of 2.

5.2 Conclusions

Based on the experimental observations and the fatigue life prediction procedures, the following conclusions can be drawn:

1. For all types of loading considered in this study, the most satisfactory fatigue life correlation are obtained using the energy-based JV model. This finding can be attributed to the fact that the JV fatigue life equation includes both axial and shear energy-based terms. The fatigue life estimations based on the FS model are also sound for both axial and shear data. With the SWT model, only the fatigue life predictions for axial loading are acceptable.
2. The comparison of the results of the HL and LH experiments demonstrate that load sequence does have an effect on fatigue life. The application of the linear damage rule shows that the effect of load sequence under axial loading is more significant than its effect under pure torsion loading. Because some of the fatigue life estimations obtained from the linear damage approach under VAL are satisfactory, it appears that the load sequence effect could vary depending on the applied VAL history.
3. Mean stress relaxation can be observed for 30CrNiMo88HH steel with, in some cases, negligible half-life mean stress. Nevertheless, the applied mean strain still has an influence on fatigue life, as indicated by the overestimated fatigue life predictions for the mean strain loading tests.

5.3 Recommendations

The following future research is recommended:

1. For estimations of fatigue life under VAL based on the SWT and FS models, the half-life hysteresis loops were extracted from the test output, whereas for the JV model, the total energy densities were estimated using the proposed formulas. It is recommended that plasticity models be applied in order to estimate the cyclic stress–strain response of the material. Based on the results of previous work, the plasticity models developed by Mroz and Chaboche are recommended for 30CrNiMo88HH steel.
2. To omit the empirically determined constants, the Manson and Marco–Starkey damage accumulation methods were modified based on the experimental observations from the two-

step loading tests. The possibility of generalizing those modifications for other materials should be investigated.

3. Due to time limitations, multiaxial VAL was not included in this study. The assessment of fatigue life under multiaxial VAL requires further analysis with respect to counting the cycles from the applied VAL histories. One of the methods suggested in the literature is to perform the counting for both axial and torsional VAL histories and then to adopt the one that produces the greater damage total.

Appendix A

Hysteresis Loops

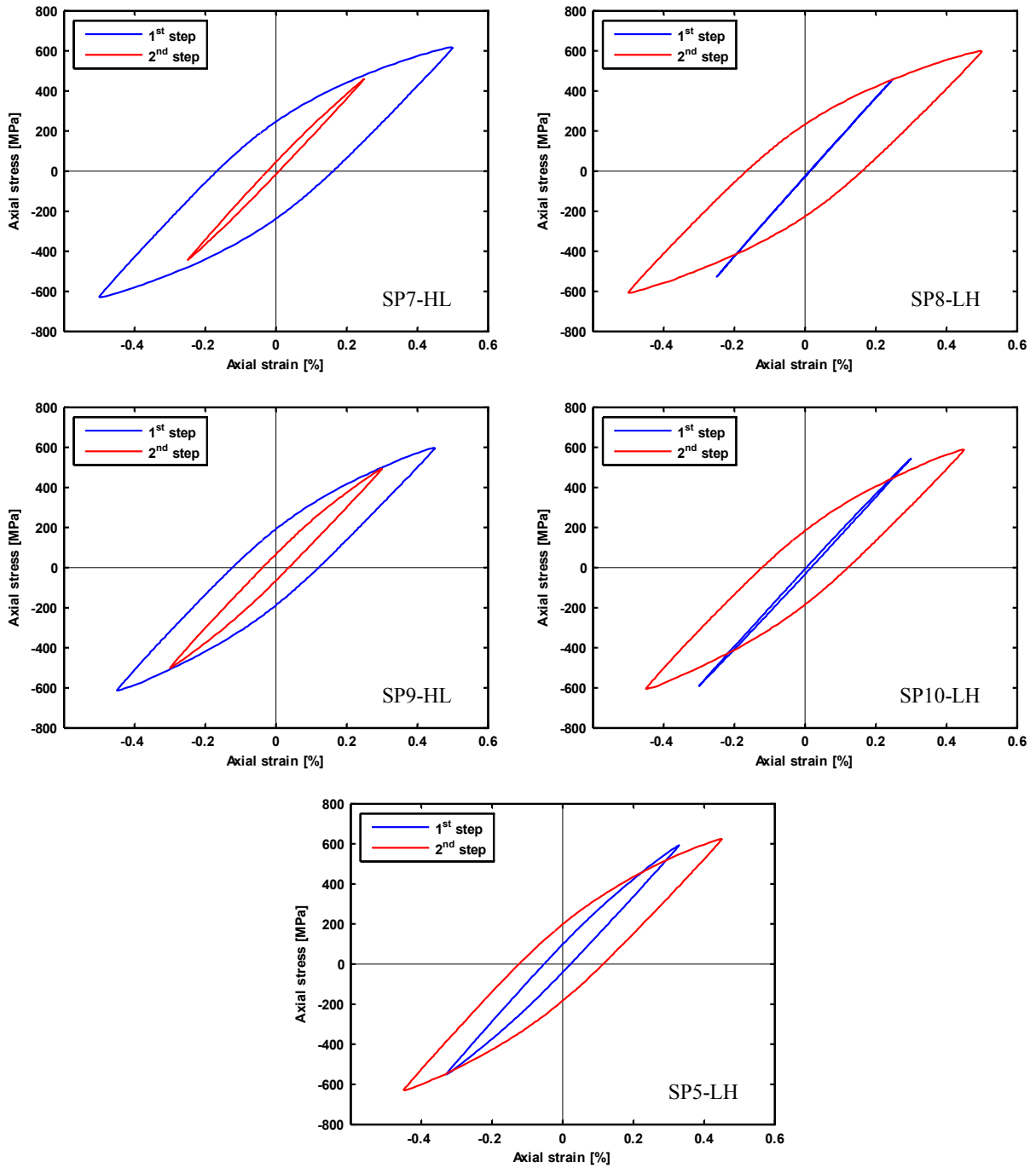


Figure A.1: Two-step hysteresis loops for axial loading

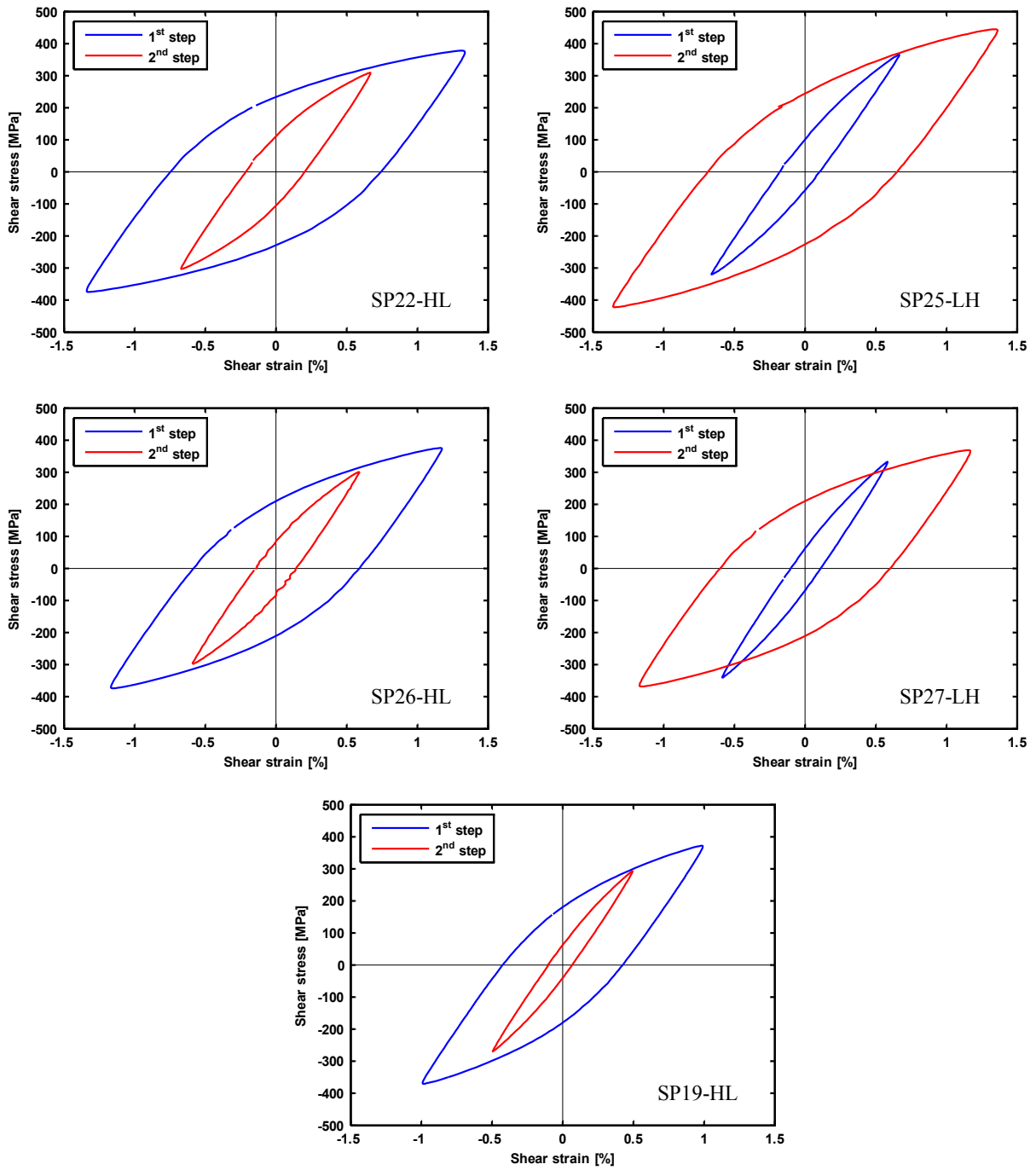


Figure A.2: Two-step hysteresis loops for shear loading

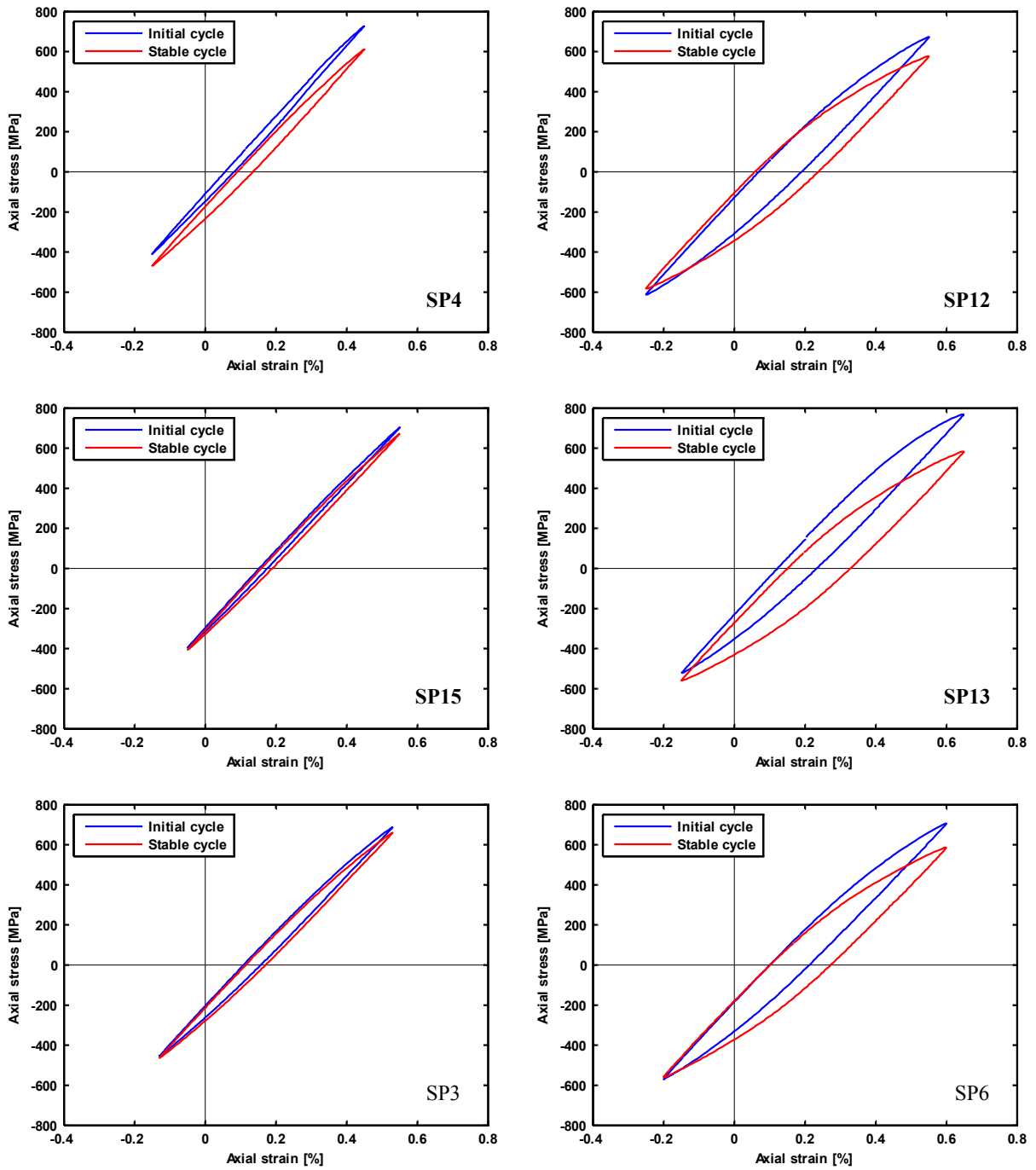


Figure A.3: Hysteresis loops for axial mean strain

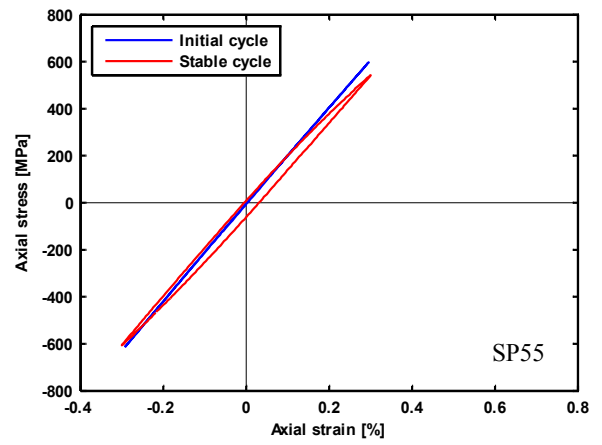
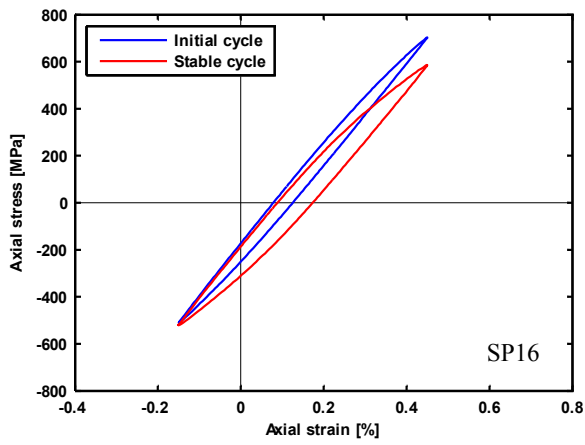
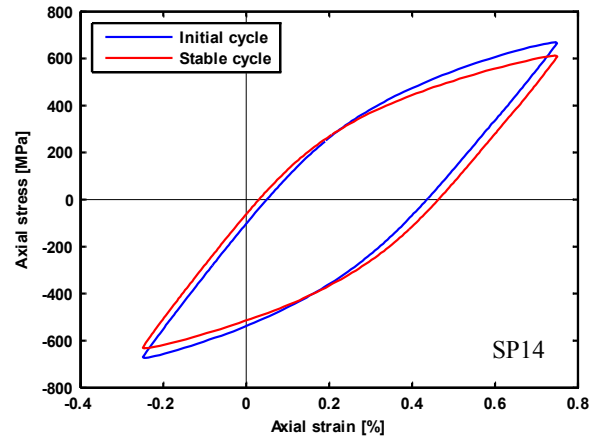
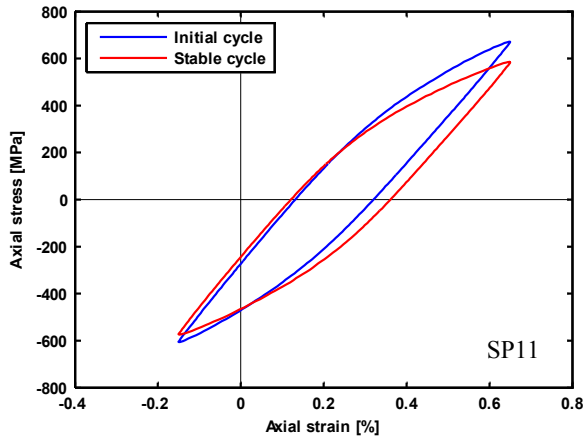


Figure A.3: Hysteresis loops for axial mean strain (continued)

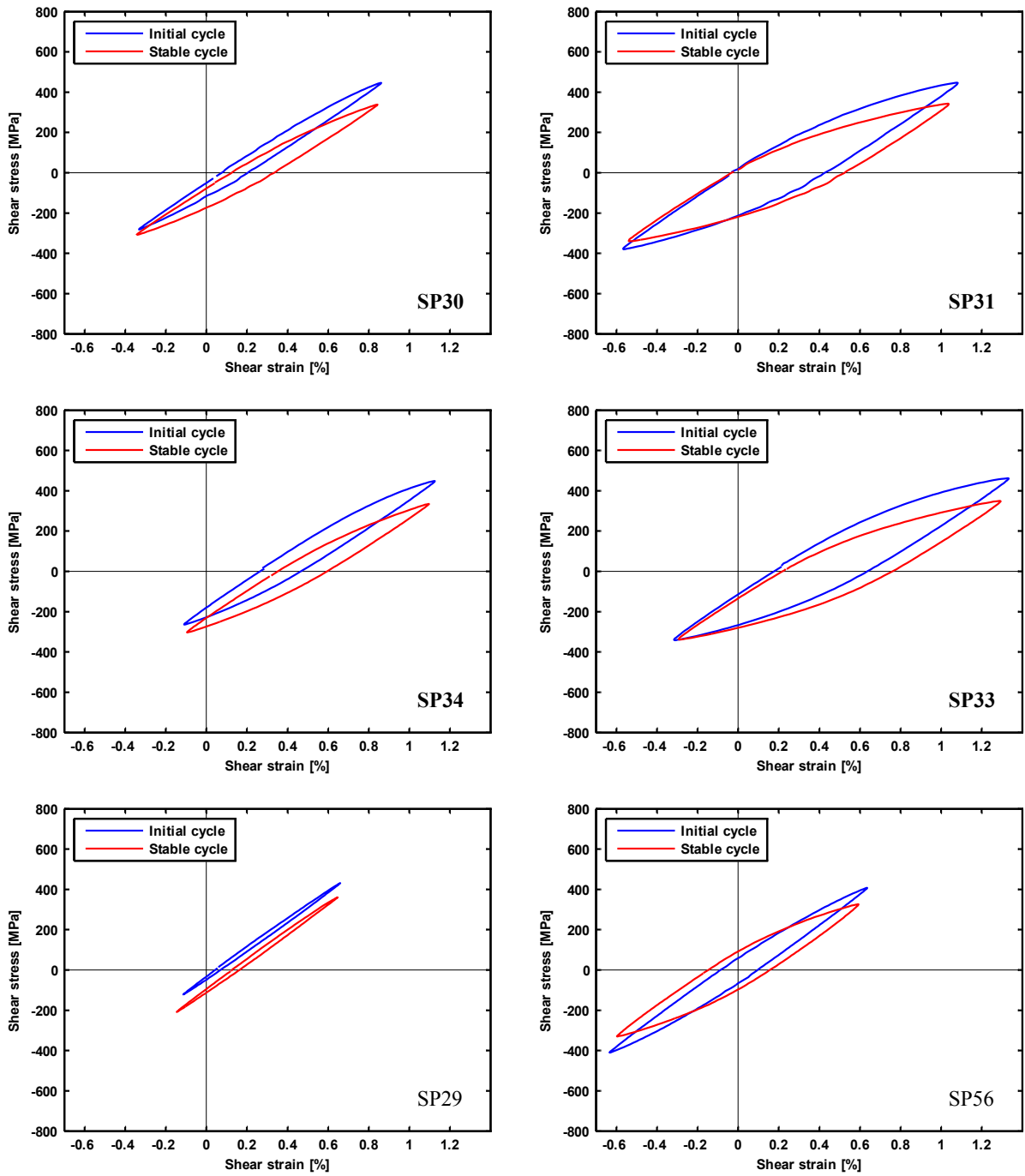


Figure A.4: Hysteresis loops for shear mean strain

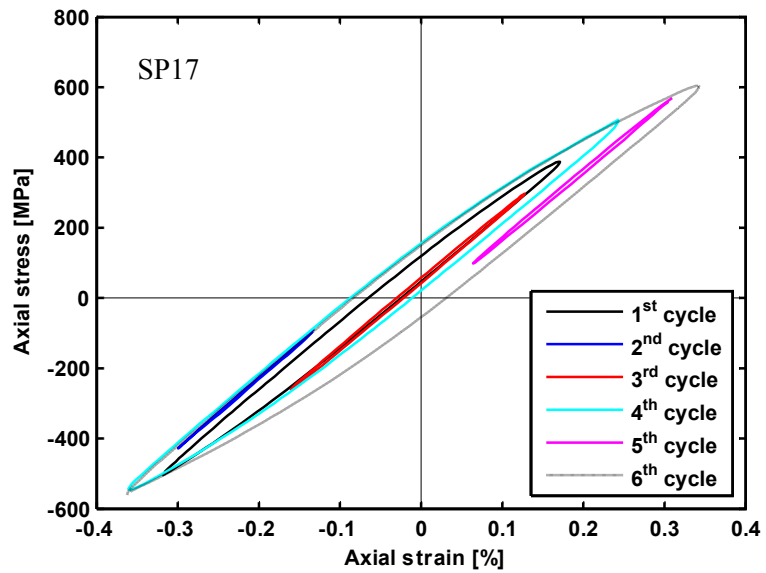
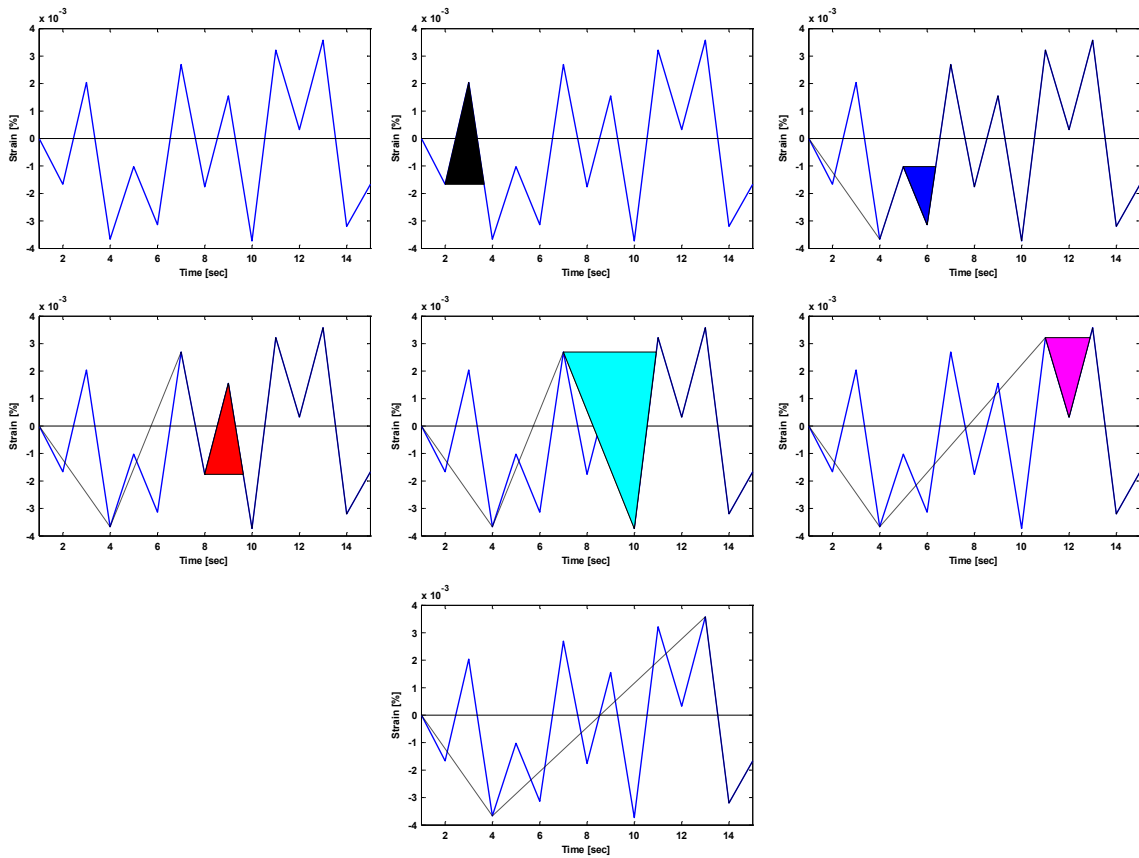


Figure A.5: Counted cycles and hysteresis loops for VAL [without repeated cycles]

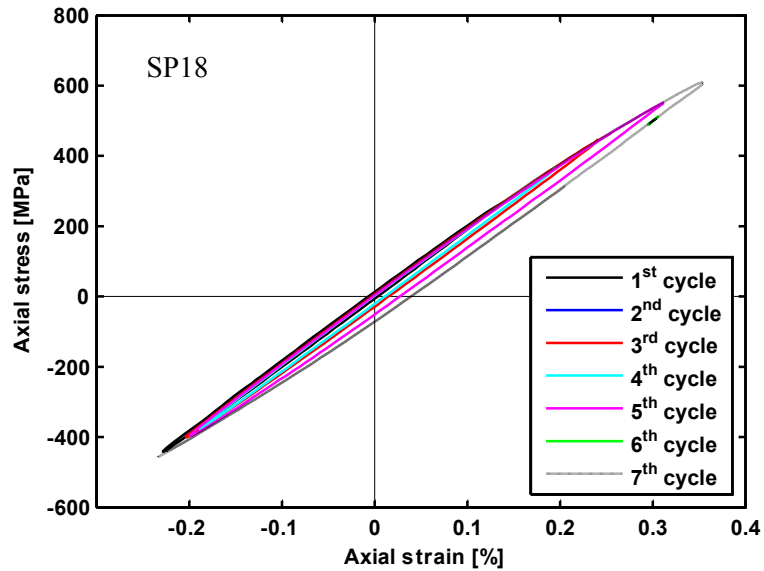
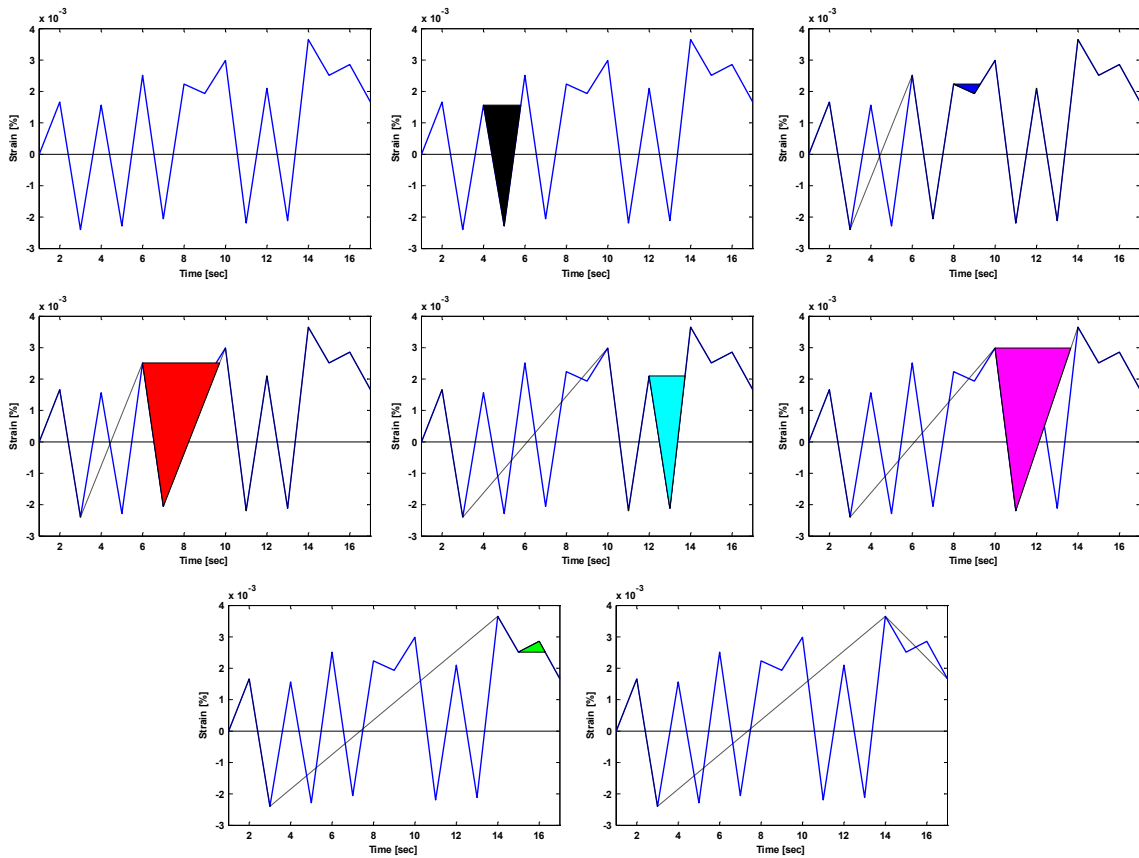


Figure A.5: Counted cycles and hysteresis loops for VAL [without repeated cycles] (continued)

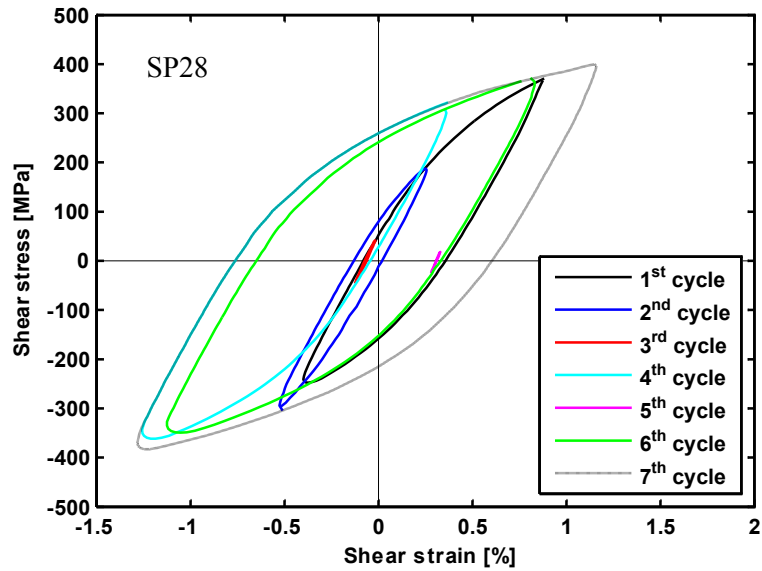
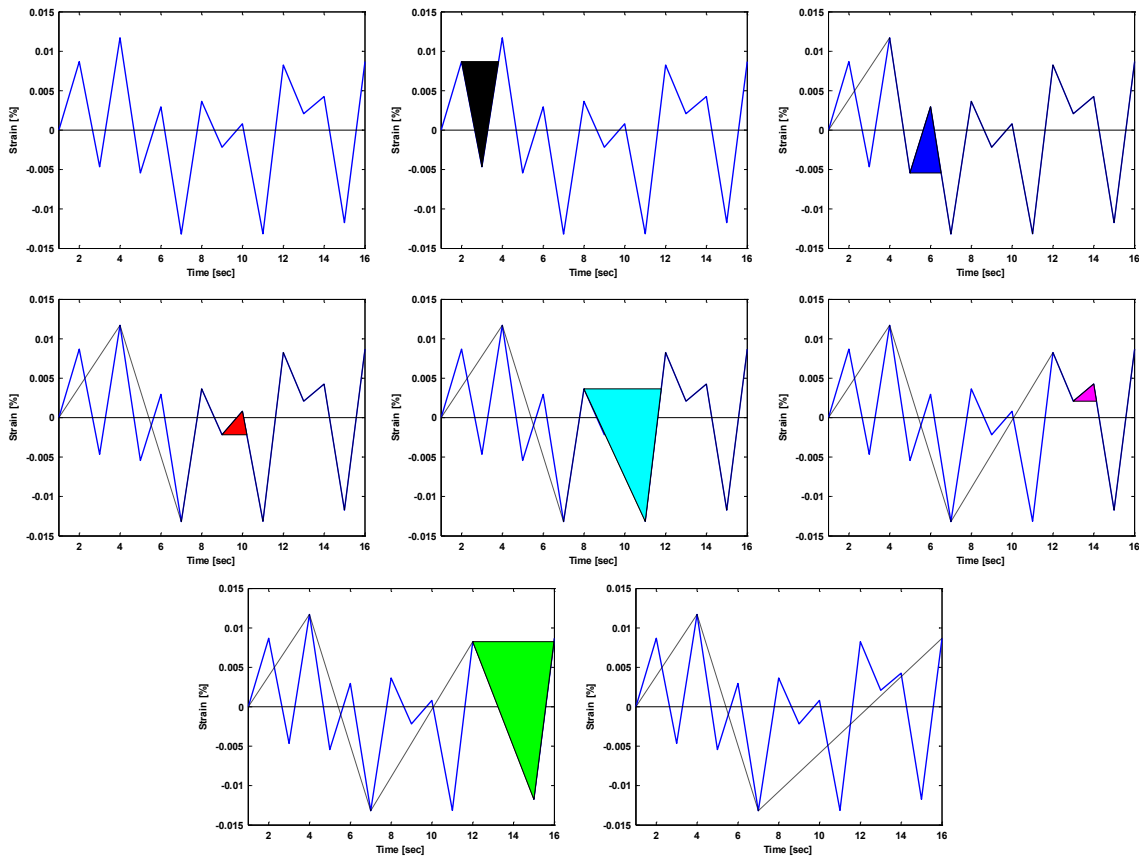


Figure A.5: Counted cycles and hysteresis loops for VAL [without repeated cycles] (continued)

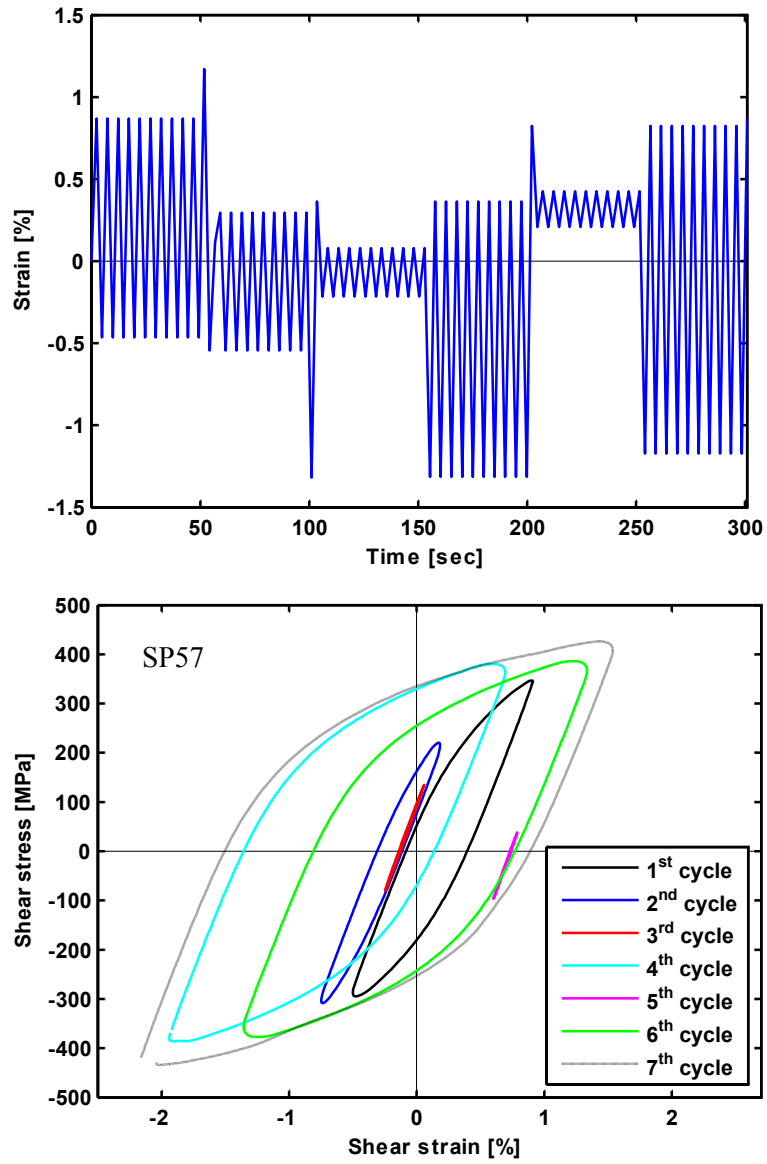


Figure A.6: VAL history and hysteresis loops [with repeated cycles]; same counted cycles as for SP28 but with each cycle counted (except the largest) repeated 50 times within the block

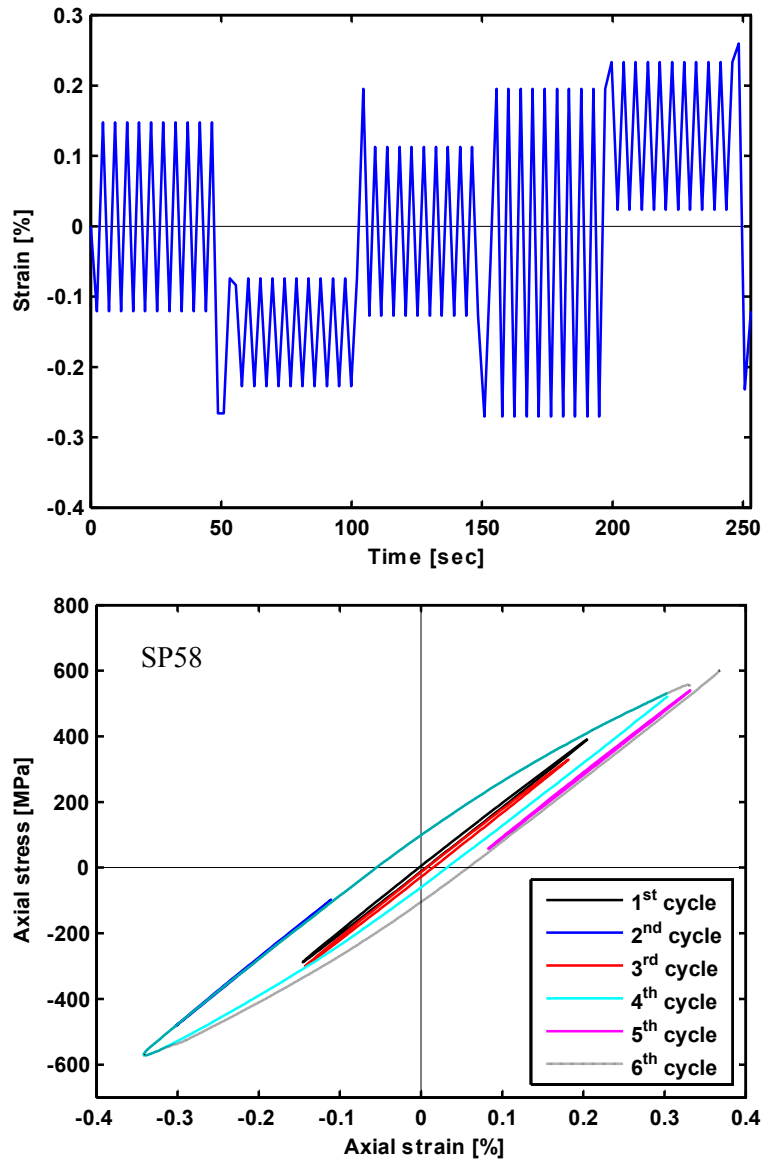
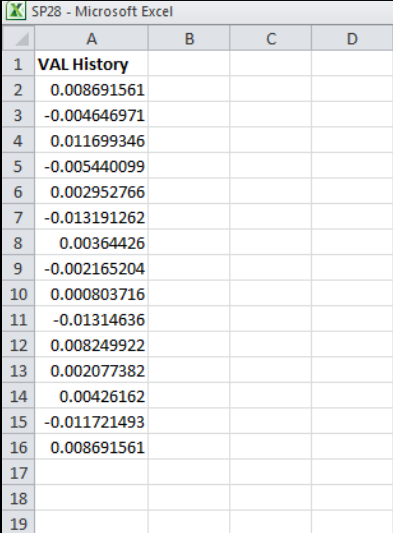


Figure A.6: VAL history and hysteresis loops [with repeated cycles] (continued); same counted cycles as for SP17 but with each cycle counted (except the largest) repeated 50 times within the block

Appendix B

MATLAB Code for the Rainflow Counting Method

This appendix includes the MATLAB code that counts and plots the cycles obtained from the VAL history. The input file for this program is an Excel file with only one column containing the VAL data points, as shown in Figure B.1.



The image shows a screenshot of a Microsoft Excel spreadsheet titled "SP28 - Microsoft Excel". The spreadsheet has four columns labeled A, B, C, and D. Column A contains the VAL history data points, while columns B, C, and D are empty. The data points in column A are: 0.008691561, -0.004646971, 0.011699346, -0.005440099, 0.002952766, -0.013191262, 0.00364426, -0.002165204, 0.000803716, -0.01314636, 0.008249922, 0.002077382, 0.00426162, -0.011721493, and 0.008691561. The first cell in column A is labeled "VAL History".

| | A | B | C | D |
|----|--------------------|---|---|---|
| 1 | VAL History | | | |
| 2 | 0.008691561 | | | |
| 3 | -0.004646971 | | | |
| 4 | 0.011699346 | | | |
| 5 | -0.005440099 | | | |
| 6 | 0.002952766 | | | |
| 7 | -0.013191262 | | | |
| 8 | 0.00364426 | | | |
| 9 | -0.002165204 | | | |
| 10 | 0.000803716 | | | |
| 11 | -0.01314636 | | | |
| 12 | 0.008249922 | | | |
| 13 | 0.002077382 | | | |
| 14 | 0.00426162 | | | |
| 15 | -0.011721493 | | | |
| 16 | 0.008691561 | | | |
| 17 | | | | |
| 18 | | | | |
| 19 | | | | |

Figure B.1: SP28 input file for VAL history

```

% UNIVERSITY OF WATERLOO
% FATIGUE & STRESS ANALYSIS LABORATORY (FATSLAB)
% MECHANICAL & MECHATRONICS ENGINEERING DEPARTMENT (MME)

clc
clear all

disp('*****');
disp('*          RAINFLOW COUNTING METHOD          *');
disp('*    (WITHOUT HISTORY REARRANGEMENT)    *');
disp('*          AUTHOR: ELFAITORI IBRAHIM          *');
disp('*****');

% ----- INPUT DATA -----

% THE INPUT FILE FOR VAL HISTORY CONTAINS ONLY ONE COLUMN FOR VAL BLOCK.
% THE VAL BLOCK (REPEATED BLOCK) MUST NOT START WITH ZERO.
% SPECIFY THE INPUT FILE INCLUDING ITS PATH
% (e.g., 'E:\Rainflow_input\VAL.xlsx')
input_file = '';

% THE OUTPUT LOCATION CONTAINS THE COUNTING RESULTS IN AN EXCEL FILE AND
% THE FIGURES THAT SHOW THE COUNTING STEPS.
% SPECIFY THE OUTPUT LOCATION (e.g., 'E:\Rainflow_output')
output_location = '';

% ----- END INPUT. SAVE AND RUN -----

% READING VAL HISTORY
data = xlsread(input_file);
data = [0;data];
t = 1:length(data);

% PLOTTING VAL HISTORY BEFORE COUNTING
h1=figure;
plot(t,data,'-b','LineWidth',1)
hold on
plot([1 length(data)],[0 0],'k-')
xlim([1 length(data)])
xlabel('Time [sec]')
ylabel('Strain [%]')

% SAVE VAL BEFORE COUNTING
file=strcat(output_location,'/Figure',num2str(1));
print(h1,'-dtiff',file)

% PLOT VAL HISTORY AGAIN AND HOLD ON
h2=figure;
plot(t,data,'-b','LineWidth',1)
hold on
plot([1 length(data)],[0 0],'k-')

```

```

xlim([1 length(data)])
xlabel('Time [sec]')
ylabel('Strain [%]')
hold on

data0 = data;
t0 = t;

i=1;
m=2;
n=3;
p=2;

% WHILE LOOP FOR COUNTING.
% THE COUNTING WILL END IF THE LAST POINT IN VAL HISTORY IS REACHED
while data(n) ~= data(end)

    slope1 = (data(n)-data(m))/(t(n)-t(m));
    slope2 = (data(n+1)-data(n))/(t(n+1)-t(n));

    range1 = abs(data(n)-data(m));
    range2 = abs(data(n+1)-data(n));

% CRITERIA FOR COUNTING
if range2 >= range1 && slope1*slope2 < 0

% CALCULATE RANGE, MAX, MIN, MEAN, AND AMPLITUDE FOR COUNTED CYCLE
DltStrain(i) = range1;
MaxStrain(i) = max(data(n),data(m));
MinStrain(i) = min(data(n),data(m));
MeanStrain(i) = (MaxStrain(i)+MinStrain(i))/2;
StrainAmp(i) = (MaxStrain(i)-MinStrain(i))/2;

% MARK THE COUNTED CYCLE ON THE FIGURE
xx = t(n) + (data(m)-data(n))/slope2;
fill([t(m) t(n) xx],[data(m) data(n) data(m)], 'y')
box on

% SAVE THE FIGURE
file=strcat(output_location, '/Figure', num2str(p));
print(h2, '-dtiff', file)
p=p+1;
hold off

% PLOT ANOTHER FIGURE FOR THE NEXT COUNTING STEP
h2=figure;
plot(t0,data0, '-b', 'LineWidth',1)
hold on
plot([1 t0(end)], [0 0], 'k-')
xlim([1 length(data0)])
xlabel('Time [sec]')

```

```

        ylabel('Strain [%]')

% REMOVE THE COUNTED CYCLE FROM THE HISTORY
data(m:n) = [];
t(m:n) = [];

hold on

% PLOT DASHED LINE AFTER REMOVING THE COUNTED CYCLE
plot(t,data,'--k','LineWidth',.5)

    i=i+1;
    m = 2;
    n = 3;

end

if slope1* slope2 < 0
    m = m+1;
end

n = n +1;

end

% SAVE THE LAST FIGURE AFTER THE COUNTING ENDS
file=strcat(output_location,'/Figure',num2str(p));
print(h2,'-dtiff',file)

% ADD THE LAST (LARGEST) CYCLE THAT ENCOMPASSES ALL COUNTED CYCLES
DltStrain(i) = max(data0)-min(data0);
MaxStrain(i) = max(data0);
MinStrain(i) = min(data0);
MeanStrain(i) = (max(data0)+min(data0))/2;
StrainAmp(i) = (max(data0)-min(data0))/2;

% COUNTING RESULTS
results = [StrainAmp' MaxStrain' MinStrain' MeanStrain' DltStrain'];

% SAVE COUNTING RESULTS IN AN EXCEL FILE
heading = {'Amplitude','Maximum','Minimum','Mean','Range'};
file2=strcat(output_location,'/Counting results.xlsx');
xlswrite(file2,heading,'A1:E1')

interval = ['A',num2str(2),':','E',num2str(i+1)];

xlswrite(file2,results,interval)

% COUNTING IS OVER!
disp('Done! Open the output folder for counting results and figures')

```

Bibliography

- [1] M. Noban, H. Jahed, S. Winkler, A. Ince, Fatigue characterization and modeling of 30CrNiMo8HH under multiaxial loading, *Materials Science and Engineering: A*, 528 (2011) 2484-2494.
- [2] M. Noban, H. Jahed, E. Ibrahim, A. Ince, Load path sensitivity and fatigue life estimation of 30CrNiMo8HH, *International Journal of Fatigue*, (2011).
- [3] J.A. Bannantine, J.J. Comer, J.L. Handrock, *Fundamentals of metal fatigue analysis*, Prentice Hall, 1990.
- [4] R.I. Stephens, A. Fatemi, R.R. Stephen, H.O. Fuchs, *Metal fatigue in engineering*, Second ed., John Wiley & Sons, Inc., 2001.
- [5] J.A. Collins, *Failure of materials in mechanical design: analysis, prediction, prevention*, John Wiley, 1993.
- [6] M. Matsuishi, T. Endo, Fatigue of metals subjected to varying stress, *Japan Society of Mechanical Engineers*, Fukuoka, Japan, (1968) 37-40.
- [7] S.D. Downing, D.F. Socie, Simple rainflow counting algorithms, *International Journal of Fatigue*, 4 (1982) 31-40.
- [8] I. Rychlik, A new definition of the rainflow cycle counting method, *International Journal of Fatigue*, 9 (1987) 119-121.
- [9] C. Amzallag, J.P. Gerey, J.L. Robert, J. Bahuaud, Standardization of the rainflow counting method for fatigue analysis, *International Journal of Fatigue*, 16 (1994) 287-293.
- [10] Standard Practices for Cycle Counting in Fatigue Analysis, in: *ASTM Standard E1049-85*, American Society for Testing and Materials, ASTM International, West Conshohocken, 2011.
- [11] G. Glinka, J.C.P. Kam, Rainflow counting algorithm for very long stress histories, *International Journal of Fatigue*, 9 (1987) 223-228.
- [12] A. Fatemi, L. Yang, Cumulative fatigue damage and life prediction theories: a survey of the state of the art for homogeneous materials, *International Journal of Fatigue*, 20 (1998) 9-34.
- [13] A. Palmgren, Durability of ball bearings, *ZVDI*, 68 (1924) 339-341.
- [14] M.A. Miner, Cumulative damage in fatigue, *J. Appl. Mech.*, 12 (1945) A159-A164.
- [15] L. Yang, A. Fatemi, Cumulative fatigue damage mechanisms and quantifying parameters: a literature review, *Journal of Testing and Evaluation*, 26 (1998) 89-100.

- [16] S. Manson, Interpretive report on cumulative fatigue damage in the low cycle range (Palmgren-Miner, Manson, Fuller, and Valluri methods of predicting fatigue life in spectrum loading), *Welding Journal, Research Supplement*, 43 (1964).
- [17] S. Manson, A. Nachtigall, J. Freche, A proposed new relation for cumulative fatigue damage in bending, in, 1961, pp. 679-703.
- [18] S. Manson, S.o.A. Engineers, A.S.o.M. Engineers, Further investigation of a relation for cumulative fatigue damage in bending, *Society of Automotive Engineers*, 1964.
- [19] S. Marco, W. Starkey, A concept of fatigue damage, *Trans. ASME*, 76 (1954) 627-632.
- [20] S.K. Koh, R.I. Stephens, Mean Stress Effects on Low Cycle Fatigue for a High Strength Steel, *Fatigue & Fracture of Engineering Materials and Structures*, 14 (1991) 413-428.
- [21] T. Wehner, A. Fatemi, Effects of mean stress on fatigue behaviour of a hardened carbon steel, *International Journal of Fatigue*, 13 (1991) 241-248.
- [22] F. Ellyin, *Fatigue damage, crack growth, and life prediction*, Chapman & Hall, 1997.
- [23] J. Schijve, *Fatigue of Structures and Materials*, Springer, 2009.
- [24] A. Fatemi, P. Kurath, Multiaxial Fatigue Life Predictions Under the Influence of Mean-Stresses, *Journal of Engineering Materials and Technology*, 110 (1988) 380-388.
- [25] Y.L. Lee, M.E. Barkey, H.T. Kang, *Metal Fatigue Analysis Handbook: Practical Problem-solving Techniques for Computer-aided Engineering*, Elsevier Science, 2011.
- [26] J.A. Graham, J.F. Millan, F.J. Appl, S.o.A.E. Iron, S.T.C.D.F.D. Subcommittee, *Fatigue design handbook: a guide for product design and development engineers*, Society of Automotive Engineers, 1968.
- [27] S.S. Manson, G.R. Halford, Practical implementation of the double linear damage rule and damage curve approach for treating cumulative fatigue damage, *International Journal of Fracture*, 17 (1981) 169-192.
- [28] Standard Test Methods for Tension Testing of Metallic Materials, in: ASTM Standard E8/E8M-11, American Society for Testing and Materials, ASTM International, West Conshohocken, 2011.
- [29] Standard Test Method for Shear Modulus at Room Temperature, in: ASTM Standard E143-02, American Society for Testing and Materials, ASTM International, West Conshohocken, 2008.
- [30] K.N. Smith, P. Watson, T.H. Topper, A stress-strain function for the fatigue of metals, *Journal of Materials*, 5 (1970) 767-778.
- [31] D. Socie, Multiaxial Fatigue Damage Models, *Journal of Engineering Materials and Technology*, 109 (1987) 293-298.

- [32] A. Fatemi, D.F. Socie, A Critical Plane Approach to Multiaxial Fatigue Damage Including out-of-Phase Loading, *Fatigue & Fracture of Engineering Materials and Structures*, 11 (1988) 149-165.
- [33] M.W. Brown, K.J. Miller, A theory for fatigue failure under multiaxial stress-strain conditions, *ARCHIVE: Proceedings of the Institution of Mechanical Engineers 1847-1982 (vols 1-196)*, 187 (1973) 745-755.
- [34] D. Socie, G. Marquis, *Multiaxial fatigue*, Society of Automotive Engineers, 2000.
- [35] H. Jahed, A. Varvani-Farahani, Upper and lower fatigue life limits model using energy-based fatigue properties, *International Journal of Fatigue*, 28 (2006) 467-473.
- [36] K. Golos, F. Ellyin, Generalization of cumulative damage criterion to multilevel cyclic loading, *Theoretical and Applied Fracture Mechanics*, 7 (1987) 169-176.
- [37] K. Golos, F. Ellyin, A Total Strain Energy Density Theory for Cumulative Fatigue Damage, *Journal of Pressure Vessel Technology*, 110 (1988) 36-41.
- [38] G. Masing, Eigenspannungen und verfestigung beim messing, *Proc. Second Int. Cong. Appl. Mech.*, (1926) 332-335.
- [39] J. Morrow, Cyclic plastic strain energy and fatigue metals, *ASTM/STP 378*, (1965) 45-78.
- [40] D. Lefebvre, F. Ellyin, Cyclic response and inelastic strain energy in low cycle fatigue, *International Journal of Fatigue*, 6 (1984) 9-15.
- [41] Z. Mróz, On the description of anisotropic workhardening, *Journal of the Mechanics and Physics of Solids*, 15 (1967) 163-175.
- [42] J.L. Chaboche, Time-independent constitutive theories for cyclic plasticity, *International Journal of Plasticity*, 2 (1986) 149-188.
- [43] J. Bannantine, A variable amplitude multiaxial fatigue life prediction method, in, *University of Illinois at Urbana-Champaign, United States -- Illinois, 1989*, pp. 286 p.
- [44] A. Bannantine, D. Socie, A Multiaxial Fatigue Life Estimation Technique, *Advances in fatigue lifetime predictive techniques*, 51 (1992) 249.
- [45] T. Lagoda, E. Macha, Fatigue life estimation for 30CrNiMo8 steel under in- and out-of-phase combined bending and torsion with variable amplitudes, *Materials Science*, 31 (1996) 23-31.
- [46] D.S. Tchankov, K.V. Vesselinov, Fatigue life prediction under random loading using total hysteresis energy, *International Journal of Pressure Vessels and Piping*, 75 (1998) 955-960.
- [47] K.S. Kim, J.C. Park, Shear strain based multiaxial fatigue parameters applied to variable amplitude loading, *International Journal of Fatigue*, 21 (1999) 475-483.
- [48] F. Kandil, M. Brown, K. Miller, Biaxial low-cycle fatigue fracture of 316 stainless steel at elevated temperatures, *Book*, 280 (1982) 203-210.

[49] B.L. Lee, K.S. Kim, K.M. Nam, fatigue analysis under variable amplitude loading using an energy parameter, *International Journal of Fatigue*, 25 (2003) 621-631.

[50] J. Colin, A. Fatemi, Variable amplitude cyclic deformation and fatigue behaviour of stainless steel 304L including step, periodic, and random loadings, *Fatigue & Fracture of Engineering Materials & Structures*, 33 (2010) 205-220.

[51] Standard Practice for Strain-Controlled Fatigue Testing, in: *ASTM Standard E606-92*, American Society for Testing and Materials, ASTM International, West Conshohocken, 2004.

[52] Standard Practice for Strain-Controlled Axial-Torsional Fatigue Testing with Thin-Walled Tubular Specimens, in: *ASTM Standard E2207-08*, American Society for Testing and Materials, ASTM International, West Conshohocken, 2008.

[53] D.C. Montgomery, *Design and analysis of experiments*, Wiley, 2008.